

RAYTHEON COMPANY
Microwave and Power Tube Division
Waltham, Massachusetts 02254

**MICROWAVE BEAMED POWER
TECHNOLOGY IMPROVEMENT
FINAL REPORT**

JPL Contract No. 955104

by
W.C. Brown

**PT-5613
15 May 1980**



**This work was performed for the Jet Propulsion
Laboratory, California Institute of Technology,
sponsored by the National Aeronautics and
Space Administration under Contract NAS 7-100.**

**(NASA-CR-163043) MICROWAVE BEAMED POWER
TECHNOLOGY IMPROVEMENT Final Report
(Raytheon Co.) 48 p HC A03/NF A01**

N80-26785

**Unclas
G3/44 27908**

RAYTHEON COMPANY
Microwave and Power Tube Division
Waltham, Massachusetts 02254

MICROWAVE BEAMED POWER
TECHNOLOGY IMPROVEMENT

FINAL REPORT

JPL Contract No. 955104

by
W.C. Brown

PT-5613
15 May 1980

**This work was performed for the Jet Propulsion
Laboratory, California Institute of Technology,
sponsored by the National Aeronautics and
Space Administration under Contract NAS 7-100.**

TABLE OF CONTENTS

<u>Section</u>	<u>Title</u>	<u>Page</u>
1.0	INTRODUCTION	1-1
2.0	THEORY OF OPERATION OF THE MAGNETRON DIRECTIONAL AMPLIFIER	2-1
2.1	Introduction	2-1
2.2	The Operating Properties of the Magnetron Directional Amplifier	2-5
3.0	GENERAL PERFORMANCE DATA ON THE MAGNETRON DIRECTIONAL AMPLIFIER	3-1
3.1	Introduction	3-1
3.2	Phase Shift Through the Magnetron Directional Amplifier and Power Output of the Magnetron Directional Amplifier as a Function of Anode Current, Anode Voltage, and Level of Microwave Drive	3-2
3.3	Frequency Locking Range of the Magnetron Directional Amplifier as a Function of Magnetron Anode Current and Voltage, and Level of Microwave Drive	3-4
4.0	NOISE MEASUREMENTS OF THE MAGNETRON DIRECTIONAL AMPLIFIER	4-1
4.1	Introduction	4-1
4.2	Background Noise as a Function of Operating Conditions	4-2
4.3	Phase Modulation Noise Added by the Magnetron Directional Amplifier	4-6
4.4	The Measurement of Harmonic Power Levels	4-15
4.4.1	Introduction	4-15
5.0	CATHODE LIFE CONSIDERATIONS	5-1
5.1	Introduction	5-1
5.2	Cathode Temperature as a Function of Anode Current, Magnetic Field, and Load Coupling	5-9
5.3	Correlation of Operating Temperature with the Richardson-Dushman Equation for Primary Emission	5-11
5.4	A Review of the Engineering Background on the Life of the Carburized Thoriated Tungsten Cathode Including Experimental Data	5-14

TABLE OF CONTENTS (Cont'd)

<u>Section</u>	<u>Title</u>	<u>Page</u>
5.5	Distribution of Cathode Temperature as a Function of Axial Distance Along the Cathode	5-22
5.6	Observations of the Impact of Cathode Poisoning upon Cathode Operating Temperature and Tube Efficiency	5-24
6.0	OPERATION OF THE MICROWAVE OVEN MAGNETRON AT HIGH EFFICIENCY AND POWER LEVEL	6-1
6.1	Introduction and Engineering Approach to High Efficiency	6-1
6.2	Test Arrangements and Test Results	6-3
7.0	DESIGN, CONSTRUCTION, AND EVALUATION OF A THIN-METAL LOW-COST, LOW-LOSS S-BAND SLOTTED WAVEGUIDE ARRAY	7-1
7.1	Introduction	7-1
7.2	Basic Approach to the Fabrication Method	7-2
7.3	The Electric Design and Its Development	7-6
7.4	Testing Methods and Test Results for the Finished Arrays	7-15
7.5	Measurement of the Dissipative Loss in the Slotted Waveguide Array	7-21
8.0	CONCLUSION AND SUMMARY OF RESULTS	8-1
8.1	Phase Shift and Power Output as a Function of Anode Current, Anode Voltage, and Drive Level	8-1
8.2	Evaluation of Noise Properties	8-1
8.3	Investigation of Long Cathode Life Potential	8-2
8.4	Investigation of High Efficiency in the Microwave Oven Magnetron	8-3
8.5	Investigation of a Novel Method for Fabricating Slotted Waveguide Arrays from Thin Sheet Metal	8-4
9.0	RECOMMENDATIONS	9-1
10.0	NEW TECHNOLOGY	10-1

LIST OF ILLUSTRATIONS

<u>Figure No.</u>	<u>Title</u>	<u>Page</u>
2-1	Gain Properties of Directional Amplifier.	2-2
2-2	Directional Amplifier Approaches Utilizing Crossed Field Devices.	2-3
2-3	The central portion of the load diagram for a magnetron showing that the tube cannot distinguish between a reflection from a passive load and a signal of equal magnitude injected from another source. The tube adjusts itself to an injected signal by operating at the frequency of the injected signal and changing its output phase to accommodate the magnitude of the injected signal and the frequency difference between the injected signal and the free-running frequency of the magnetron.	2-6
3-1	Test arrangement for observing phase shift across magnetron directional amplifier as a function of operating voltage and current.	3-3
3-2	Curves of constant power output and phase shift as functions of magnetron directional amplifier voltage and current for drive power of 25 watts.	3-5
3-3	Curves of constant power output and phase shift as functions of magnetron directional amplifier voltage and current for drive power of 10 watts.	3-6
3-4	Curves of constant power output and phase shift as functions of magnetron directional amplifier voltage and current for drive power of 2.5 watts.	3-7
3-5	Curves of constant frequency and power output for undriven magnetron directional amplifier as function of voltage and current.	3-8
3-6	Simplified Test Setup Block Diagram.	3-10
3-7	Effect of Injection Power on Locking Range.	3-11
3-8	Locking Performance - Low Voltage Region.	3-13
3-9	Locking Performance - Mid Voltage Region.	3-14
3-10	Locking Performance - High Voltage Region.	3-15
4-1	Test Arrangement to Photograph Spectra of Microwave Output of Magnetron Directional Amplifier.	4-3
4-2	Signal to Noise as a Function of Voltage and Current	4-5

LIST OF ILLUSTRATIONS (Cont'd)

<u>Figure No.</u>	<u>Title</u>	<u>Page</u>
4-3	Signal to Noise as a Function of Frequency Deviation	4-7
4-4	Signal to Noise as a Function of Drive Level	4-8
4-5	Typical Data Obtained from CNA-10 Analyzer for Phase Modulation Noise.	4-10
4-6	Test Arrangement for Measuring Close-In Phase Modulation Noise Added by the Magnetron Directional Amplifier.	4-11
4-7	Measurements of close-in phase modulation noise added by magnetron directional amplifier. See text for detailed explanation.	4-12
4-8	Direct transmission of QKH2000 magnetron directly to 7/8 inch coaxial line. Transition arrangement preserves the normal external coupling of the tube.	4-16
4-9	Coaxial Output Fitted Directly to the Microwave Oven Magnetron.	4-17
4-10	Test Set-up for Measuring Harmonic Power.	4-19
4-11	Harmonic Power Level as a Function of Pulling Slug's Position.	4-24
5-1	Test arrangement for viewing the temperature of the filament-type cathode in the microwave oven magnetron as a function of anode current, applied magnetic field, and microwave load. Optical pyrometer is in the right foreground. Transparent window is visible outside of solenoid-type electromagnet.	5-3
5-2	Carburized Thoriated Tungsten Filament Optical Pyrometer Reading vs True Temperature.	5-4
5-3	Four (4) turns of the filament-type cathode are visible in the photograph. The filament wire diameter is approximately one half millimeter. Filament is observed between the tips of two vanes so full diameter of cathode is not observed.	5-6
5-4	Experimentally Observed and Theoretically Predicted Relationship Between Cathode Temperature and Anode Current.	5-8
5-5	Anode Voltage and Cathode Brightness Temperature as Function of Magnetic Field.	5-10

LIST OF ILLUSTRATIONS (Cont'd)

<u>Figure No.</u>	<u>Title</u>	<u>Page</u>
5-6	Cathode Brightness Temperature and Power Output as Function of Loading.	5-12
5-7	Relationship of Diode Current to Anode Voltage as Function of Observed Brightness Temperature.	5-15
5-8	Cross section of carburized thoriated tungsten filament and curve showing life for different thickness of carbide shell. After Ayer.	5-17
5-9	Carbide Loss Versus Operating Temperature.	5-18
5-10	Distribution of Temperature Along Filament.	5-23
5-11	Impact of gas poisoning on filament temperature, tube efficiency, and anode voltage as function of operating time.	5-26
6-1	Operation of conventional microwave oven magnetron at high magnetic field and voltages on a well-filtered DC power supply. At high voltages and currents, overall efficiency reached 81.7% Also shown on the chart is the normal operating line for the magnetron which is required in its normal operation to alternate between a peak current of over 900 milliamperes and zero current at a sixty Hz rate.	6-4
6-2	Water flow schematic for eliminating water flow rate and absolute temperature calibration of thermocouples as variables in the measurement of efficiency.	6-6
6-3	Theoretical and experimentally observed DC to rf conversion efficiencies of conventional microwave oven magnetron and 915 MHz magnetron. Conversion efficiency is efficiency of conversion of DC power into microwave power. Overall efficiency includes circuit inefficiencies which can be ascertained from cold test data.	6-10
7-1	Proposed method for precision forming and assembly of low-cost, thin-walled, slotted waveguide arrays for the SPS. Figure 7-1A shows the forming of the top and bottom section. Figure 7-1B shows the assembly of the top and bottom.	7-3
7-2	General Fabrication Procedure.	7-5
7-3	Front view of the 8x8 slotted waveguide array as constructed from 0.020 inch aluminum sheet throughout and assembled by means of spot welding.	7-7

LIST OF ILLUSTRATIONS (Cont'd)

<u>Figure No.</u>	<u>Title</u>	<u>Page</u>
7-4	Back view of the 8x8 slotted waveguide array as constructed from 0.020" aluminum throughout and assembled by means of spot welding.	7-8
7-5	Load deflection curve for section of slotted waveguide array made from 0.020" material and spot welded together.	7-9
7-6	Beam rf power technology S-band slotted waveguide subarray.	7-10
7-7	Engineering model of slotted waveguide array showing provision for rotation of coupling slots and their removal for making change in slot length.	7-13
7-8	Impedance as seen at the center line of coupling slot looking into radiating waveguide as a function of coupling slot rotation and length of coupling slot. Feed waveguide was used as standing wave detector. All coupling slots in feed waveguide were sealed off to set shorting plunger at end of feed waveguide to produce a minimum at center of outboard coupling slot. The shorting tape was then removed from the outboard coupling slot and the measurements made as shown above. Holes in the feed waveguide cover plate that were used to obtain standing wave information are shown in Figure 7-7. Phase information as well as amplitude information was taken when the probe was inserted into the holes to obtain accurate minimum data from plotting phase and amplitude information on polar coordinate paper. Impedance values above have been normalized to the 50 ohm Smith chart paper. Actual values, of course, are related to the characteristic impedance of the feed waveguide.	7-14
7-9	Probe arrangement for measuring phase and amplitude of microwave power radiated at individual slots. The phase and amplitude sensed by the probe were compared by means of a Hewlett-Packard network analyzer with the amplitude and phase of the power input to the single waveguide feed to the slotted waveguide array.	7-16
7-10	Arrangement for checking for any error in phase and amplitude slot measurements introduced by rf pickup of the support rod for probe. Data indicated no significant error was introduced.	7-17
7-11	Matrix Array of Amplitude and Phase Information on Thin Metal Slotted Array #1.	7-19

LIST OF ILLUSTRATIONS (Cont'd)

<u>Figure No.</u>	<u>Title</u>	<u>Page</u>
7-12	Beam rf power technology 8-slot x 8-stick slotted waveguide antenna, E-plane pattern.	7-22
7-13	Beam rf power technology 8-slot x 8-stick slotted waveguide antenna, H-plane pattern.	7-23
7-14	Test Arrangement for Measuring Internal Losses of Microwave Slotted Waveguide Radiator.	7-29
7-15	Arrangements for Checking Slotted Waveguide for Internal Dissipation Losses.	7-30
7-16	System Check with Immersion Heater at the 5-Watt Level	7-34
7-17	VSWR Looking into Feed Waveguide to Slotted Waveguide Before and After Impedance Matching.	7-35
7-18	Dissipated power in slotted waveguide section measured by thermal means. Microwave power of 480 watts enters the slotted waveguide and all but 4.8 watts is radiated through the slots. Microwave power is applied as a step function for approximately ten minutes and then turned off.	7-37

ABSTRACT

The purpose of the investigation was to add experimentally-derived information in two critical technology areas to the data base for microwave beamed power. The first was the investigation of the combination of a microwave oven magnetron and a passive directional device to provide a low cost, efficient, microwave amplifier. The second was an investigation of a new method for fabricating a slotted waveguide array from thin sheet metal that would result in low cost.

The magnetron directional amplifier was tested for (1) phase shift and power output as a function of gain, anode current and anode voltage, (2) background noise and harmonics in the output, (3) long life potential of the magnetron cathode and (4) high operational efficiency. Examples of results were an adequate range of current and voltage over which 20 dB of amplification could be obtained, spectral noise density 155 dB below the carrier, 81.7% overall efficiency, and potential cathode life of 50 years in a design for solar power satellite use.

A new fabrication method was used to fabricate a 64-slot, 30" square slotted waveguide array module from 0.020" thick aluminum sheet. The test results on the array are discussed.

1.0 INTRODUCTION

This report is primarily concerned with two different subjects. The first of these is an investigation of the magnetron as a directional amplifier with special attention being given to a number of characteristics that are of importance to its application to microwave power transmission. The second of these is the successful implementation of a new method of fabricating slotted waveguide modules from thin metal.

Although seemingly unrelated from a technology point of view, these two investigations are both key developments in reducing the estimated cost of the transmitting portion of the microwave power transmission system. The previous broad range in cost estimates and the conservative tendency to use the higher estimates have been an inhibiting factor in applying microwave power transmission technology.

The investigation has shown that the common microwave oven magnetron that is available as a shelf item at very low cost is suitable for most earth based transmitting arrays. Similarly, the approach to a low cost, slotted waveguide array that has been demonstrated under this contract has resolved a situation in which the range of estimated costs varied by a factor of as much as ten to one.

In addition, both of these investigations are related to the development of the solar power satellite. The magnetron investigation has indicated that a design suitably scaled in voltage and power from the microwave oven magnetron could probably be successfully incorporated into the SPS transmitter. The construction techniques involved in the fabrication of the thin metal slotted waveguide array and the resulting low mass meet the requirements imposed by the SPS transmitting antenna for mass and fabrication in space.

Because of their basically different nature and background the two new developments will be discussed separately. The magnetron directional amplifier will be discussed first.

It is believed that the proposed use of the combination of the microwave oven magnetron and a passive directional device in microwave power transmission systems was first made by Richard Dickinson of Jet Propulsion Laboratory in the 1974 to 1975 time period. At the time of the proposal the microwave oven magnetron had a reputation for being "much too noisy" for any application where its output would be radiated directly into free space. However, the author discovered in 1975 that when the tube was operated with a well-filtered DC power supply and without external filament power, the background noise level was very low. It was so low, in fact, that it could not be measured on the Hewlett Packard spectrum analyzer. In addition to the noise, other characteristics of the magnetron directional amplifier were also examined. A written report describing the results of the Kaytheon-sponsored investigation was distributed by the author in the summer of 1975.

There was little further investigation of the magnetron directional amplifier until the effort under this contract was initiated in the summer of 1978. One thing that had been done was to increase the sensitivity of the noise measurements by incorporating a notch filter to remove most of the carrier signal while permitting the remaining energy output of the magnetron to flow more directly into the spectrum analyzer. These measurements had indicated signal to noise ratios of as high as 160 dB/Hz at noise frequencies removed by 50 MHz or more from the carrier.

One of the first steps under the contract was to reduce the bandwidth of the notch filter so that background noise closer to the carrier could be examined. Although this arrangement was still limited in sensitivity and did not bring the noise level from the magnetron above the background noise level in the spectrum analyzer, the carrier to noise ratios were sufficiently high to justify a special effort to present the results to both Johnson Space Center and Marshall Space Flight Center who were concerned with the microwave generator for the SPS. These presentations were received with considerable interest. However, the

question was raised as to the expected life of such a tube, because the SPS application requires that the tube have a very long lifetime, measured in terms of twenty to fifty years.

As explained in the main text of this report, the ensuing investigation which was based in part upon visual examination of the cathode temperature in special tubes and in part upon the extensive literature on the carburized thoriated tungsten cathode indicated that the life could be very long indeed, perhaps as high as fifty years. In addition it is believed that this investigation was the first of its kind on a CW magnetron and has led to much new knowledge about the automatic control of its cathode temperature by backbombardment.

The investigation into the life of the cathode had not been anticipated at the inception of the contract. But most other aspects of the study dealing with the magnetron directional amplifier were anticipated. Harmonic noise measurements were made on the tube with the values being lower than had been anticipated. Measurements of added-phase-noise close in to the carrier were made and found to be low. Measurements of signal to noise ratio as a function of (1) current and voltage, (2) rf drive level and gain and (3) difference of drive frequency and free-running frequency of magnetron were made. Graphs showing the phase shift through the magnetron directional amplifier and power output as a function of voltage, current, and drive level were made. A special effort to obtain high efficiency that was accurately measured was made. An overall efficiency of 81.5% was obtained. The corresponding DC power to microwave power efficiency was estimated to be 87%.

The investigation of the approach to a low cost, slotted waveguide array based upon the use of thin sheet metal and a unique metal folding process was a completely different kind of activity. It had first been proposed as an approach to a low cost collector of microwave energy. In this format the proposed size would be about fifteen inches square. However, an opportunity arose to build a much larger slotted waveguide array based upon a JPL design. Although the 30 inch

square array that was designed and constructed could be used for the collection of energy, a much more likely use for it would be as a transmitting antenna.

The physical slotted waveguide array that resulted from this investigation was based upon the use of 0.020" thick aluminum. It was so rugged and strong as to immediately suggest that it could be made from 0.005" material. If this judgement is correct, the resulting structure could be used in the SPS satellite transmitter.

The information obtained under this contract, especially that having to do with the magnetron directional amplifier, is expected to have an important impact upon the design of the microwave power transmission system for the SPS. The high signal to noise ratio data, the efficiency data, and the data indicating long cathode life, are all of interest in the selection of the microwave generator for the SPS.

2.0 THEORY OF OPERATION OF THE MAGNETRON DIRECTIONAL AMPLIFIER

2.1 Introduction

An understanding of the operation of the magnetron directional amplifier may be approached from a number of points of view. First it should be made clear as to what constitutes a magnetron directional amplifier, and why it is called a magnetron directional amplifier rather than a locked oscillator or a reflection amplifier which would identify it better to most readers. It is called a directional amplifier to identify it with a larger class of crossed-field devices which exhibit the same behavior but which may be constructed differently. A directional amplifier is defined, as shown in Figure 2-1, as a two-port device that amplifies a signal injected in one port and accepts a signal in the other port but does not amplify it nor significantly attenuate it as it is transmitted internally to the other port.

There are basically two types of crossed-field directional amplifiers. One type requires the addition of passive devices with directional properties to achieve the overall performance. The other type does not require this but contains the directional feature as an inherent property of the device. The first type of device can also be broken down into two sub-classes - those using ferrite circulators as the passive directional device, and those using a 3 dB hybrid or a "Magic T" to obtain their directional property. Figure 2-2 summarizes these devices and shows how they are connected to the passive devices, if any, to form a component with two ports that interface with the outside world.

All of the devices shown in Figure 2-2 have been considered at one time or another for application to the SPS transmitter. The first device is the Amplitron device which needs no external passive device for its operation but which is handicapped by its relatively low gain, a mechanical complication of arranging two ports for the device, and a lack of detailed knowledge as to its signal to noise behavior.

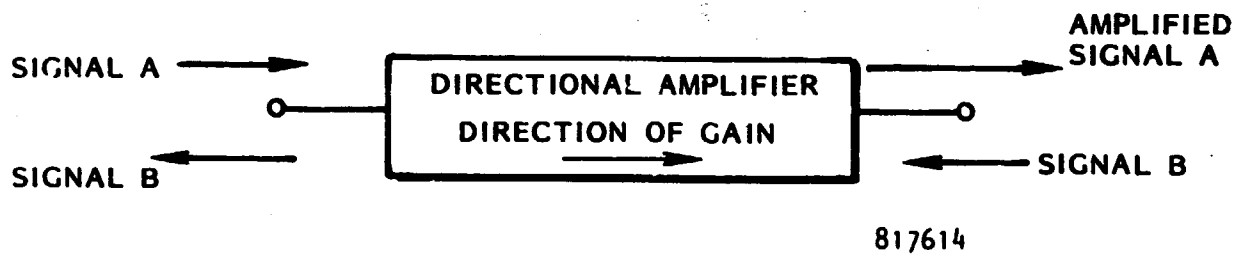
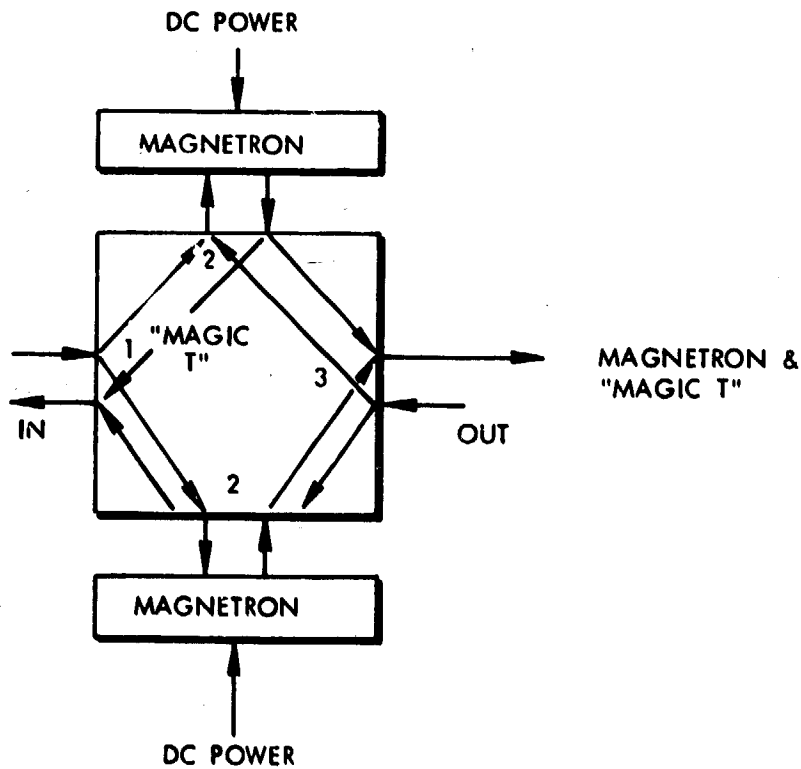
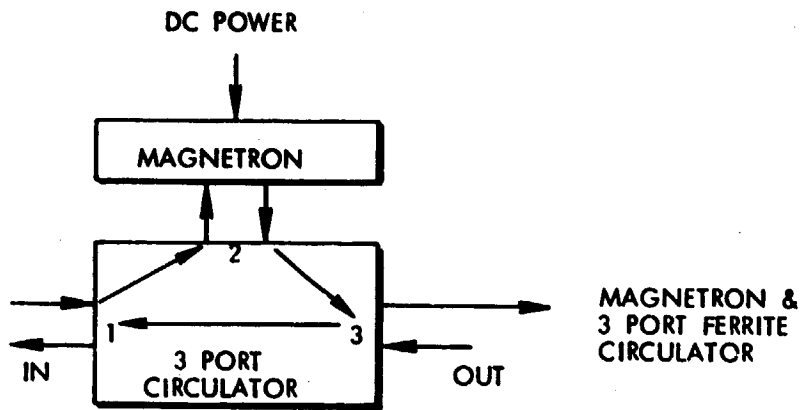
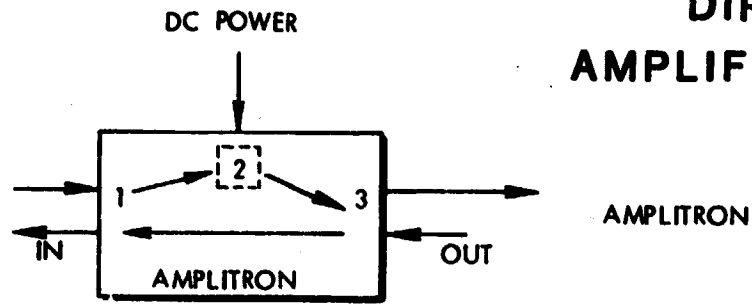


Figure 2-1. Gain Properties of Directional Amplifier.

DIRECTIONAL AMPLIFIER APPROACH



967607

Figure 2-2. Directional Amplifier Approaches Utilizing Crossed Field Devices.

The amplatron, however, is able to operate over a broad range of frequencies, over all values of current and voltage up to its maximum power handling capability, and has relatively small phase shift caused by a variation of anode current. It has found wide use in applications such as radar where these properties are desirable.

The second directional amplifier device is the combination of a ferrite circulator and a single conventional magnetron oscillator to form a directional amplifier. This arrangement has a distinct advantage in the development period of microwave power transmission just ahead because it can utilize the conventional microwave oven magnetron which is efficient, readily available, low in cost, and which has been shown to have a very high signal to noise ratio that is adequate for most purposes. In addition, the magnetron directional amplifier has a considerable amount of gain: 20 dB is a number that is practical for many applications. For the SPS application it has the basic disadvantage that it uses a ferrite circulator which for several reasons does not appear to be compatible with the SPS environment in space. It also has a limited range of operation in terms of anode current and must have a phase comparator circuit and a control system which actuates some compensating phase shifter or other device to maintain the desired phase at the output of the tube. However, this has now been accomplished very satisfactorily, and does not constitute a basic problem in most applications.

The third directional amplifier device is the device that makes use of the Magic T or 3 dB hybrid. This device makes it possible to eliminate the ferrite circulator, which is a big advantage in the SPS application. It is necessary to use a pair of matched tubes, although analysis indicates that the tubes need not be necessarily well balanced. It has been successfully operated at JPL. Some thought now needs to be given to whether sensors at the output of each tube are necessary for tracking purposes, and how the sensing and control problems are impacted by the need to remove all solid state devices from the high temperature operating environment that surrounds the tube. These, of course, are problems only in a space application.

With respect to these three different directional amplifier devices, this report will deal exclusively with the approach combining the magnetron with the ferrite circulator.

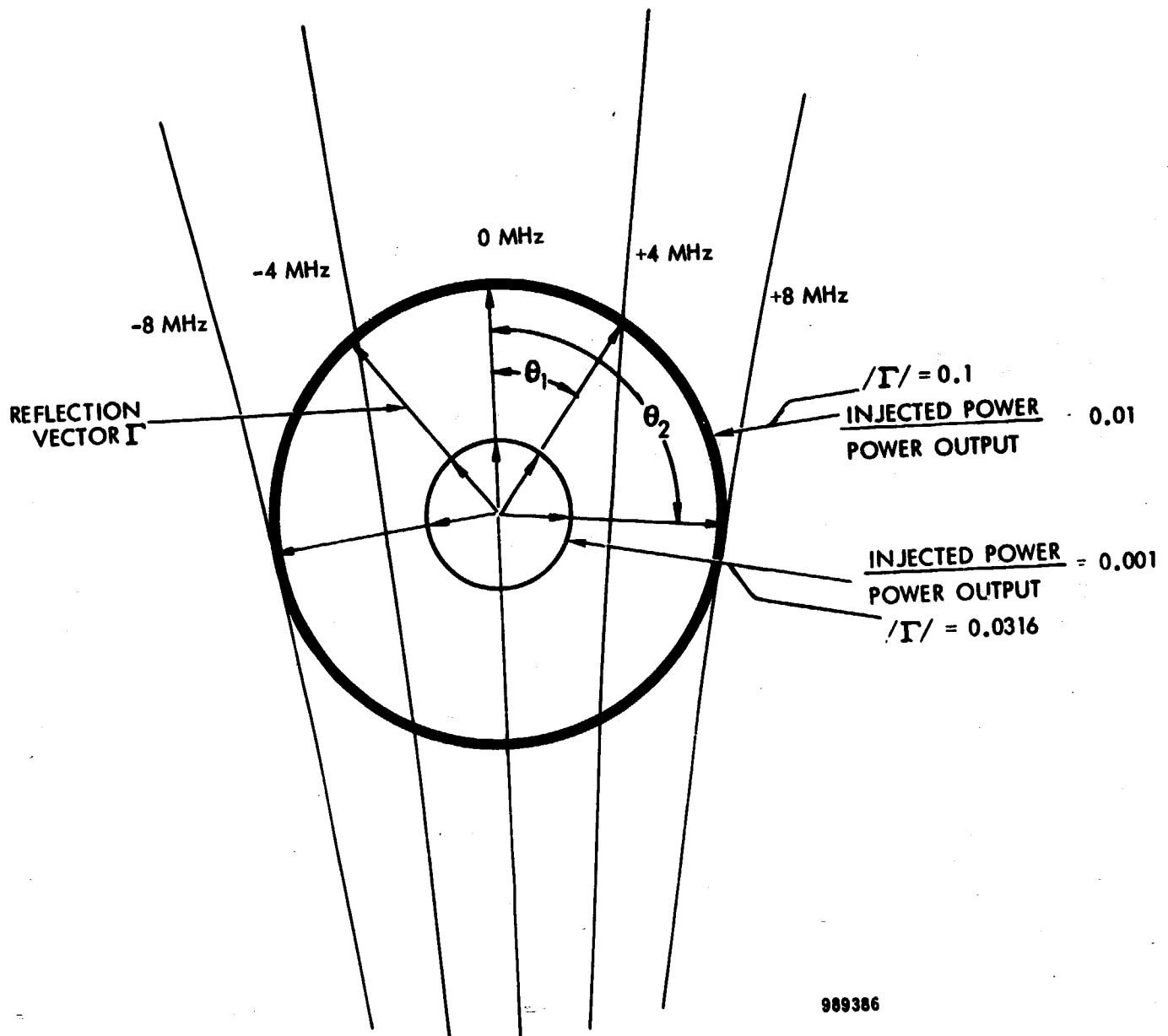
2.2 The Operating Properties of the Magnetron Directional Amplifier

An understanding of the operation of the magnetron directional amplifier may be approached either by setting down an equation for the interaction between two different sources, one of which is an oscillator and the other a fixed frequency source, or by analogy with how the magnetron oscillator behaves when it is coupled to the outside world, and its ability to distinguish between the reflection from a passive load and an injected signal. We will use the second approach first and then discuss the useful results of the theory.

The magnetron oscillator is connected to the outside world through a single port to which the load is connected. The free running frequency of the oscillator is changed by a reflection from the external load if this reflection is out of phase with the phase of the outgoing power. The expanded central portion of a typical load diagram is shown in Figure 2-3. The exact center of the load diagram of Figure 2-3 corresponds to a matched load and therefore to no reflection. As the load is varied from the matched condition, the reflection vector Γ changes and the frequency changes accordingly. Now the key point to the frequency control of the magnetron by an injected signal is that under steady state conditions the tube cannot distinguish between reflected power from the mismatched passive load and power which is injected into it from another source.

With this key point established, it is now possible to determine the phase of the output of the magnetron relative to the phase of the injected signal. The injected signal represents a reflection vector Γ whose magnitude is

$$|\Gamma| = \sqrt{\frac{\text{Injected Power}}{\text{Output Power of Magnetron}}}$$



989386

Figure 2-3. The central portion of the load diagram for a magnetron showing that the tube cannot distinguish between a reflection from a passive load and a signal of equal magnitude injected from another source. The tube adjusts itself to an injected signal by operating at the frequency of the injected signal and changing its output phase to accommodate the magnitude of the injected signal and the frequency difference between the injected signal and the free-running frequency of the magnetron.

One end of this vector must lie at the center of the load diagram while the other end must lie on a frequency contour corresponding to the difference in the frequency of the injected signal and the free running magnetron oscillator. If the frequency of the free-running magnetron and the frequency of the injected signal are the same there will be no phase difference between the injected signal and the output of the magnetron. If, however, there is a difference in frequency, the phase difference will depend upon that difference and also upon the magnitude of the reflection vector Γ represented by the injected signal.

To pursue this relationship further, refer to the large circle and the reflection vector associated with it in Figure 2-3. When the frequency of the external source is equal to the free running frequency of the oscillator, the phase shift is 0. If the frequency of the injected signal is now changed by 4 MHz, the associated phase shift in the output of the tube will be θ_1 . As the frequency is changed further to a maximum of 8 MHz θ will have increased to θ_2 . If the frequency is changed further the injected signal will not cause the magnetron to oscillate at a single frequency.

The phase shift through the magnetron directional amplifier as a function of difference between the frequency of the injected signal and the free running frequency of the magnetron is a characteristic of this kind of device. With small frequency differences the phase shift will be substantially linear with the difference. As the frequency difference increases, however, the phase change will become nonlinear, as is evident from Figure 2-3.

It is also evident that if the free running frequency of the oscillator should change for any reason while the drive frequency remains constant, there will be a phase shift associated with that change. Such changes in the magnetron occur principally as a result of a change in the anode current and to a lesser extent from changes in operating voltage and in changes of temperature. The latter changes the dimensions of the tube and therefore its frequency.

Figure 2-3 may also be used to illustrate how the frequency locking range varies with the amplitude of the injected signal. In Figure 2-3 the large dark circle is for an injected signal which corresponds to a reflection vector of 0.1, while the smaller circle corresponds to a reflection vector of 0.0316. The corresponding gains are 20 and 30 dB. The associated frequency locking range has decreased by a factor of 3.16.

With respect to the formal theory for the magnetron directional amplifier one of the best references is "Phasing of RF Signals" by E.E. David in Okress, Crossed Field Microwave Devices, Volume 2, Academic Press, 1961 pp. 375-399. This reference volume is available in most technical libraries. The useful results of the theory follow.

Defining ω_1 as the injected frequency and ω^1 as the oscillation frequency which ensues in the absence of the injected signal, David finds that there is a phase shift, ϕ , between the injected signal and the locked oscillator output signal which can be written.

$$\sin \theta = \frac{Q_E (\omega_1 - \omega^1)}{|\rho| \omega_0} \quad (2-1)$$

Here, $|\rho|$ is the square root of the ratio of the injected power P_i to the oscillator power P_o , and ω_0 is natural frequency of the cold magnetron internal structure.

The variable of greatest interest in this equation is Q_E , the external Q of the system which, in this case, reflects the degree of coupling of the magnetron to its load as given by the circuit efficiency.

ω depends on ω_0 , the load admittance and the electronic admittance. In the usual case of a signal injected into a magnetron via a three-port circulator, the load admittance approaches $1 + j0$. On the other hand, the electronic admittance is affected by operating current through the magnetron's pushing characteristics.

Under small signal conditions, ϕ varies from -90° to $+90^\circ$ in accordance with (3-1). The excursion in frequency is symmetrical about ω^1 and its amplitude is

$$\frac{\omega_o \sqrt{P_i/P_o}}{Q_E} \quad (2-2)$$

Returning to equation (2-1), it is interesting to examine the relationship between Q_E and the magnetron circuit efficiency, η_c , as follows

$$\eta_c = \frac{Q_o}{Q_o + Q_E} \quad (2-3)$$

where Q_o is the unloaded Q of the magnetron from (2-3)

$$Q_E = \frac{Q_o (1 - \eta_c)}{\eta_c} \quad (2-4)$$

Therefore,

$$|\omega_1 - \omega^1| \leq \sqrt{\frac{P_i}{P_o}} \frac{\omega_o}{Q_o} \left(\frac{\eta_c}{1 - \eta_c} \right) \quad (2-5)$$

In a magnetron designed for the SPS, ω_o would be fixed and Q_o would be maximized to achieve greatest efficiency. Hence, for a given locking gain P_i/P_o , the effect of circuit efficiency on attainable locking range is most important as shown by (2-5). Here, for example, we see that an increase of circuit efficiency from 87.5% (the normal value in an oven magnetron) to 92% can yield a 76% improvement of locking bandwidth. However, the pushing figure increases as the external coupling increases so that the range of anode current which the tube can be operated does not materially change.

3.0 GENERAL PERFORMANCE DATA ON THE MAGNETRON DIRECTIONAL AMPLIFIER

3.1 Introduction

The general performance data covered in this section have to do with the power output of and the phase shift through the magnetron directional amplifier as a function of operating anode current, anode voltage, level of microwave drive and coupling between the internal circuit of the tube and the load into which it operates.

Two classes of data were taken. In one class of data the performance of the tube is noted in terms of the frequency locking range as a function of anode current, anode voltage, and drive level. In the other class, the drive frequency was held constant and the power output from and the phase shift through the tube noted as a function of magnetron anode current and voltage. Several different drive levels were used and the range of current and voltage over which the tube operated was noted.

From a practical application point of view the most dominant feature of this data is that the range of anode current and voltage over which the tube can be operated is dependent upon the rf drive level. If, as in the SPS application, it is desired to operate the tube at a fixed frequency then the operating range in terms of anode current particularly and anode voltage to a lesser extent is determined by the level of drive. Although much would depend upon the nature of the application, it would seem that in most cases the operating voltage range would be somewhat restricted and that the major consideration would be the range of current and therefore both DC power input and microwave power output over which the tube would operate. In many cases an acceptable range of operation would correspond to a drive level that is 100 times less than the power output, or a gain of 20 dB.

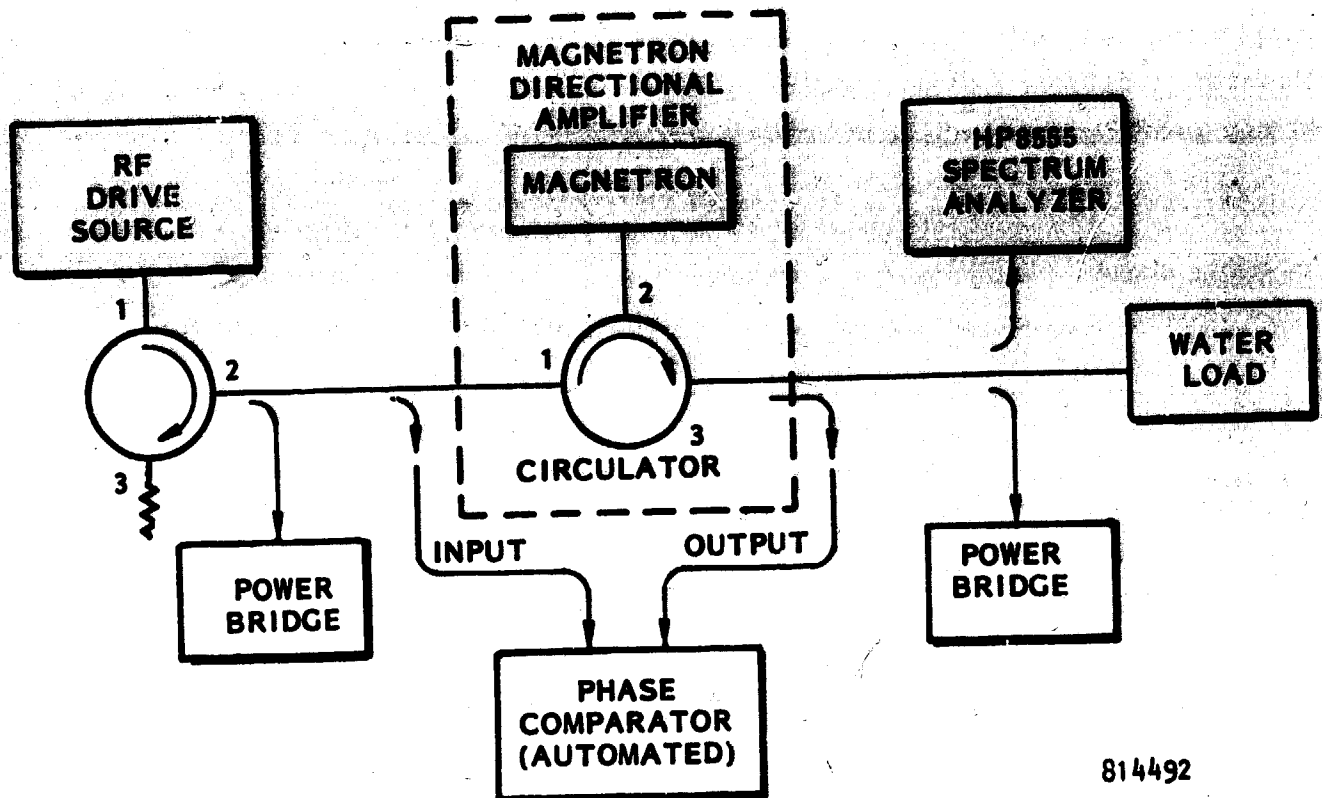
The dominating factor in limiting the range of operation is the frequency pushing characteristic of the tube when it is run as a free running oscillator. By frequency pushing is meant the change in frequency that occurs with a change in operating current. Frequency pushing is a basic property of the electronics within the tube. From a circuit point of view, the DC to microwave conversion mechanism contains within it a susceptance component which varies as a function of DC anode current and which is in parallel with the passive susceptance represented by the inductance and the capacitance of the cavities of the magnetron and the conductance and susceptance coupled in from the microwave circuit outside of the tube. With respect to the dominating influence of the pushing figure on the range of anode current, no improvement in the range of operation generally results from changing the coupling of the magnetron to the circuit outside the tube.

Although the frequency pushing figure is the dominant factor in limiting the range of operation at a given level of drive, other known factors such as the temperature of the magnetron anode, and such unknown but presumed factors as change in resonant frequency of the magnetron anode with life must be considered. These factors are made relatively less important in their impact upon the locking range by increasing the coupling of the magnetron to the external circuit. In our tests the coupling to the external circuit corresponded to an approximate value of the external Q_e of 60.

3.2 Phase Shift Through the Magnetron Directional Amplifier and Power Output of the Magnetron Directional Amplifier as a Function of Anode Current, Anode Voltage, and Level of Microwave Drive

The test arrangement for observing phase shift across the magnetron directional amplifier and the power output as a function of operating voltage and current is shown in Figure 3-1.

The tests were run at three different injected drive power levels at a frequency of 2450 MHz. The injected drive levels were 2.5, 10, and 25 watts.



814492

Figure 3-1. Test arrangement for observing phase shift across magnetron directional amplifier as a function of operating voltage and current.

Several magnetic fields were used for each drive condition. The set of magnetic fields gave a set of relatively flat voltage versus current curves that were widely separated from each other in voltage. At each drive and voltage level rf power output, current, efficiency and phase shift data were obtained. All but the efficiency information has been presented in Figures 3-2, 3-3 and 3-4. The efficiency information was left out because of the visual problem in reading the graphs with the efficiency data superimposed on the other two sets of data. However, efficiency may be readily calculated by simply dividing the power output at any point by the product of anode current and voltage at that point.

The general format of data presentation that is used will be recognized as being closely analogous to the manner in which magnetron performance data are often presented, that is, curves of a constant value of the parameter of interest against coordinate system of current and voltage.

Figure 3-5, which shows how the frequency of the free running magnetron oscillator varies as a function of anode current and voltage, has been added to show how closely these contours of frequency follow the contours of phase shift through the device when it is driven at a fixed frequency. There was no change made in converting to the free running case other than the removal of drive. The coupling of the tube to the external circuit remained the same.

The conspicuous difference in the data of the three figures 3-2, 3-3 and 3-4 are the ranges of current over which locked operation occurs and which depend upon the drive level. The quality of performance, however, in terms of efficiency, and signal to noise ratio do not change as a function of the drive level.

3.3 Frequency Locking Range of the Magnetron Directional Amplifier as a Function of Magnetron Anode Current and Voltage, and Level of Microwave Drive

This section looks at the frequency locking range of the magnetron directional amplifier as a function of several parameters. In terms of time sequence

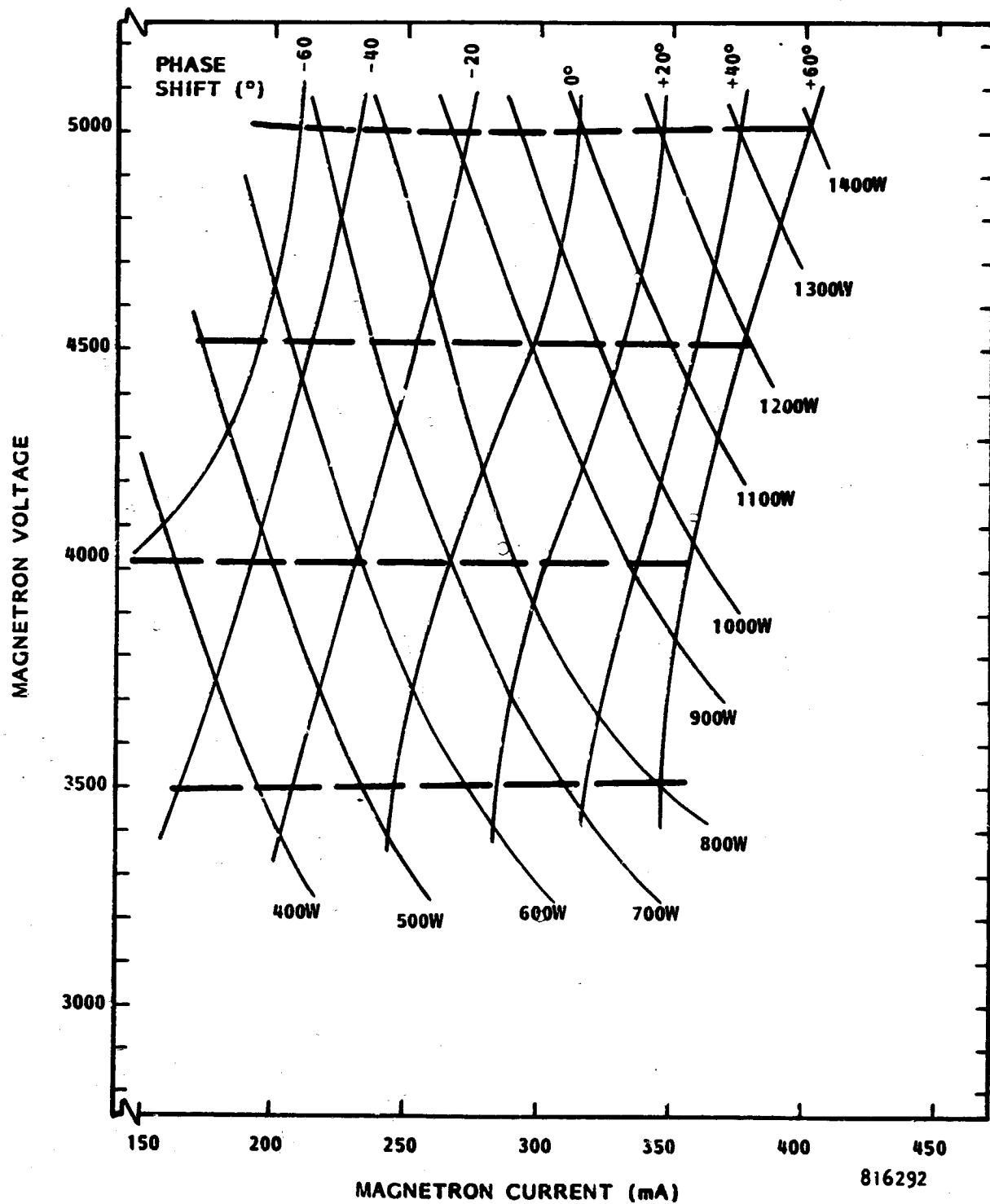


Figure 3-2. Curves of constant power output and phase shift as functions of magnetron directional amplifier voltage and current for drive power of 25 watts.

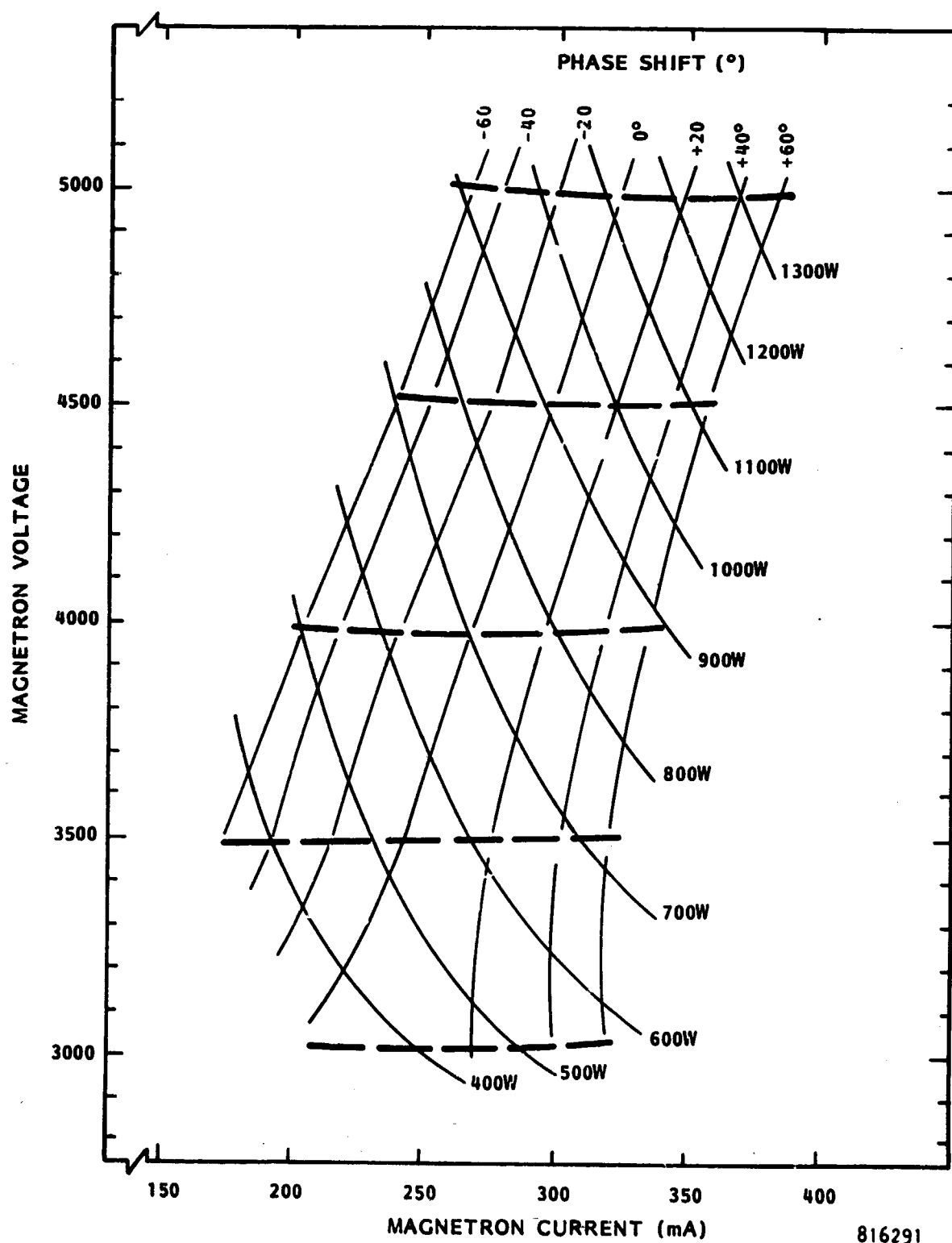


Figure 3-3. Curves of constant power output and phase shift as functions of magnetron directional amplifier voltage and current for drive power of 10 watts.

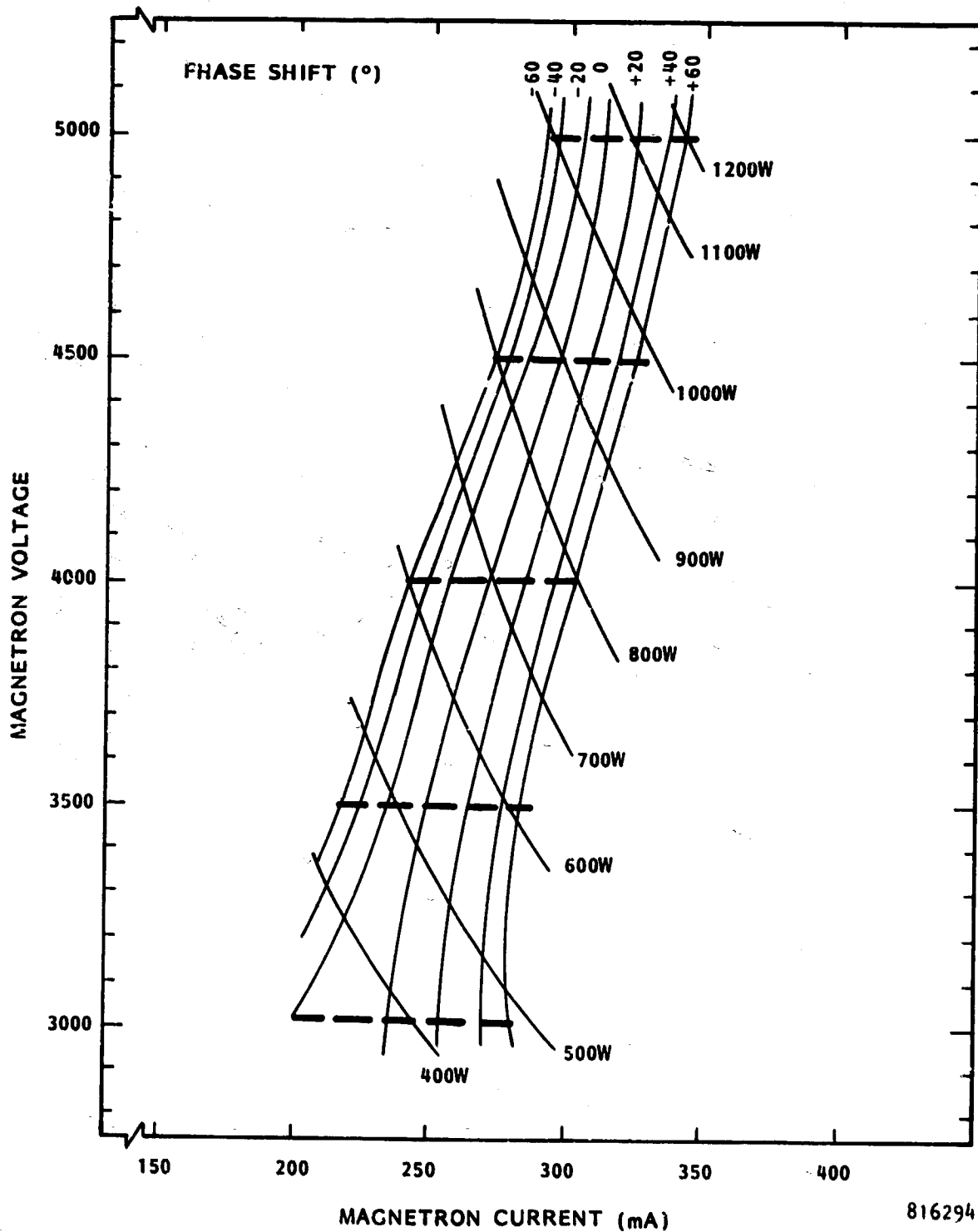


Figure 3-4. Curves of constant power output and phase shift as functions of magnetron directional amplifier voltage and current for drive power of 2.5 watts.

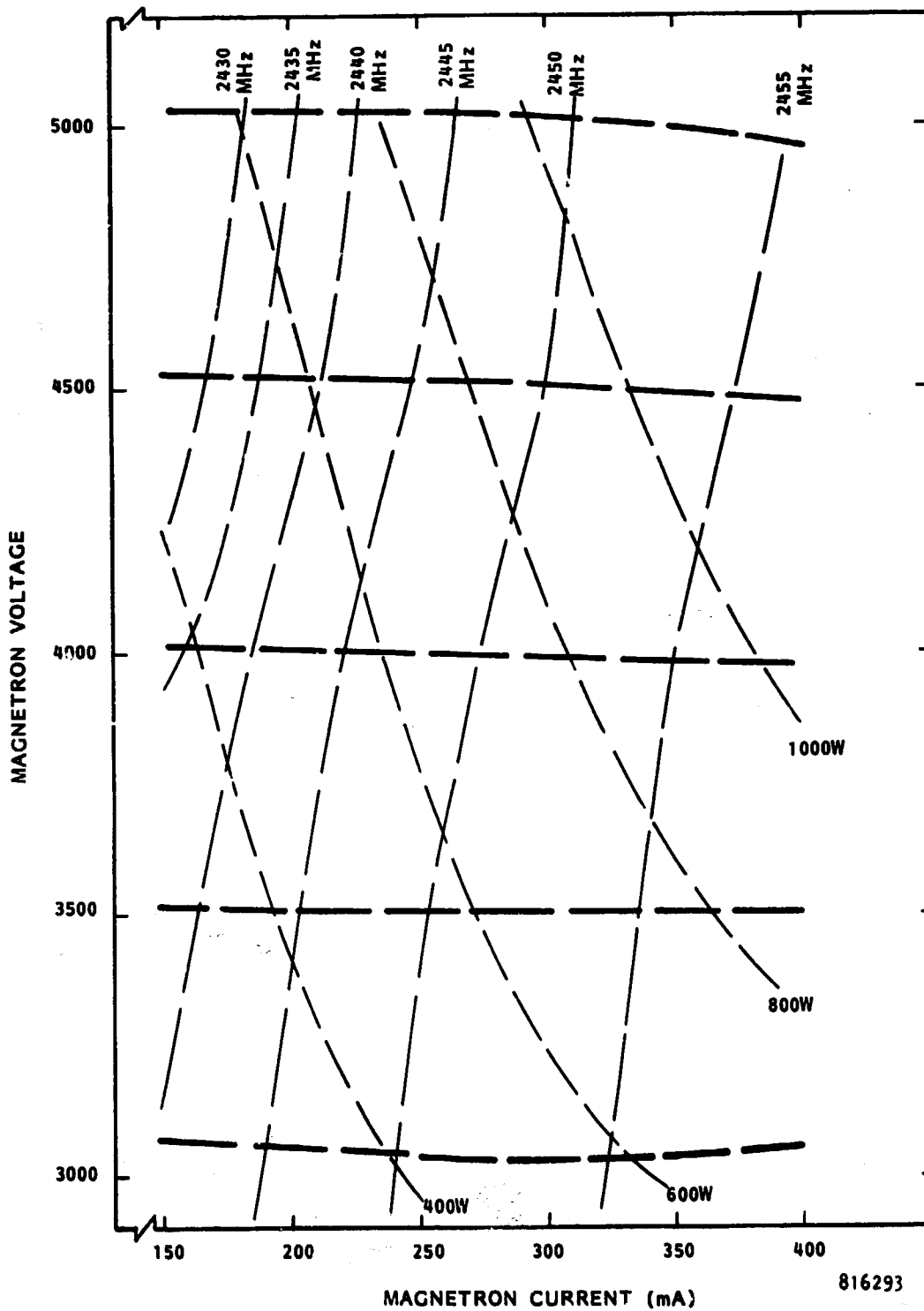


Figure 3-5. Curves of constant frequency and power output for undriven magnetron directional amplifier as function of voltage and current.

the data in this section were obtained prior to that in Section 3.2 and involved a slightly different set-up as shown in Figure 3-6.

In setting up the tube for the locking range test it was necessary to increase the coupling of the tube to the external circuit to increase the locking range for a given rf drive. The initial unadjusted coupling of the tube to the load produced a locking range that was considered insufficient. The small locking range would be expected from a consideration of the load diagram for a typical microwave oven magnetron in its normal application. An injected power level that is 20 dB below the output signal represents a reflection factor of 0.1 which would provide a locking range of only 6-7 MHz in the normally coupled tube.

Two means for increasing the coupling were available and used. First, the spacing between the short in the back of the coax to waveguide transition and the centerline of the tube's antenna was reduced. In addition a waveguide tuning screw was placed on the load side of the tube antenna and varied to adjust the conductance seen by the tube. In this manner the coupling was increased so that a locking range of from 17 to 20 MHz was obtained with the injection of 10 watts of power. The external Q corresponding to the locking range is approximately 60. However, the coupling arrangement had enough frequency sensitivity to affect some of the locking range data.

In addition to increasing the locking range, tighter coupling produces a higher circuit efficiency and therefore a higher overall operating efficiency of the tube.

Figure 3-7 shows the locking range for the magnetron directional amplifier with the readjusted coupling as a function of the injected power. The data was taken with an anode current of 250 milliamperes and thus the change in frequency of the tube as a function of current remained constant. The data was also taken for three different values of magnetic field and therefore anode voltage.

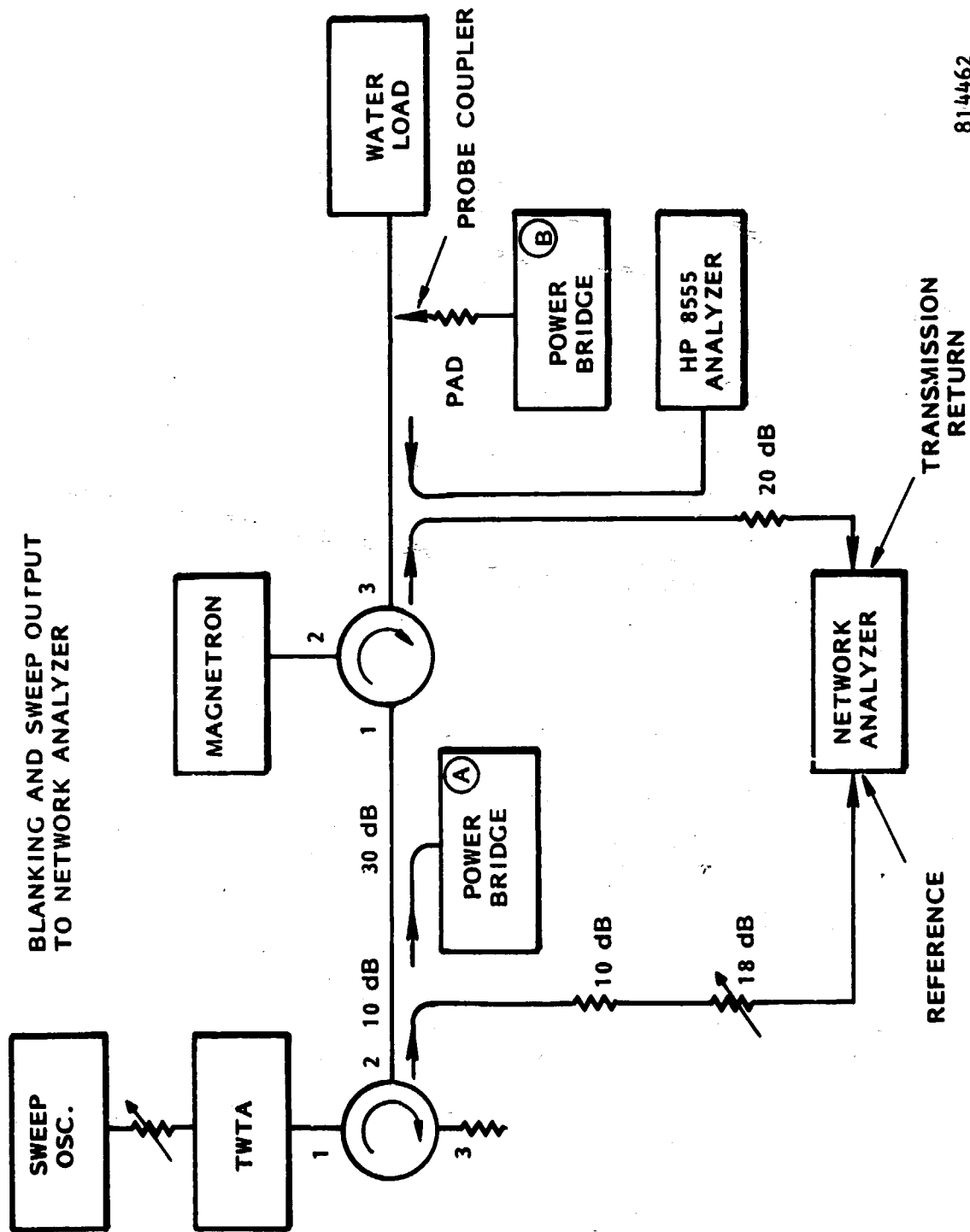
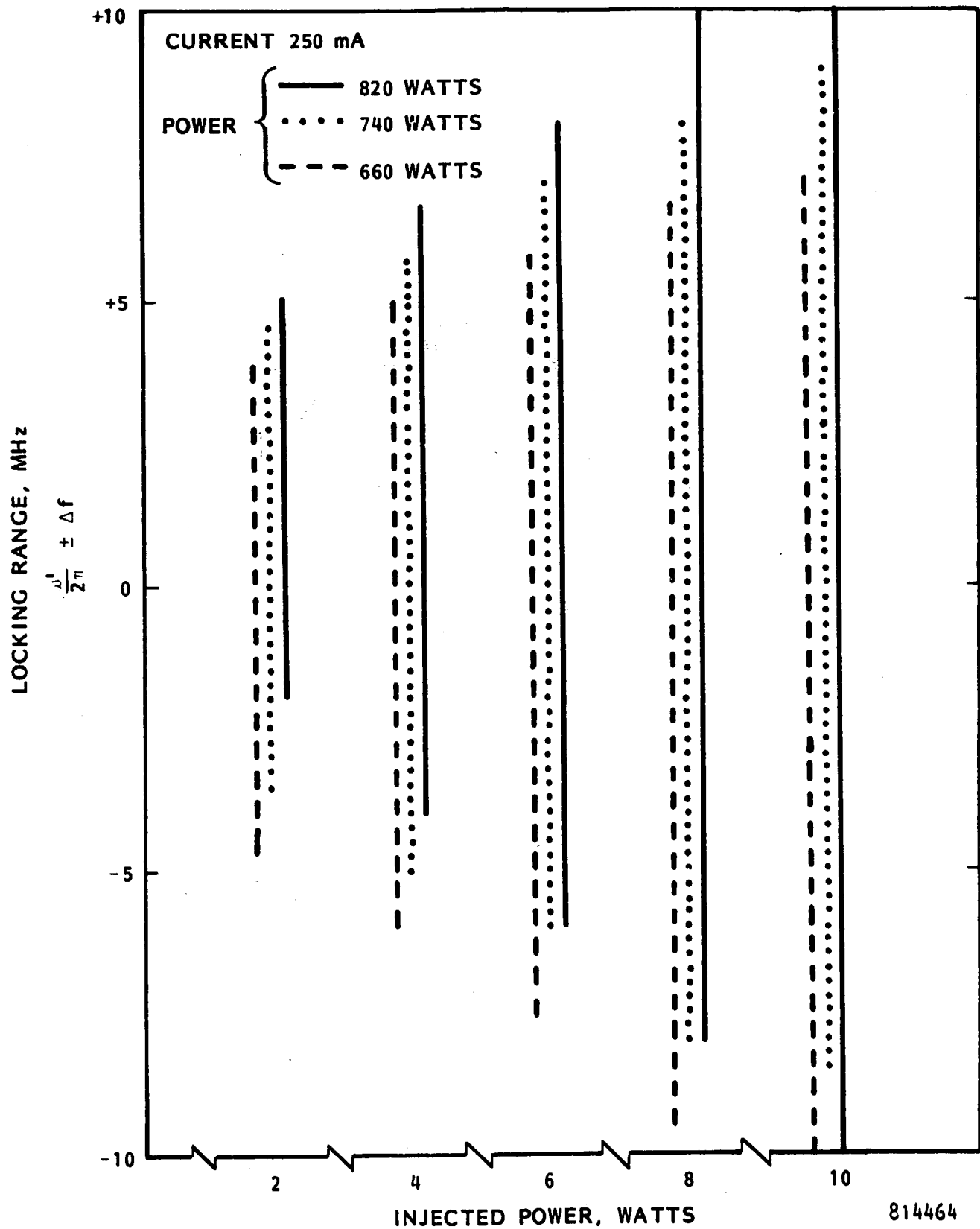


Figure 3-6. Simplified Test Setup Block Diagram.



814464

Figure 3-7. Effect of Injection Power on Locking Range.

The voltage levels were 3730, 4330 and 4860. There is some dependency of the free running frequency of the magnetron upon the value of operating voltage and this is shown in Figure 3-7 as an upward change in the frequency of the locking range associated with the higher operating power levels; the highest power output corresponds to the highest value of voltage.

The data indicate that the locking range is approximately proportional to the square root of the injected power which is predicted from theory.

Figures 3-8, 3-9 and 3-10 indicate how the locking range varies as a function of the anode current for three different values of anode voltage. These figures indicate the great influence that the pushing figure of the tube has upon determining the top and bottom frequencies of the locking range. The solid curve in the middle of the locking ranges is the frequency of zero phase shift through the magnetron directional amplifier as determined by a network analyzer placed around the directional amplifier is shown in Figure 3-6. The reference feed to the analyzer was adjusted in length so that the phase indication on the analyzer did not vary significantly with frequency when the magnetron directional amplifier was inactive. There was some variation which may explain in part why the solid line is not always at the center of the ranges but there was also some lack of symmetry in the behavior of the magnetron directional amplifier.

The decrease in locking range as the anode current is increased is explained in part by the reduced ratio of microwave drive to the microwave power output. However, this is not sufficient to account for all of it. No search was made for other causes.

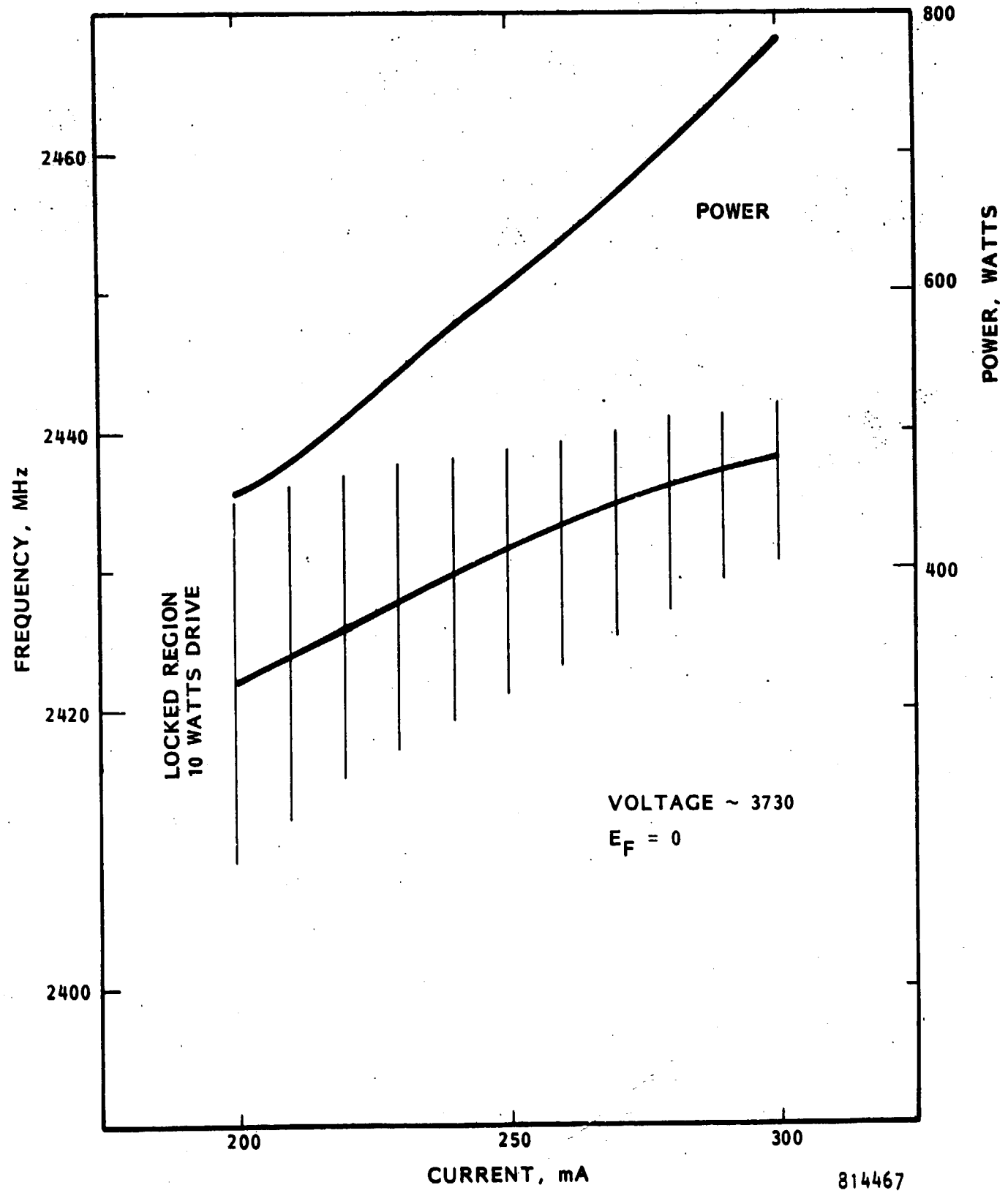


Figure 3-8, Locking Performance - Low Voltage Region.

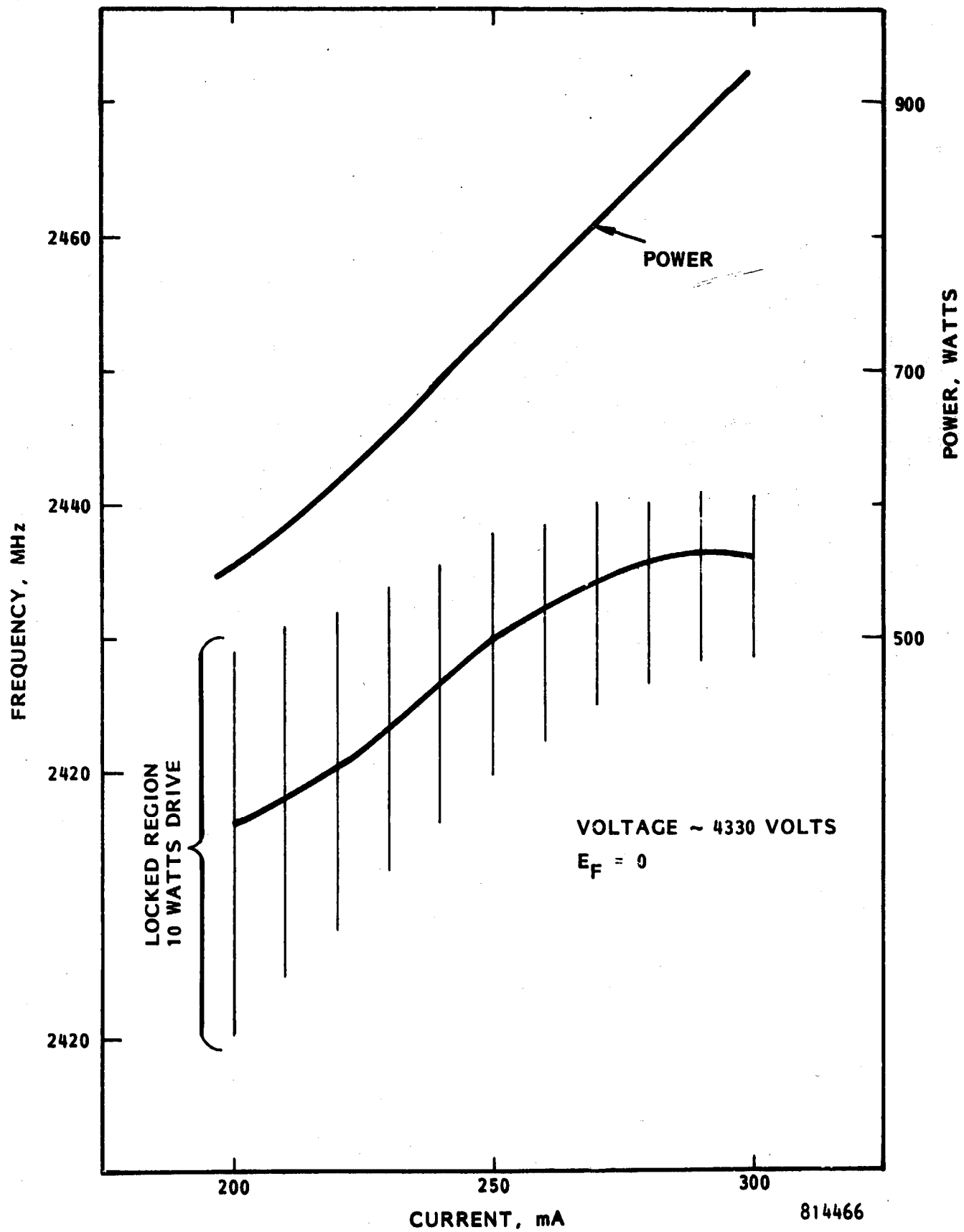


Figure 3-9. Locking Performance - Mid Voltage Region.

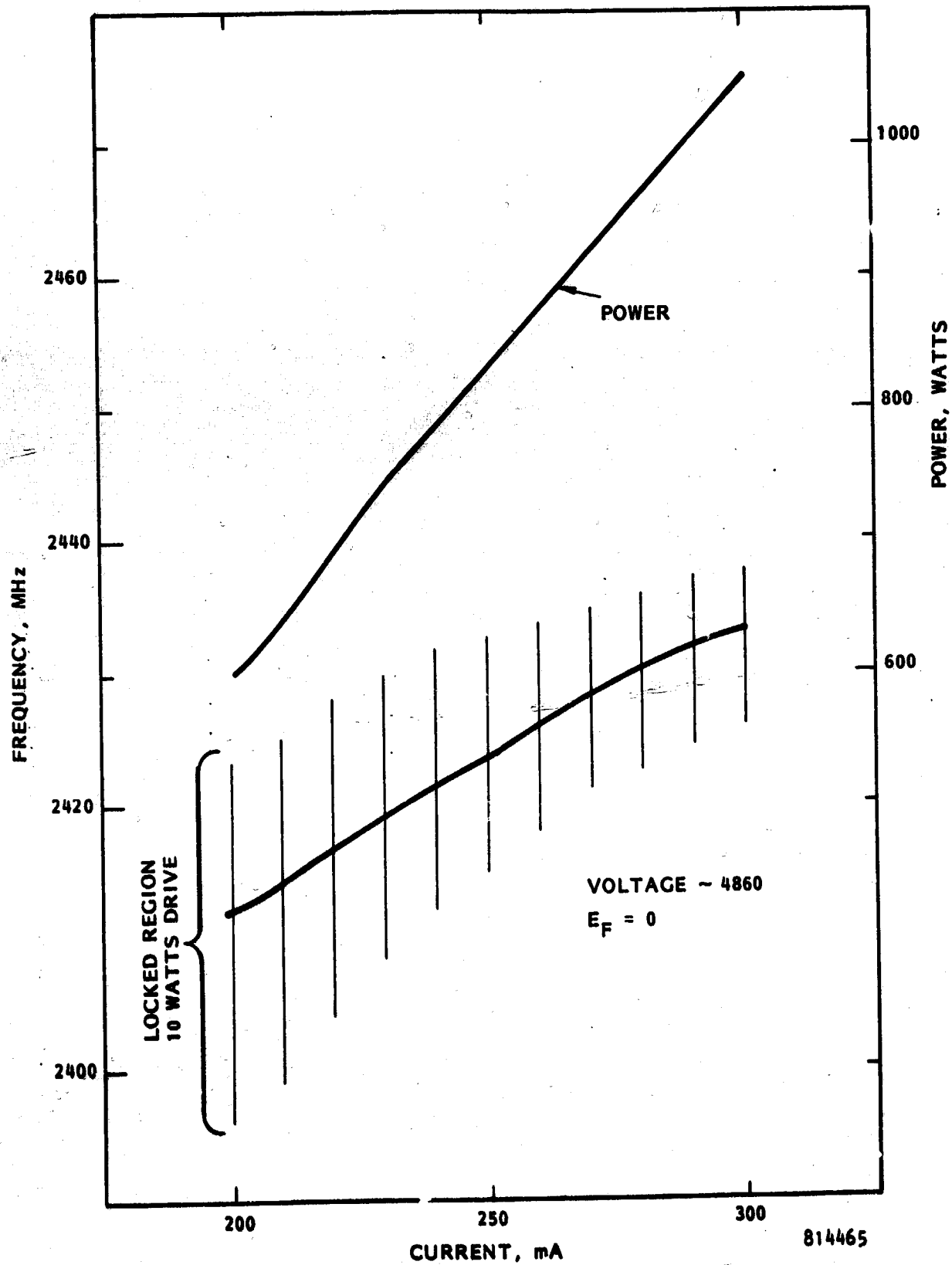


Figure 3-10. Locking Performance - High Voltage Region.

4.0 NOISE MEASUREMENTS ON THE MAGNETRON DIRECTIONAL AMPLIFIER

4.1 Introduction

The noise measurements that have been made on the magnetron directional amplifier are basically of three types: (1) measurement of background noise that is removed from the carrier signal by more than 10 MHz; (2) measurement of close-in phase modulation noise added by the magnetron directional amplifier to the driver; and (3) harmonic noise power.

The first of these types is of great concern to SPS because of the potential radio frequency interference which would occur over a large portion of the radio frequency spectrum if the level is high. But such background noise is of little concern in most applications of tubes so that data do not generally exist. Nor is it easy to obtain such data because the level of noise that would be injurious from the SPS point of view is far below the capability of the spectrum analyzer to measure while still admitting the carrier signal. The result is that special measurement setups must be made to reject almost all of the carrier signal that would normally reach the spectrum analyzer.

From the amplifier evaluation point of view it is desirable to see how this background noise varies as a function of voltage and current applied to the magnetron, of the level of rf drive, and of a change in drive frequency.

The close-in noise of the magnetron directional amplifier is of some interest, particularly in comparing it with other classes of tubes which are used for CW Doppler radar where the close-in noise is of importance.

Because of the nature of power conversion all microwave generators possess some harmonic output. Although the harmonic power may be relatively pure, it still represents a source of interference. In the SPS harmonic power is

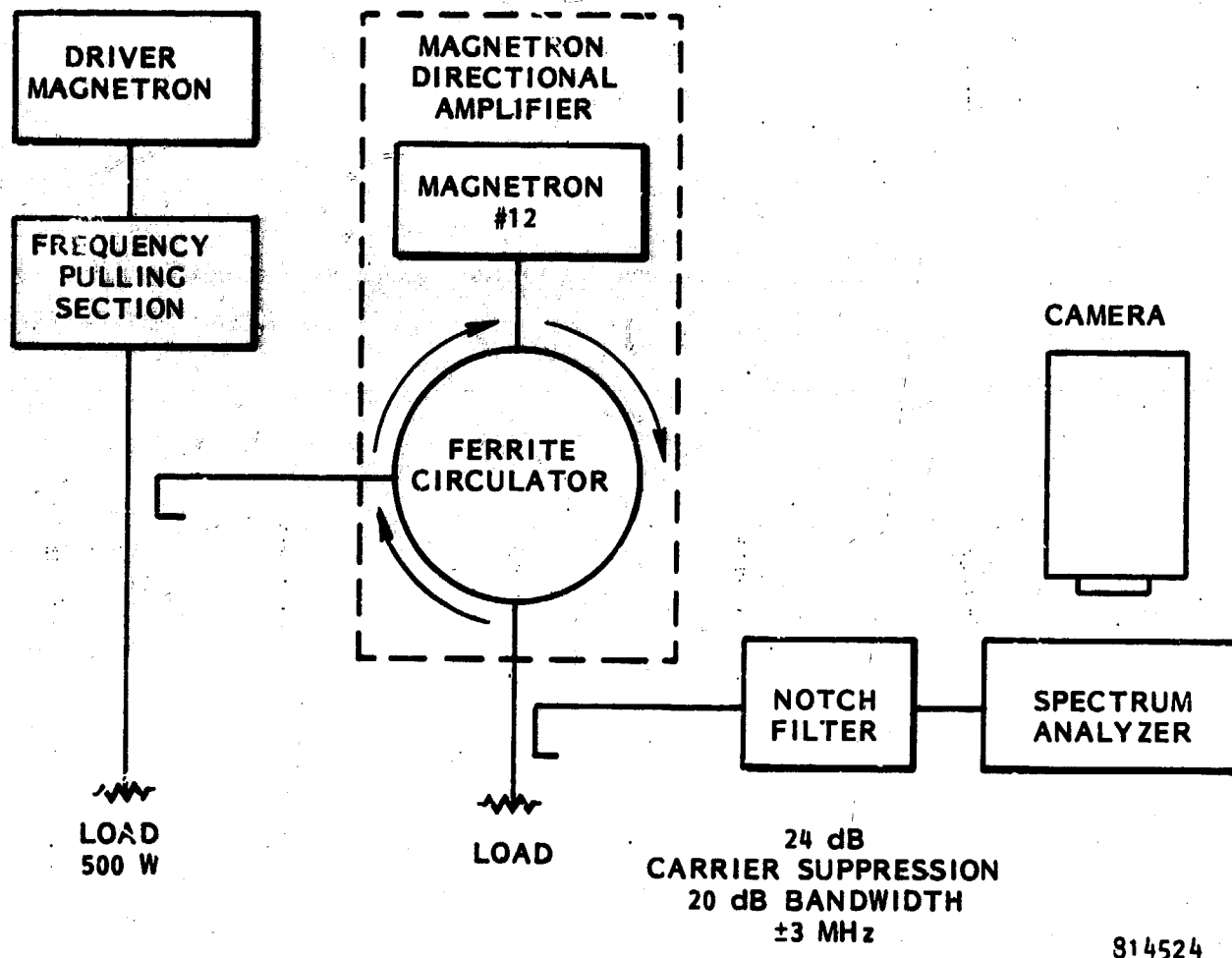
of major concern and quite possibly beyond the capabilities of engineering practice to remove without a great increase in mass and a great reduction in efficiency.

In reviewing the material in Section 4.2 on the level of the background noise, the reader should be aware that when the data that appear in this report were taken, the measurement of the background noise level was still limited by the test arrangement although at the time it represented a high degree of sensitivity because of a 25 dB suppression of the carrier by a notch filter that made it possible to obtain much useful data. More recently, the sensitivity of the test arrangement has been extended by another 35 dB which has revealed that the noise level is still very low if tubes are initially selected for relatively low noise and if certain changes that have been introduced into the cathode input circuit are adjusted for minimum noise. These recent measurements will not be discussed in this report but the reader should be aware that more recent material does exist. For example, signal to background noise ratio measurements of as high as 195 dB/Hz have been recorded from selected microwave oven magnetrons.

4.2 Background Noise as a Function of Operating Conditions

The measurement of background noise is in the form of carrier to noise ratio measurements. But since the carrier level is known it is possible to infer absolute values of the noise spectra. The major problem in making such noise measurements is that the carrier level saturates the input of the spectrum analyzer before the noise level becomes visible. The test arrangement approach to minimize this problem is to attenuate the carrier by means of a narrow notch filter.

The test setup that was used to obtain the data is shown in Figure 4-1. Because of the very high ratio of signal to noise that was being measured, it was necessary to use another microwave oven magnetron as a quiet driver



814524

Figure 4-1. Test Arrangement to Photograph Spectra of Microwave Output of Magnetron Directional Amplifier.

because the 10 watt traveling wave tube has a noise level that is much too high for such measurements. The driver magnetron was operated into a frequency pulling section and a matched load so that its frequency could be varied. A small fraction of the output power was coupled off for injection through the ferrite circulator to drive the magnetron directional amplifier.

The output from the magnetron directional amplifier was then sampled by a probe. The probe picked up several watts of power and was fed into a notch filter that suppressed the carrier by 24 dB. The bandwidth of the notch filter was very narrow, resulting in an attenuated signal of only 4 dB at two megahertz at either side of the carrier.

The signal to noise ratio measurements obtained from the test arrangement of Figure 4-1 were limited by the residual noise level of the spectrum analyzer. The residual noise level in a 300 kHz bandwidth which was used in the measurements was 103 dB down from the unsuppressed carrier level. The equivalent noise level in a 1 MHz bandwidth is 97.8 dB.

Figure 4-2 is a pictorial presentation of the spectral output of the magnetron directional amplifier as presented on the Hewlett Packard spectrum analyzer after the sampled output has been passed through the 24 dB notch filter to suppress the carrier, as a function of operating voltage and current. The total sweep presented on each photograph is 200 MHz. The flat portion of each spectra is the residual noise level of the spectrum analyzer. All of the photographs taken show that the noise level has reached this residual noise level at the edges of the 200 MHz band, except for those taken at 5 kilovolts. However, near the carrier there is a marked difference in the noise level as a function of the magnetic field (higher anode voltage). The cleanest spectra are seen to be at the lower values of magnetic field and at the higher current levels.

The "gauss lines", or the relationship between voltage and current at various values of magnetic field, are shown on Figure 4-2 and appear as nearly

SIGNAL TO NOISE AS A FUNCTION OF VOLTAGE AND CURRENT

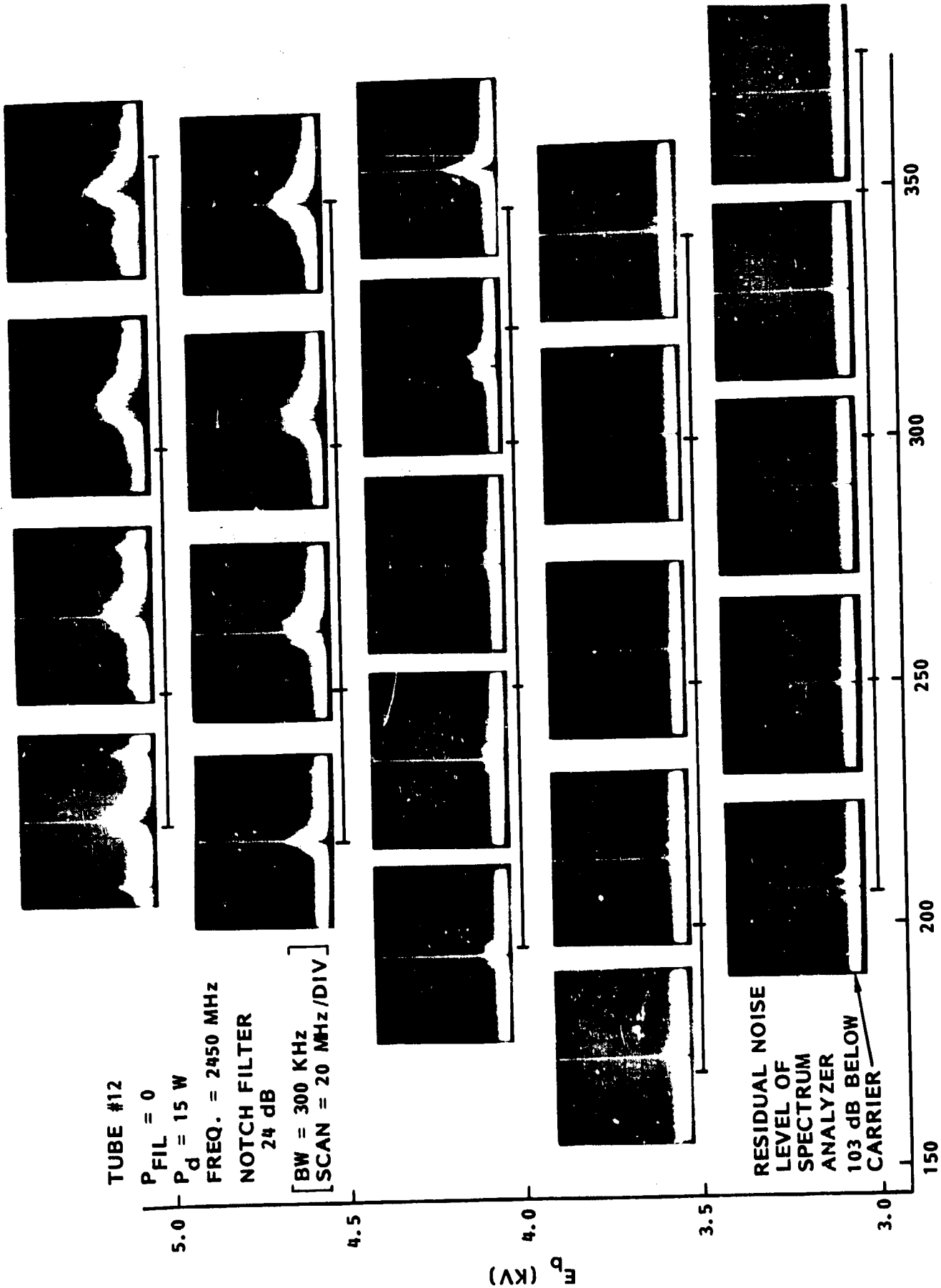


Figure 4-2.

horizontal lines. The values of current at which each spectra was taken is shown as a dot on the gauss line.

Complementary data with respect to power output and phase shift as a function of anode voltage and current in the magnetron directional amplifier are shown in Figure 3-3. The same tube and the same degree of coupling of the tube to the external circuit was used for the noise data as was used for the data of Figure 3-3.

Figure 4-3 is a pictorial presentation of the spectral output of the magnetron directional amplifier as a function of the driver frequency, at two values of magnetic field and voltage and at a fixed anode current of 300 milliamperes, and at a drive level of 10 watts. It is observed that the spectra are impacted to only a minor degree by a change in the driver frequency. The spectra are shown for total frequency sweeps of 200 MHz and 50 MHz.

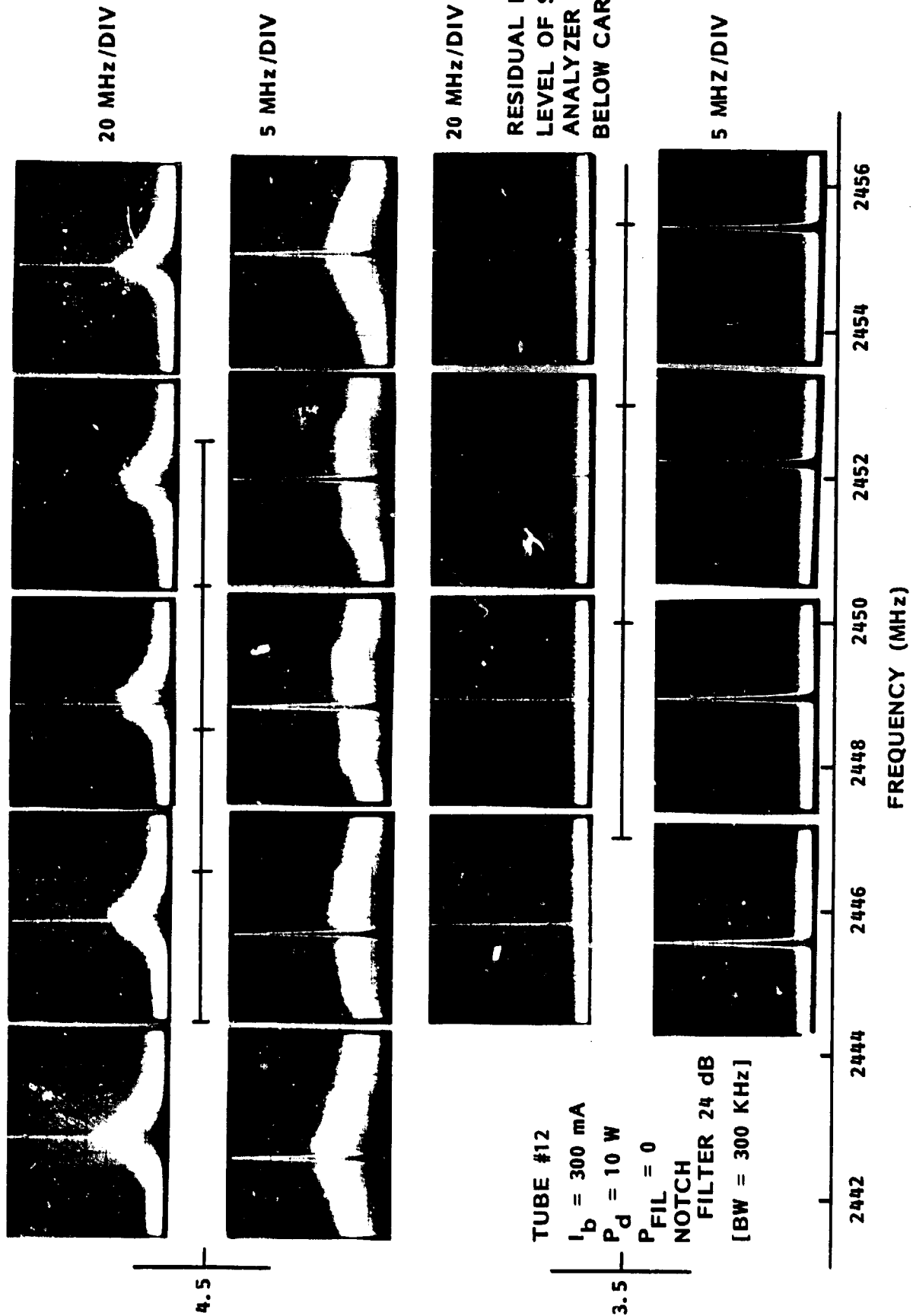
Figure 4-4 is a pictorial presentation of the spectral output of the magnetron directional amplifier as a function of the drive level for two voltage levels. Again it is noted that the spectral output changes little even when the gain is approximately 30 dB. One photograph was taken of the spectra of the tube running without drive, or as an oscillator. It is seen that the spectra are not different from those for all of the driven examples.

The lack of sensitivity of the noise spectra to changes of drive frequency and values of gain are to be expected from the fact that at reasonably high values of gain the tube looks into a load that is very close to the matched load point as noted in Section 2.0.

4.3 Phase Modulation Noise Added by the Magnetron Directional Amplifier

The noise that is emitted by the magnetron directional amplifier outside of the ISM band is of primary importance in the context of interference

SIGNAL TO NOISE AS A FUNCTION OF FREQUENCY DEVIATION



PT-5613

Figure 4C3.

SIGNAL TO NOISE AS A FUNCTION OF DRIVE LEVEL

TUBE #12
 FREQ. = 2450 MHz
 PFIL = 0
 NOTCH FILTER 24 dB
 [BW = 300 KHz
 SCAN 20 MHz/DIV]



20 W



10 W



5.0 W



2.5 W



UNDRIVEN

4.5

(A) E_p (KV)
 4-8



20 W

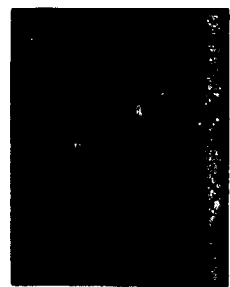
RESIDUAL NOISE LEVEL
 OF SPECTRUM ANALYZER
 105 dB BELOW CARRIER
 T-5613



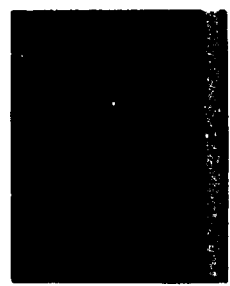
10 W



5.0 W



2.5 W



0.6 W

$P_o = 890 W$ $I_b = 300 mA$

DRIVE LEVEL

Figure 4-4.

ORIGINAL PAGE IS
 OF POOR QUALITY

with other users of the frequency spectrum. But it is also important to determine the level of noise that is in close to the carrier to enable a comparison to be made of the magnetron directional amplifier with other amplifiers. The data may also be of practical significance in the study of noise mechanisms within the crossed-field device and it may be important in the context of interference with the pilot beam uplinks in the SPS that may be relatively close to the carrier (power transmit) frequency. The noise around the harmonics caused by the close-in noise around the carrier may also be a consideration.

The close-in noise added by the magnetron directional amplifier is either of an amplitude modulated or phase modulated type. The aspect with which this section is concerned is the added phase modulation.

The close-in phase modulation noise in the magnetron directional amplifier was measured with special equipment loaned to the project by a specialist group in Raytheon that makes specialized equipment for measuring close-in noise. This equipment is used, for example, in qualifying tubes for CW doppler radar applications. Typical data obtained from the Raytheon CNS-10 analyzer for Phase Modulation Noise from a klystron are shown in Figure 4-5. For our measurements the noise measuring equipment was inserted into the test arrangement for the magnetron directional amplifier as shown in Figure 4-6.

Figure 4-7 shows how the noise data were presented and the measured results. Figure 4-7a shows the presentation on the scope with the magnetron directional amplifier not operating. The presentation on the scope is the residual noise level of the measuring equipment. The linear horizontal scale covers a frequency range of 0-100 kHz in 10 kHz steps. The vertical scale is in grid steps of 10 dB. The bandwidth of the receiver is 1 kHz so that the noise is integrated over a 1 kHz bandwidth.

In Figure 4-7b the presentation is with the magnetron directional amplifier operating and inserting additional phase modulation noise. Figure 4-7c is a superposition of Figures 4-7a and 4-7b.

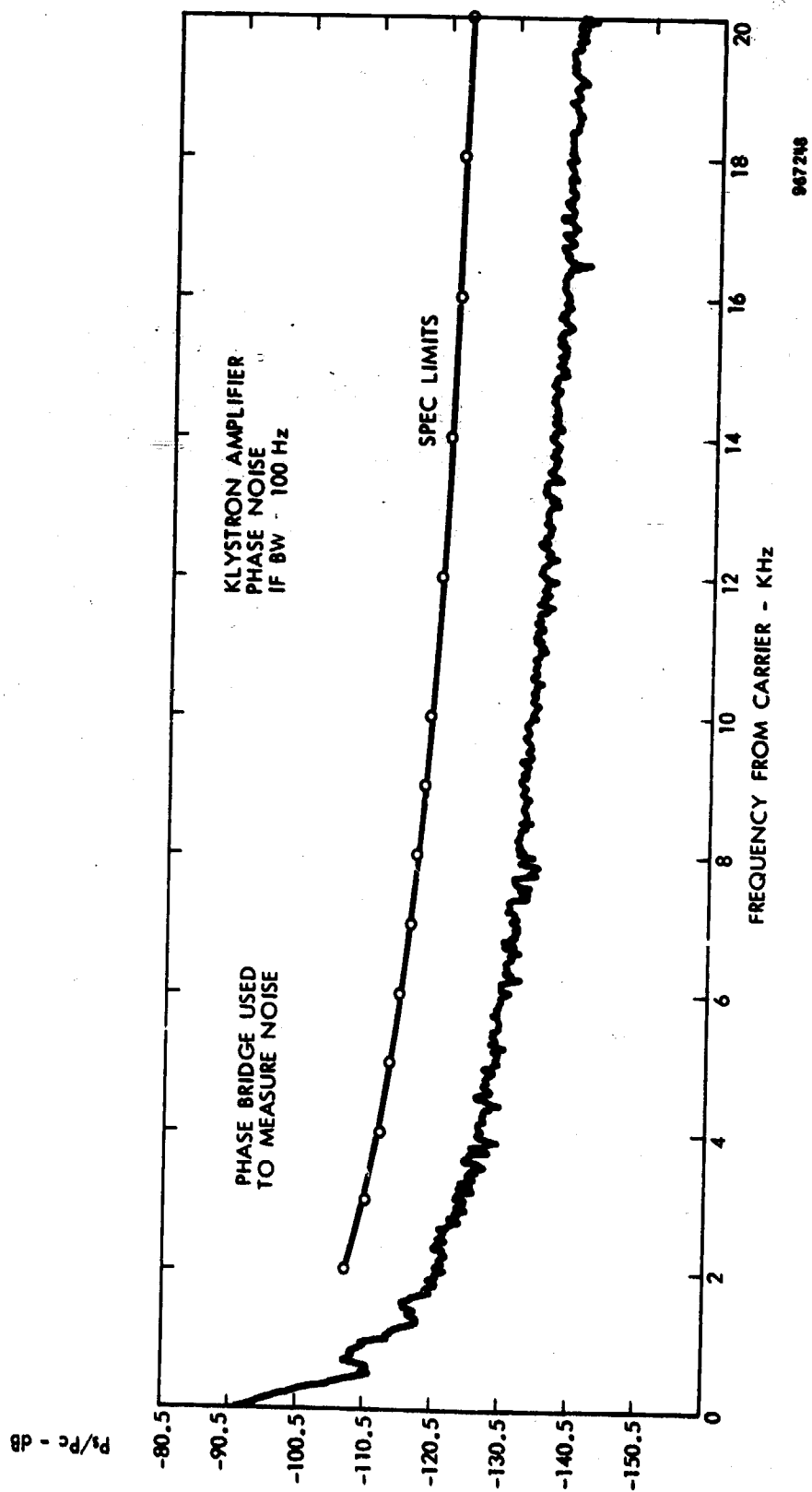
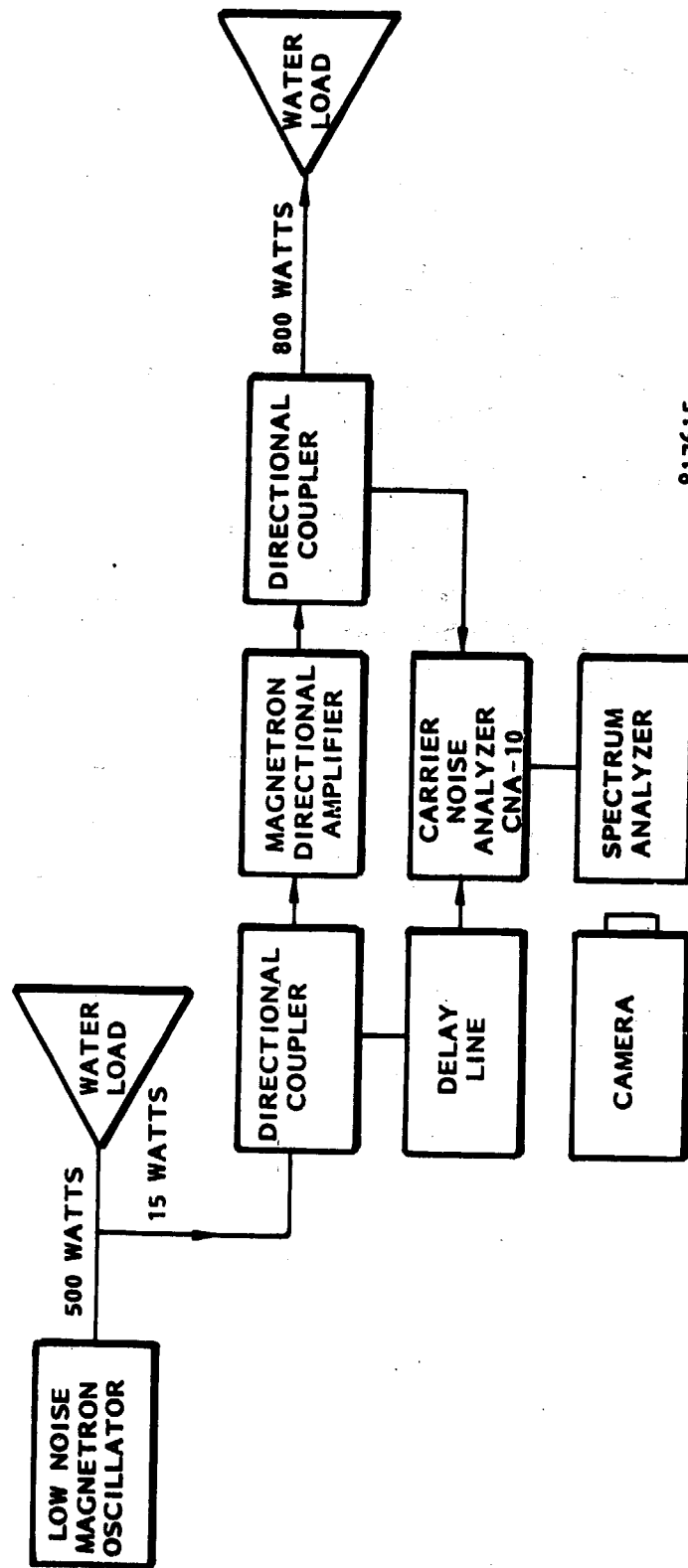


Figure 4-5. Typical data obtained from CNA-10 Analyzer for Phase Modulation Noise.



817615

Figure 4-6. Test Arrangement for Measuring Close-In Phase Modulation Noise Added by the Magnetron Directional Amplifier.

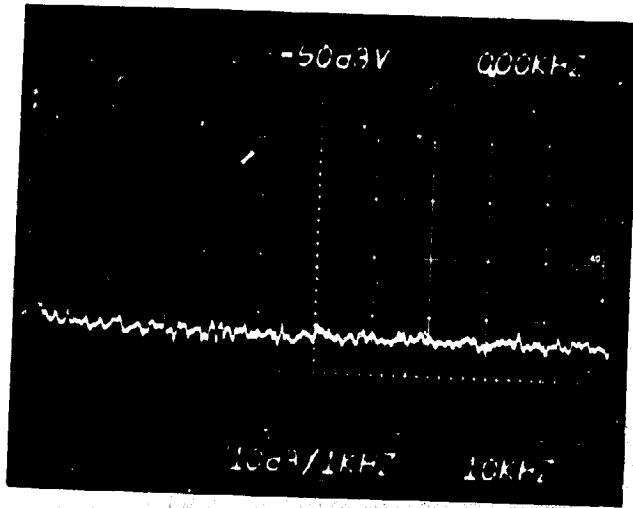


Figure 4-7a.

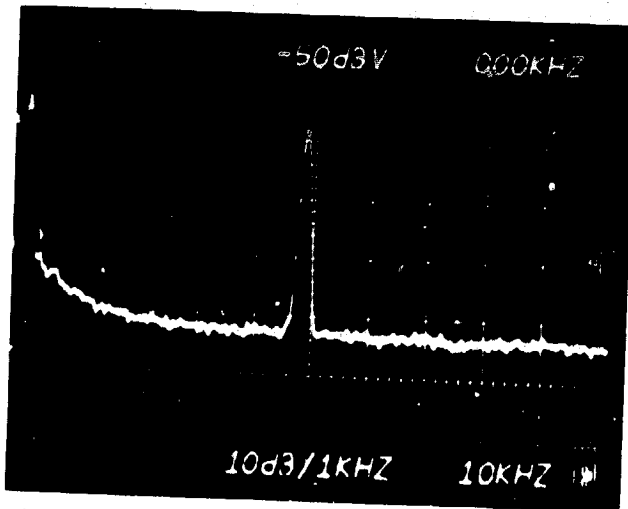


Figure 4-7b.

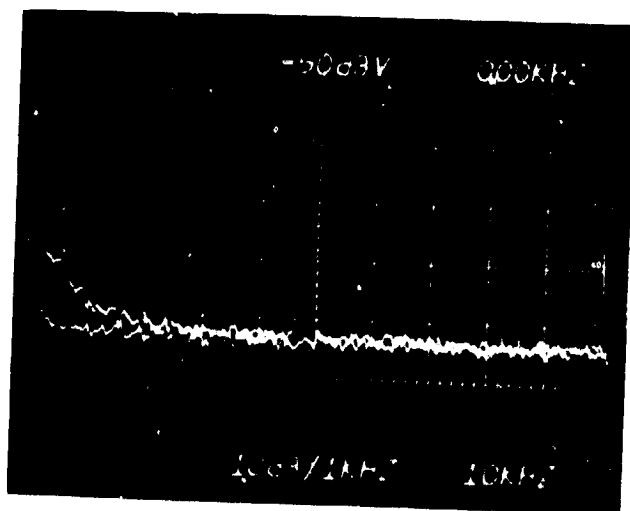


Figure 4-7c.

ORIGINAL PAGE IS
OF POOR QUALITY

Figure 4-7. Measurements of close-in phase modulation noise added by magnetron directional amplifier. See text for detailed explanation.

Both Figures 4-7b and 4-7c show a calibrating signal on the figures at approximately 50 kHz. This calibrating signal is down 80 dB from the carrier. It corresponds to a phase deviation of 0.01146 degrees which is established from the mathematical sideband level relationships for small-phase-deviation phase modulation.

The top oscilloscope trace in 4-7c, representing the noise level while the magnetron directional amplifier is operating, is 34 dB below the calibrating signal or at a noise level in a 1 kHz bandwidth that is 114 dB below the carrier. The noise contributed by the magnetron directional amplifier will be less than this value because there is a considerable contribution to the noise shown by the upper trace from the residual noise of the test equipment.

At 10 kHz the two traces are clearly separated and it would be accurate to state that the noise level in a 1 kHz band at this point is 110 dB below the carrier level. At 5 kHz the noise level in a 1 kHz band is 100 dB below the carrier level. At the close-in level the ripple of the power supply is becoming a factor that adds to the noise level.

These close-in noise measurements were made with the external source of power to the filament turned off and were made in the normal operating range for the magnetron, as shown in Table 4-1. The carrier to noise ratio for the background noise well removed from the carrier under the same operating conditions would correspond to that shown in Figure 4-3.

In summarizing the close-in noise measurement activities it is concluded that enough measurements were made to indicate that the magnetron directional amplifier adds a very small amount of phase modulation noise but would be quite suitable for most CW doppler radar applications, for example. It is not quite as good as the example for the klystron shown in Figure 4-5. (Note the 100 Hz

TABLE 4-1
Data and Operating Conditions
for the Magnetron Directional Amplifier

Magnetron Used	-	Hitachi 2M170
RF Drive Level	-	20 Watts
RF Output Level	-	710 Watts
Magnetron Anode Voltage	-	3531 Volts
Magnetron Anode Current	-	0.357 Amperes
Efficiency	-	61.5%
Frequency	-	2437 MHz

bandwidth for the klystron data when comparisons are made). It is also noted that the residual noise level of the equipment had not been tuned down to the level that would be required for the noise measurements shown in Figure 4-5.

4.4 The Measurement of Harmonic Power Levels

4.4.1 Introduction

A portion of the contractual work effort was directed toward measurements of the 2nd, 3rd, 4th and 5th harmonic output from the magnetron directional amplifier. The distinction between these measurements and those made at JPL on the magnetron were in the measurement approach. Those made at JPL were made by using special measuring equipment after the harmonic power had entered the waveguide system. Those reported upon in this section were made with the harmonic power remaining in a coaxial line system.

Ordinarily, the coaxial output of the magnetron is operated as a probe, injecting power into WR430 or other S-band waveguide, but at harmonic frequencies such waveguides will support higher orders of propagation relative to the fundamental TE_{10} mode. Fortunately the construction of the QKH2000 magnetron lends itself to a simple external transition to standard 7/8" rigid coaxial line. This line will only support a simple TEM mode of propagation for the lower harmonic frequencies, and will launch the energy into the coaxial line to preferentially excite the TEM mode of propagation for the higher harmonic frequencies.

The 7/8" line can readily handle the normal rf output of the tube. A cross sectional sketch of the transition is shown in Figure 4-8, while Figure 4-9 is a photograph of the assembly. The coaxial coupling arrangement gives values of coupling to the 50 ohm coaxial line that are comparable to those commonly used in coupling the probe to a waveguide system. The measured Q_L , Q_E and Q_U were 169, 220 and 735, respectively.

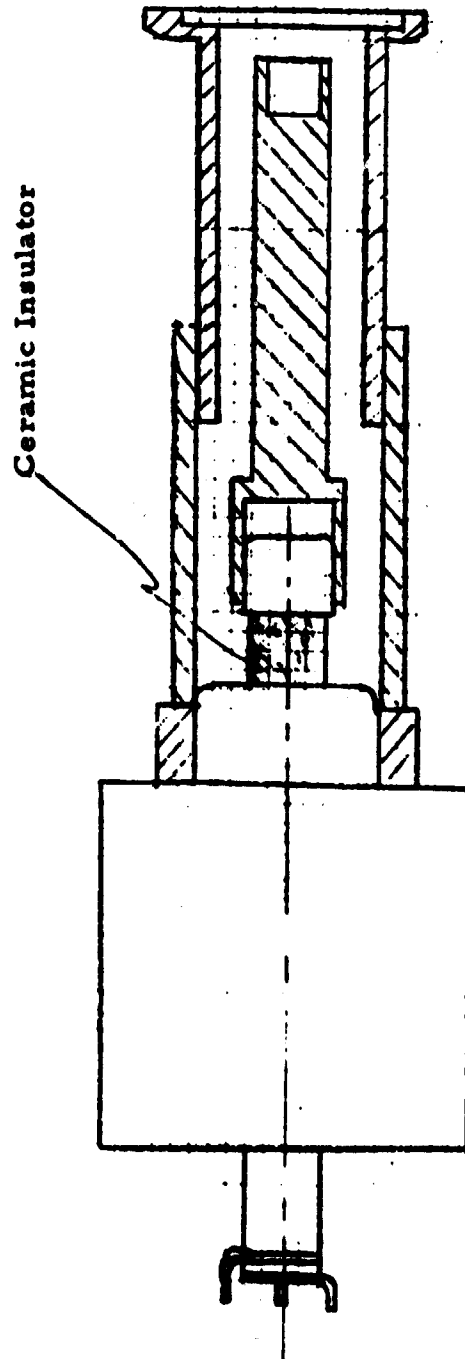


Figure 4-8. Direct transmission of QKH2000 Magnetron directly to 7/8 inch coaxial line. Transition arrangement preserves the normal external coupling of the tube.

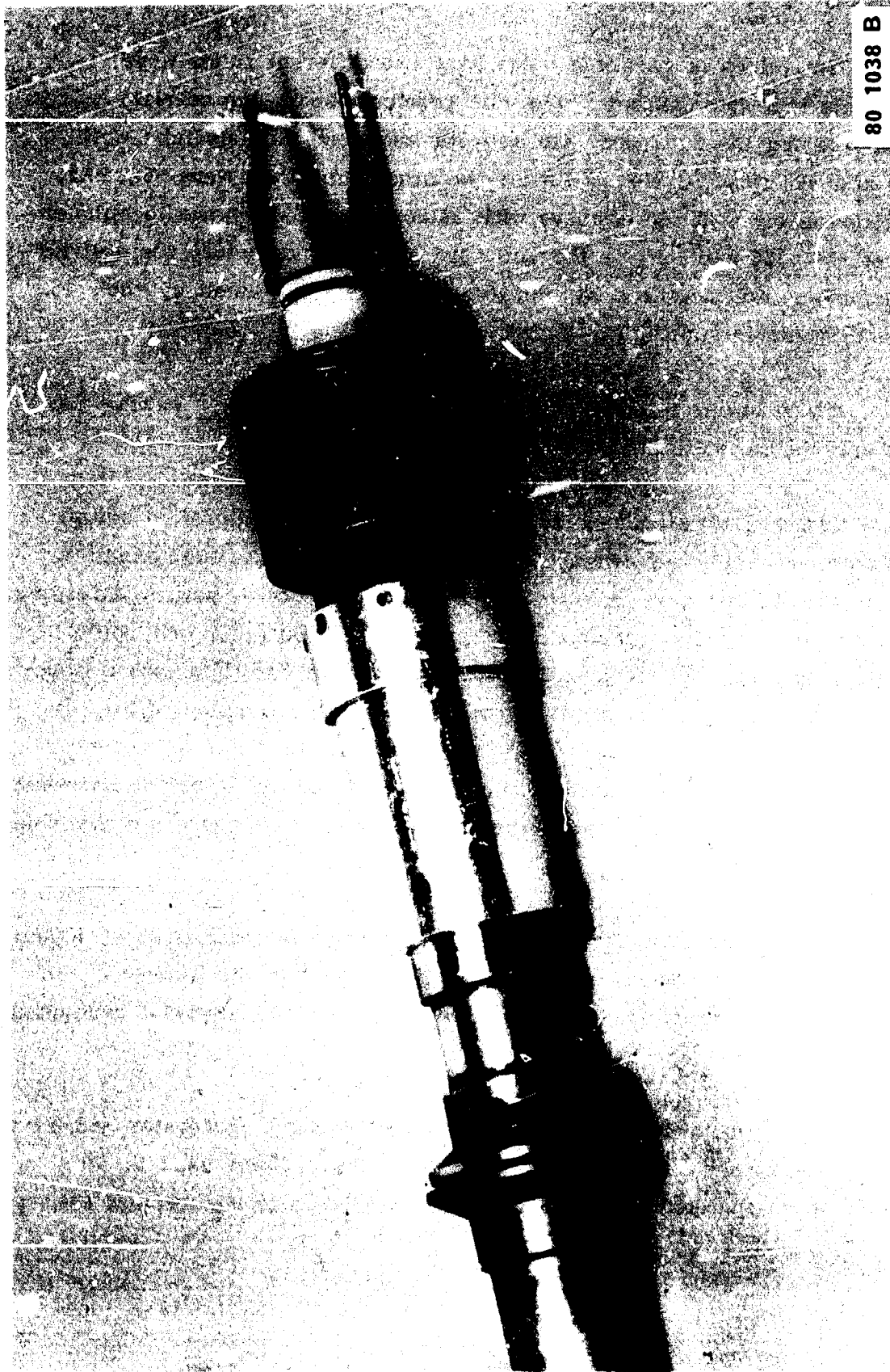


Figure 4-9. Coaxial Output Fitted Directly to the Microwave Oven Magnetron.

The values of harmonic noise from two different tubes were measured with this test arrangement. The dbc (decibels below the carrier) values that were measured for the 2nd, 3rd, 4th and 5th harmonics for one tube were -71, -97, -86 and -62 respectively, while for the other tube they were -69, -85, -93 and -64 respectively. These compare with values measured by the techniques used by JPL of -56, -65 and -67 for the 2nd, 3rd and 4th harmonics, respectively. The 5th harmonic was not measured by JPL and its value as obtained by the Raytheon measurements is suprisingly high.

The following material describes the arrangements for making the measurements and the measurements themselves in more detail.

Figure 4-10 is a block diagram of the test and calibration setup. The magnetron power supply furnished 300 mADC at 4000 v to the tube which was operated at zero heater input and which delivered 820 W of rf power. Emerging from the tube by means of the transition of Figure 4-8, this output power could be coupled directly to a waterload, or an intervening section of 7/8" line with a moveable mismatch could be inserted to study harmonic levels as a function of load impedance. Available in the waterload were two probes having coupling values of -24 dB and -33.4 dB at the magnetron fundamental frequency. For the harmonic measurements reported here, the former probe was utilized to maximize the available signal power.

A probe coupling factor for the harmonics was determined by injecting a known amount of harmonic power from a signal generator into the waterload and observing the coupled power out on the spectrum analyzer which was also calibrated in power.

A 1.0 mW calibration signal, derived from a signal generator and a variable pad, and measured with a power bridge (not shown), was used to set a reference amplitude on the analyzer display. Care was taken to ensure that the

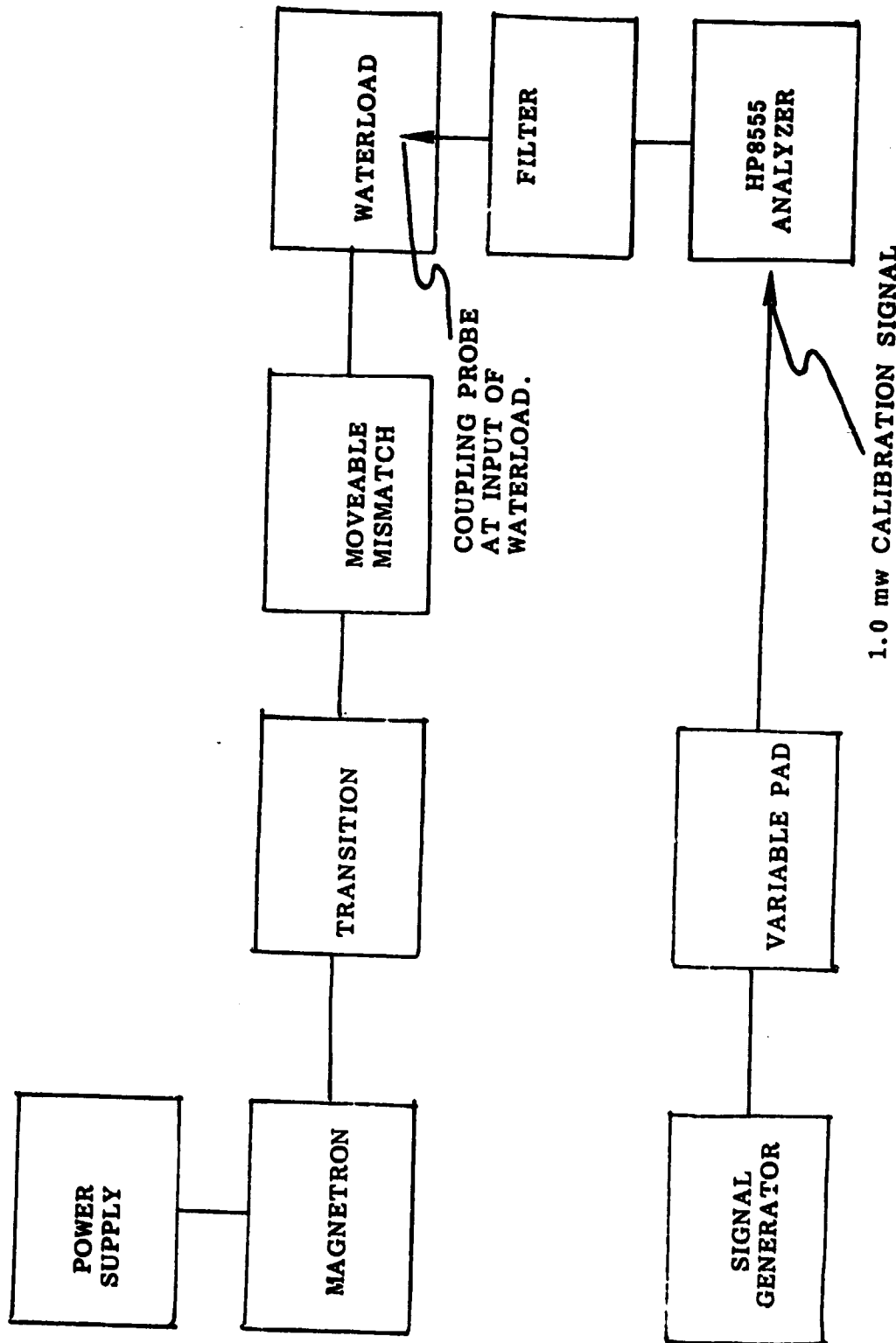


Figure 4-10. Test Set-Up for Measuring Harmonic Power.

amplitude calibration of the analyzer, nominally 10 dB/cm, was maintained over the full range of signal inputs.

To prevent saturation of the spectrum analyzer by the fundamental at 2450 MHz when viewing harmonics, waveguide filters were utilized; for the second and third harmonics a length of WR187 waveguide was chosen and for the fourth and fifth harmonics, a length of WR90 waveguide was used to prevent fundamental power entry into the analyzer. Wideband matched coaxial-waveguide couplers were used on each end of the filters. With this arrangement, harmonic levels down to -100 dbc could be measured.

The notation adopted for harmonic level calculation is indicated below:

C_p :	probe coupling factor, dB
C_f :	filter insertion loss, dB
P_a :	signal power in the spectrum analyzer, dBm
P_t :	total power in the waterload, dBm

Using these definitions, harmonic levels relative to the carrier are given (in dbc) by:

$$[P_a + C_p + C_f] - P_t$$

Calibration factors determined at the harmonic frequencies are listed in Table 4-2, where $k f_0$ denotes the k th harmonic frequency and f_1 denotes the $n = 7$ mode of the magnetron, a space harmonic of the magnetron's network which is known to be capable of generating a spurious signal.

These calibration factors are the measured insertion losses of the various components (coupling probe, WR187 filter and WR90 filter) at the nominal

TABLE 4-2

<u>Frequency</u>	<u>Nominal Frequency MHz</u>	<u>Cp dB</u>	<u>Cf dB</u>	
f_o	2450	24.6		
f_1	4360	16.6	1.7	} WR187
$2 f_o$	4900	16.0	2.4	
$3 f_o$	7350	21.5	3.8	
$4 f_o$	9800	18.2	2.0	} WR90
$5 f_o$	12250	19.2	2.0	

Calibration Factors

frequencies of the signals being examined. Since absolute frequencies can differ slightly from tube to tube, the sensitivity of the calibration factors was observed over a range large enough to accommodate this variation and their values were found relatively constant (± 1 dB) over the expected range.

Two tubes were examined, Serial Nos. 11 and 12 under matched load conditions with results as tabulated below:

<u>Frequency</u>	<u>HARMONIC LEVELS</u>	
	<u>#11</u> <u>dbc</u>	<u>#12</u> <u>dbc</u>
f_0	0	0
f_1	< -100	-73
$2 f_0$	-71	-69
$3 f_0$	< -97	-85
$4 f_0$	-86	-93
$5 f_0$	-62	-64

These findings are somewhat better than had been anticipated based on earlier experience with waveguide coupled tubes. However, with a coaxial system the harmonic impedances presented to the tube should result in less mismatch than for the waveguide case in which multimode propagation is a near certainty. On the other hand, it was recognized that for the higher order harmonics in 7/8" coaxial line, propagation of the TE_{11} mode was possible, and, therefore longitudinal loading slots colinear with the coupling probes were introduced into the line to preferentially orient this mode if it existed. The detection of significant power at the 5th harmonic despite the loading slots, coupled with the symmetrical excitation afforded by the tube construction, made it virtually certain that no TE_{11} components were present.

Since measurable power at the $n = 7$ mode frequency was detected under some conditions, a magnetron circuit was probed to ascertain the orientation of the two possible doublets of this mode.

As expected, the lower doublet was found at 4300 MHz, heavily loaded, and the upper doublet appeared at 4360, lightly loaded, the latter being the interfering frequency. No equalization of loading for damping purposes was needed for the original application of the magnetron, but, for the SPS application, equal loading of the doublet pair could be readily accomplished, thus preventing excitation of this mode frequency.

Because the harmonic impedance presented to an active microwave device can significantly affect harmonic levels (and other performance characteristics), observations of the effect of a simple mismatch were undertaken. A movable coaxial slug was used which presented the loads indicated below:

	VSWR
f_0	1.5
$2 f_0$	unknown
$3 f_0$	4 (approx.)
$4 f_0$	1.0 - 2.5
$5 f_0$	25 (approx.)

Results are given in Figure 4-11 in terms of P_a , the power input to the spectrum analyzer versus mismatch slug position. The point to recognize is that a modest impedance variation, e.g., that set up at $4 f_0$, can cause a large change (>10 dB) of the harmonic intensity. From this, two points can be brought forth:

- a) Significant variations of harmonic level from one condition to another as, for example, waveguide coupling vs coaxial coupling, are to be expected.

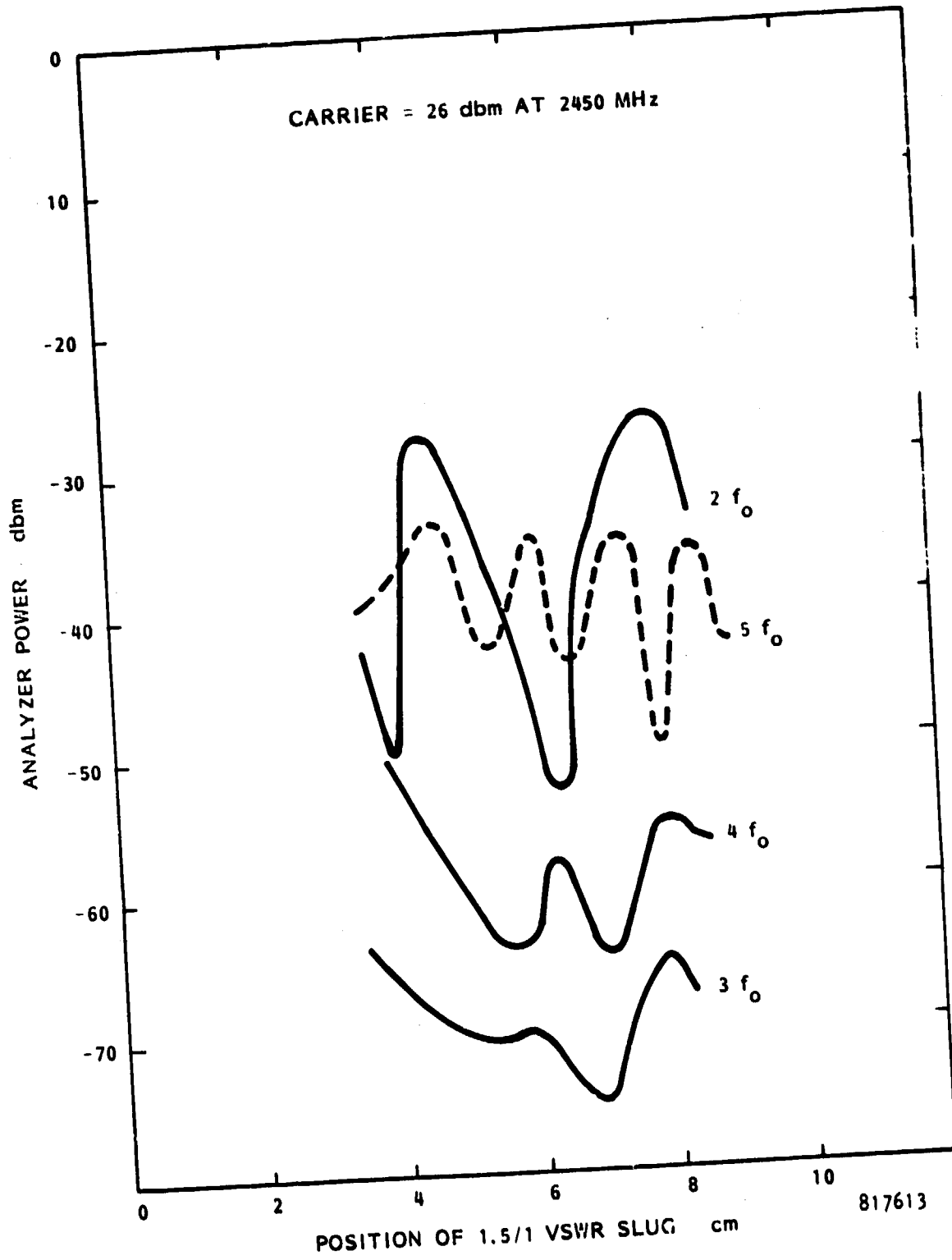


Figure 4-11. Harmonic Power Level as a Function of Pulling Slug's Position.

- b) Harmonic impedance control may offer interesting benefits in suppressing harmonic output and in optimizing other tube performance characteristics.

5.0 CATHODE LIFE CONSIDERATIONS

5.1 Introduction

The investigation into the potential life of the cathode in the magnetron directional amplifier was motivated by a question that arose during a Raytheon briefing that was primarily centered on the high signal to noise ratios that had been observed in the microwave oven magnetron when it was operated on a well filtered DC power supply and when the source of external filament power was removed. The question was simply; "What is the life of the tube when it is run under conditions of high signal to noise ratio". It is important to answer this question for it would obviously be desirable to have microwave generators with very long life in microwave power transmission applications, and particularly so in the SPS application.

It is a basic characteristic of thermionic tubes that their life is limited by the life of the cathode. In the case of the microwave oven magnetron the cathode is a carburized thoriated tungsten cathode in the form of a helix wound from 0.020" diameter thoriated tungsten wire. The filament is carburized in a subsequent treatment and it is this carburization that greatly extends the life of the cathode.

An initial study of available life test data on the carburized thoriated tungsten cathode and a review of the rather extensive design literature on such cathodes indicated that a life of fifty to one hundred years should be possible if the cathode were run at a temperature of 1900° Kelvin or below under high vacuum conditions. It was therefore necessary to know the operating temperature of the cathode in the microwave oven tube to make a prediction of life.

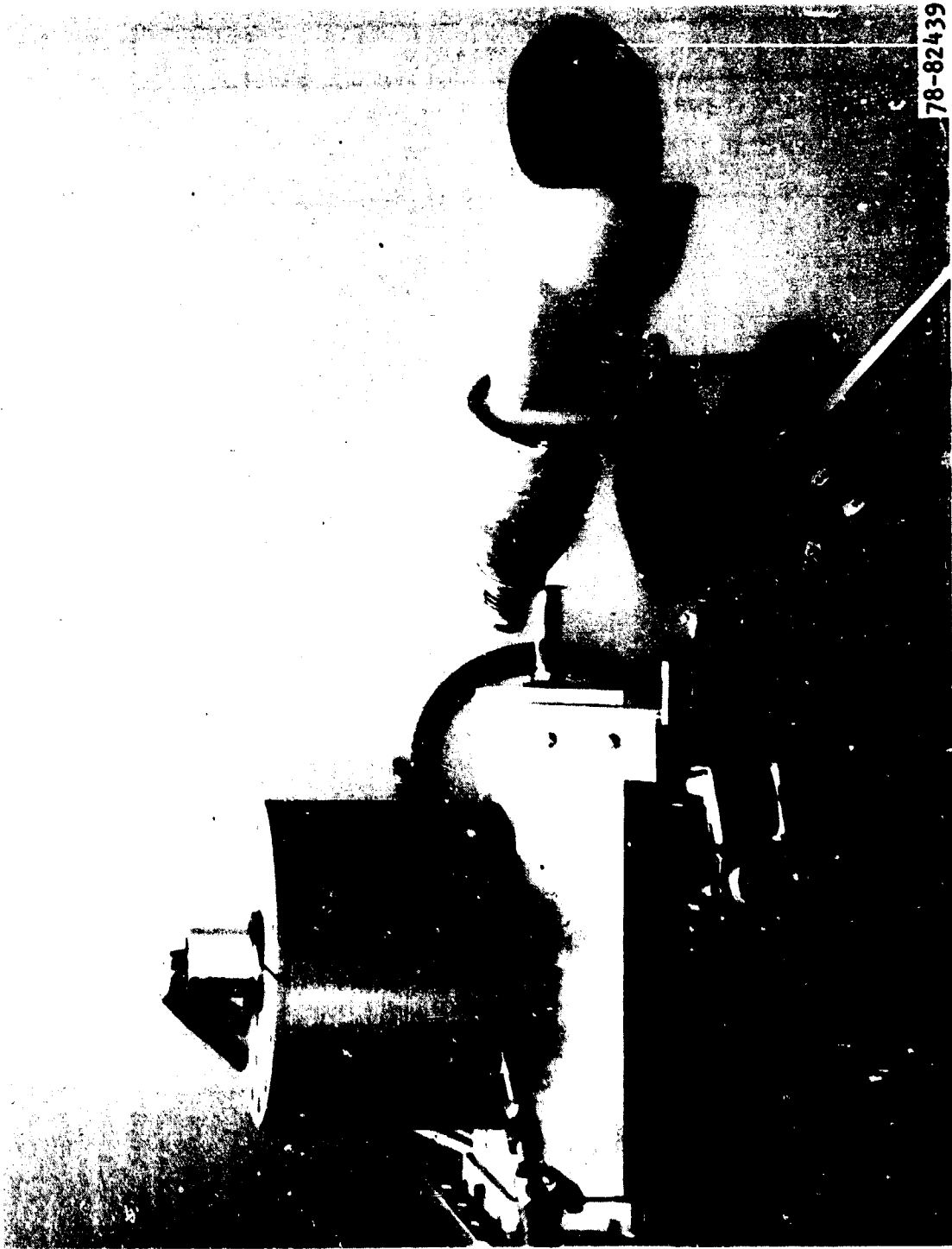
It was first proposed that the temperature of operation of the cathode be estimated on the basis of resistance measurements made on the cathode while

the tube was running. Subsequent investigation revealed, however, that without a correlation between the resistance measurement and an actual visual observation of the cathode temperature, such an approach would not give measurements of the accuracy needed.

Fortunately, Raytheon, as part of their active participation in the development of the microwave oven magnetron, had previously assembled three magnetrons in which an optical window had been inserted for viewing of the cathode temperature while the tube was operating. These tubes were transferred to this study without charge. One of these tubes, packaged with a permanent magnet, was put into our regular test facility and appeared to operate in a normal fashion, including the very high signal-to-noise ratio when the source of external filament power was removed.

In order to observe the cathode temperature as a function of magnetic field and rf load, as well as anode current, a special test arrangement was made to accommodate the optical window which is mounted on the end of a copper tube which is inserted into the wall of the tube; the axis of the viewing pipe is at right angles to the axis of the cathode. In this arrangement, shown in Figure 5-1, the permanent magnet was removed from the tube and the tube was fitted into a wire-wound solenoid so that it was possible to vary the magnetic field and view the cathode temperature at the same time. Another added feature was a water cooling jacket fitted around the anode so that the tube could be adequately cooled.

Temperature measurements were made with the Leeds and Northrop 8622C optical pyrometer which is an industry standard for making such measurements. It is shown mounted on a tripod in Figure 5-1. The readings of the instrument are calibrated in terms of brightness temperature which can then be converted into true temperature by taking the emissivity of the carburized thoriated tungsten into account. This relationship between brightness and true temperature for carburized thoriated tungsten is given in Figure 5-2, and is taken from the



78-82439

Figure 5-1. Test arrangement for viewing the temperature of the filament-type cathode in the microwave oven magnetron as a function of anode current, applied magnetic field, and microwave load. Optical pyrometer is in the right foreground. Transparent window is visible outside of solenoid-type electromagnet.

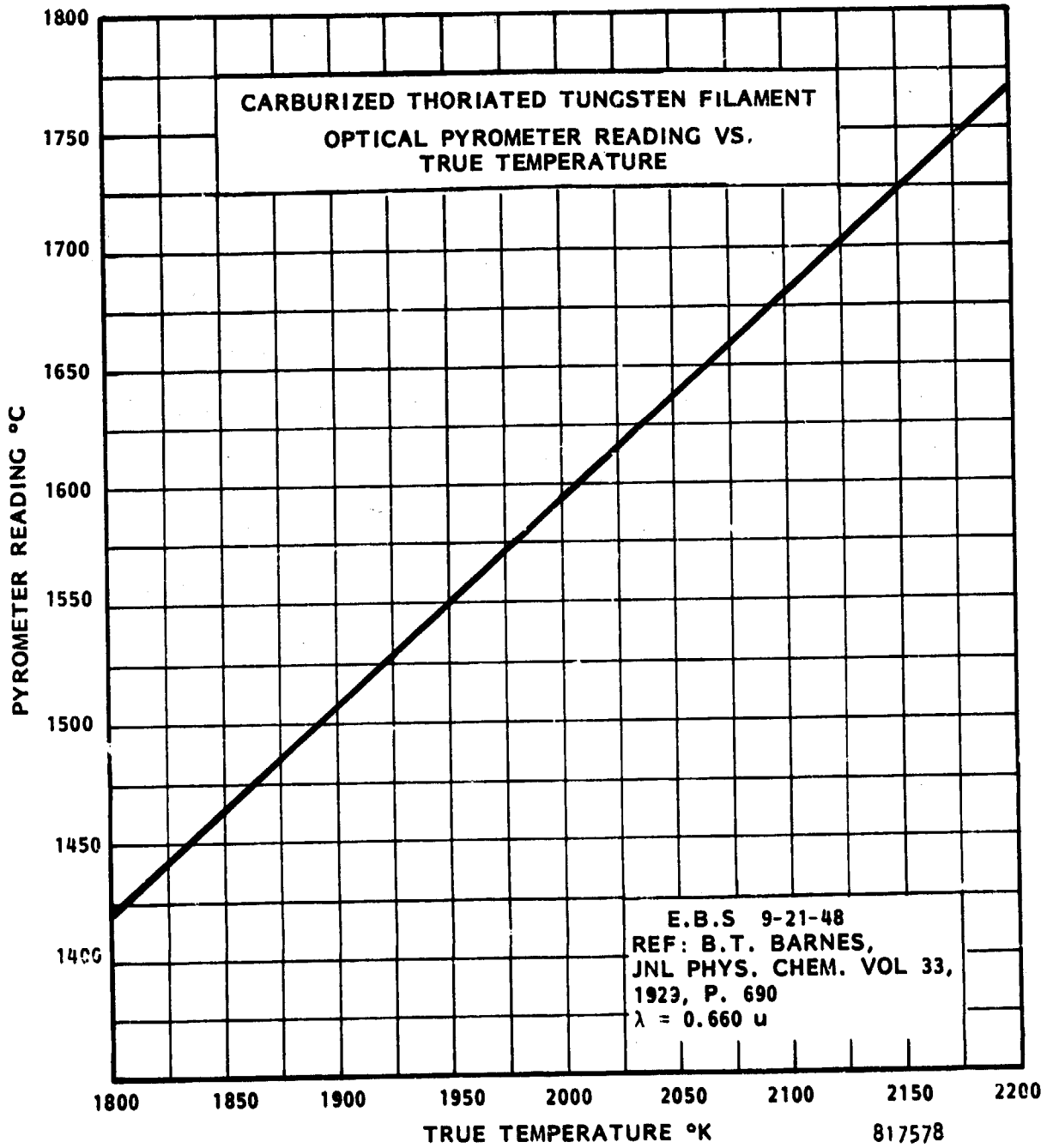


Figure 5-2.

Journal of Physical Chemistry, vol 33, 1929, page 690. It is the data that is generally used throughout the industry.

Figure 5-3 shows what is seen through the optical pyrometer. The filament type cathode cannot be seen as a whole because it is being viewed radially through the space that exists between the tips of the vanes. This space is about 0.060". Portions of four turns of the filament are visible in the photograph. It is possible to see one additional turn toward the top and the bottom by repositioning the height of the optical pyrometer.

The observations that were made on the cathode temperature as a function of several parameters indicated that it is highly dependent only upon the anode current, and that it tends to operate at a temperature which will supply the primary emission from the cathode. Quite surprisingly, it was found to be nearly independent of the magnetic field over a range of approximately two to one. The corresponding DC power input and microwave output changed by a factor of two (since the anode current is being held constant and the input voltage is proportional to the magnetic field). Similarly, a variation of the rf load by a factor of three to one had little effect upon the cathode temperature.

These observations are rather profound from the viewpoint of magnetron operation and suggest that there is a finely tuned mechanism within the magnetron which adjusts the temperature of the cathode to just provide the primary emission that is needed to match the anode current flow requirement externally imposed upon the tube by power supply adjustment. While it has been generally recognized that the backbombardment power did adjust itself to the needs of the tube, it was also believed that the backbombardment power and the temperature of the cathode increased with magnetic field and varied with changing load conditions, neither of which has been confirmed by our experimental observations over a substantial range of magnetic field and load variation. And it was not realized that the relationship between an increase in filament temperature and an

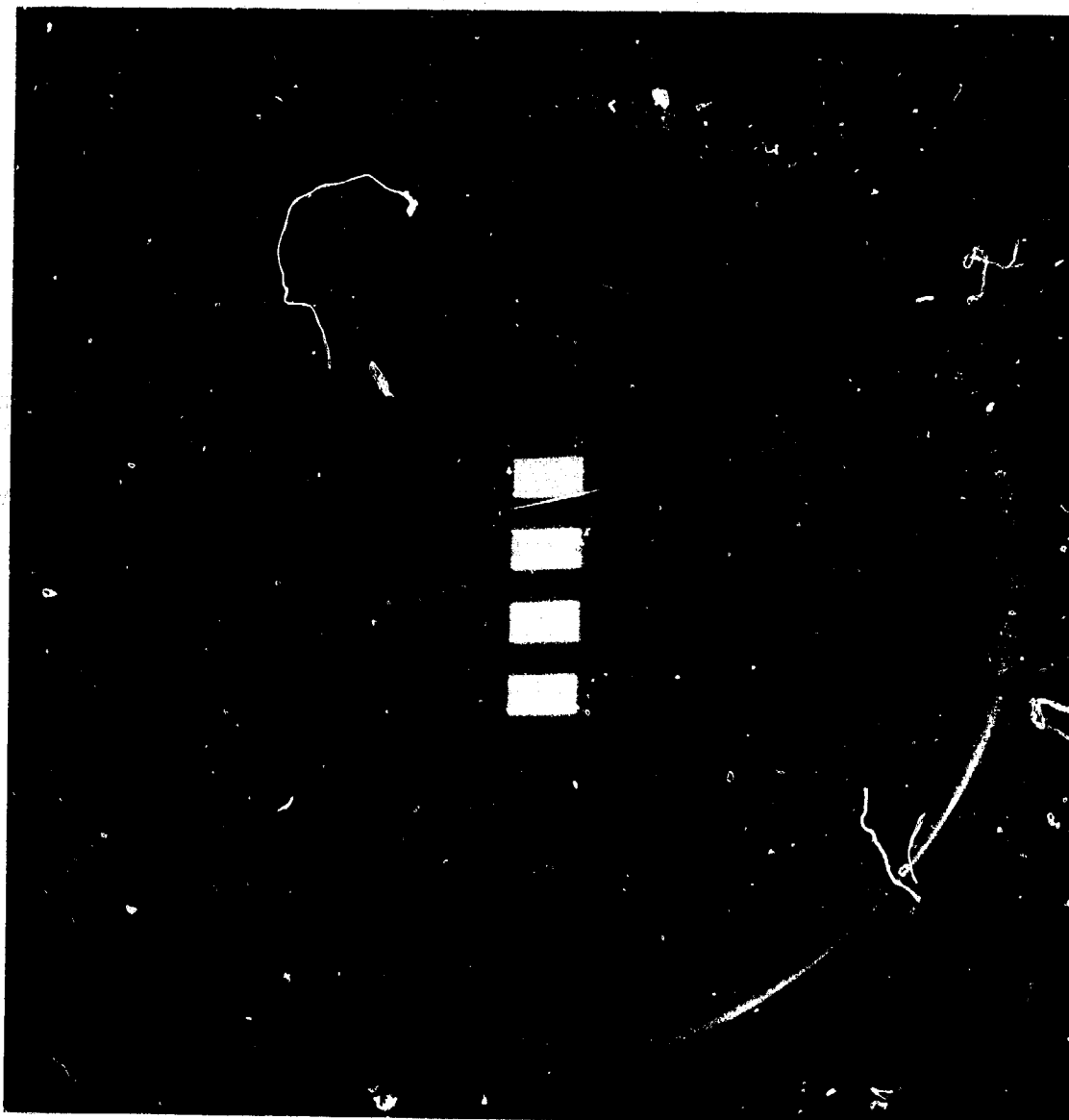


Figure 5-3. Four (4) turns of the filament-type cathode are visible in the photograph. The filament wire diameter is approximately one half millimeter. Filament is observed between the tips of two vanes so full diameter of cathode is not observed.

increase in anode current corresponded so closely to the relationship between emission limited current and temperature as given by the classical Richardson-Dushman relationship as shown in Figure 5-4.

The data that were taken also indicated that a low operating temperature could be achieved at nominal values of anode current and power output. As a result of these observations and research into the extensive literature that exists on the design and life characteristics of the carburized thoriated tungsten cathode, it seems reasonable to predict a cathode life of at least fifty years in a tube designed specifically for the SPS application.

The following material will expand upon the subjects touched upon in the introduction. There will be sections on:

- 5.2 Data obtained on cathode temperature as a function of anode current, magnetic field, and load coupling.
- 5.3 Correlation of observations on cathode operating temperature and the Richardson-Dushman equation for primary emission as a function of temperature.
- 5.4 A review of the literature on the theoretical life of the carburized thoriated tungsten cathode and corresponding experimental data.
- 5.5 Distribution of cathode temperature as a function of axial distance along the cathode.
- 5.6 Observations of the impact of cathode poisoning upon cathode operating temperature and tube efficiency.

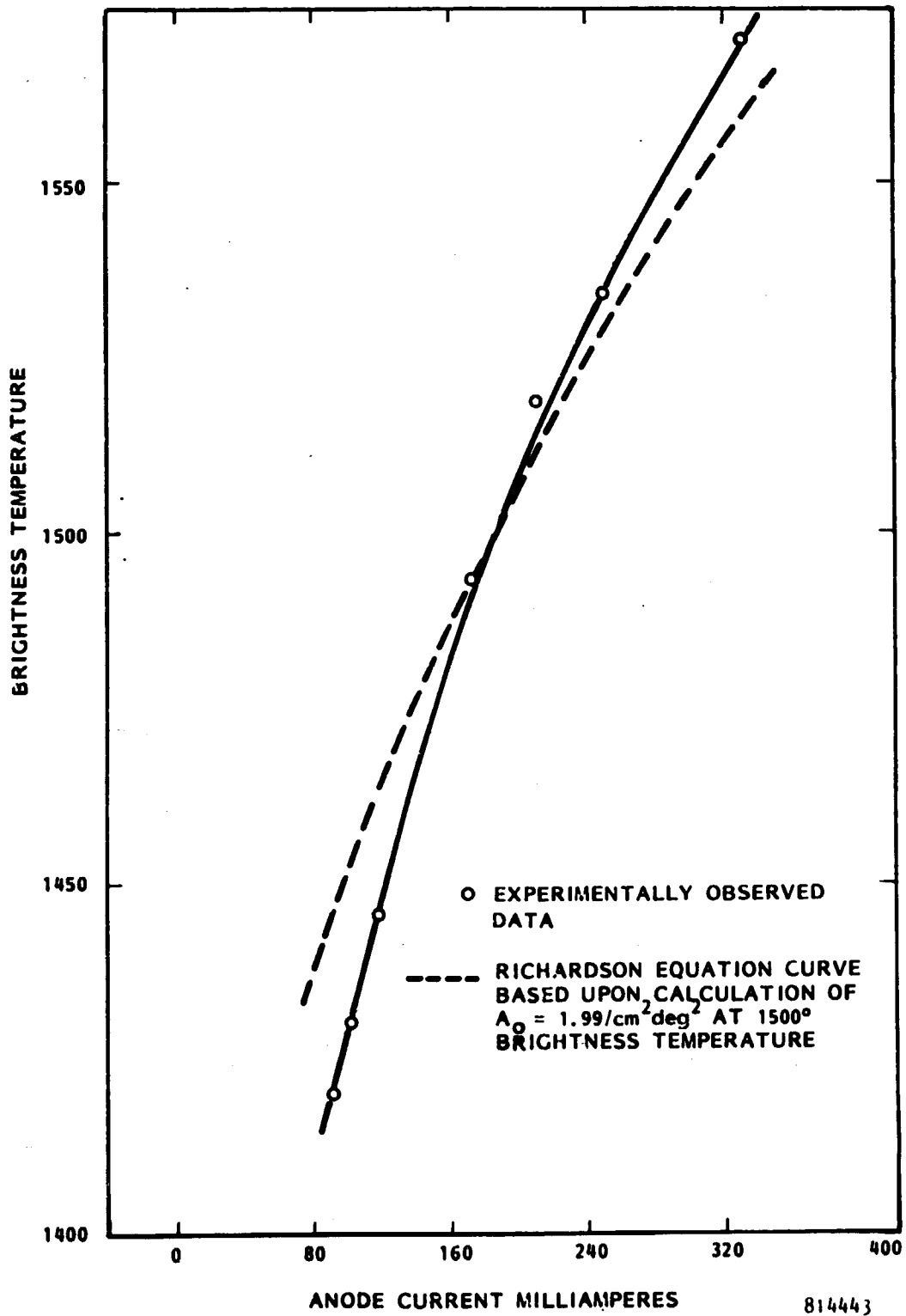


Figure 5-4. Experimentally Observed and Theoretically Predicted Relationship Between Cathode Temperature and Anode Current.

5.2 Cathode Temperature as a Function of Anode Current, Magnetic Field, and Load Coupling

In the measurements that will be discussed, the temperature observation is made in terms of brightness temperature as observed on the calibrated Leeds and Northrop 8622C optical pyrometer. From the viewpoint of predicting life and correlating with the Richardson-Dushman relationship on emission as a function of cathode temperature, a conversion into absolute cathode temperature is needed. This relationship is provided in Figure 5-2. From our viewpoint it is conservative in that the data in the graph were taken on a straight filament in a vacuum where there was little or no reflected spectral energy, while in our case the anode of the tube does reflect back into the cathode some of the emitted radiation. This would tend to reduce the gap between the brightness and absolute temperature, but we have neglected any correction for this.

Figure 5-4 shows the cathode brightness temperature as determined by the optical pyrometer as a function of anode current, for conditions with no filament power applied. Also shown in Figure 5-4 is a theoretical curve determined from the use of the Richardson equation for the temperature limited emission from a thermionic cathode. The Richardson equation is matched to the curve of experimental data at 1500° brightness temperature (the corresponding absolute temperature which goes into the equation is 1893°). The slopes of the two curves are closely matched.

Figure 5-5 shows the cathode brightness temperature and anode voltage as a function of relative magnetic field, or more precisely, as a function of relative magnetomotive force which is directly proportional to the current in the magnet solenoid. The anode voltage that must be imposed upon the magnetron to maintain anode current flow is proportional to the magnetic field across the interaction area of the magnetron. Figure 5-5 is a good demonstration not only of the independence of filament temperature from the magnetic field but also from power input to the tube since the input power is equal to the product of the anode voltage and the anode current. It should be noted that the data on cathode temperature

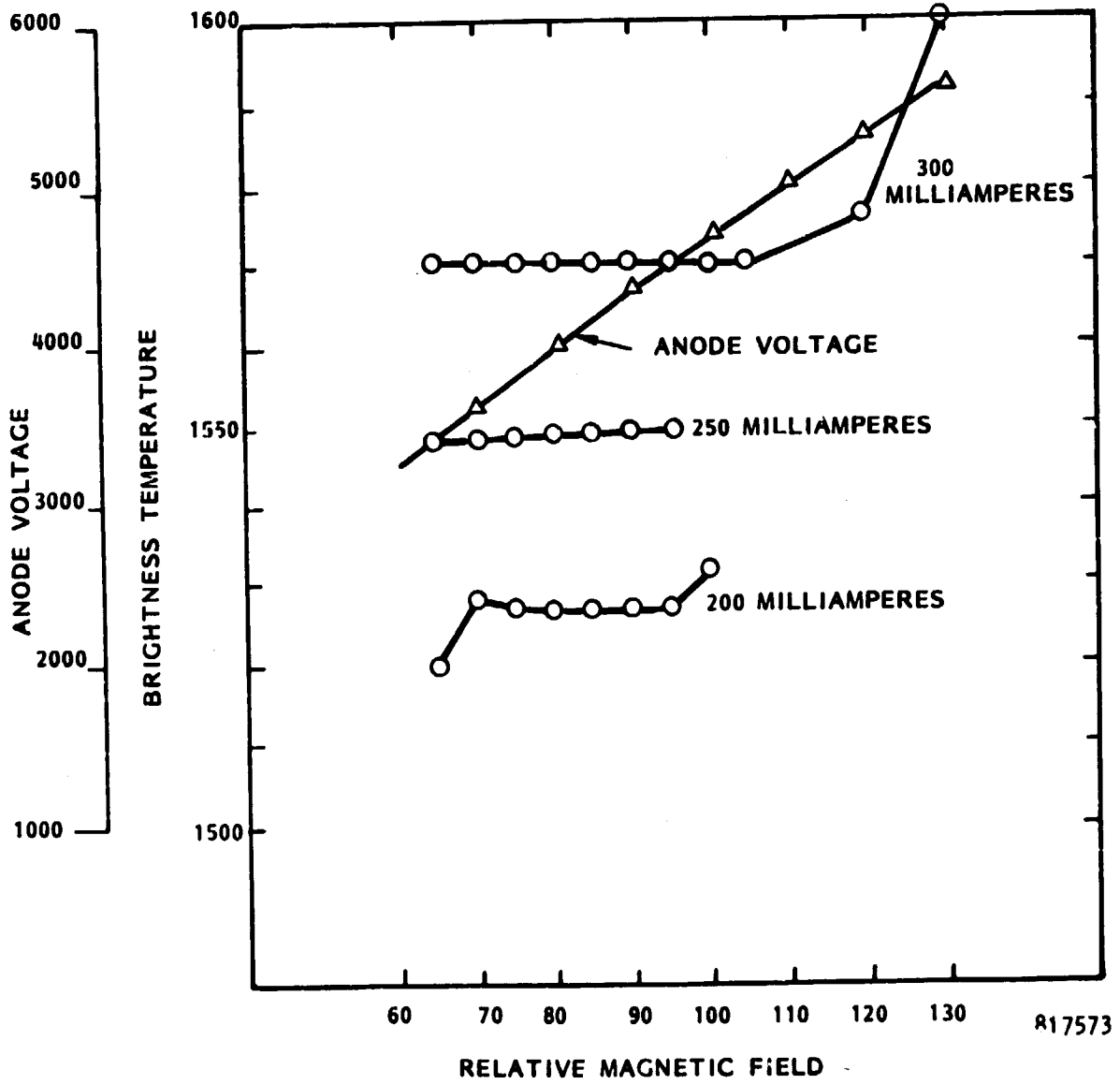


Figure 5-5. Anode Voltage and Cathode Brightness Temperature as Function of Magnetic Field.

cannot be determined by eye to better than 5 to 10°C so that the unchanging level of the data points indicates that the temperature has not changed enough to be perceptible to the eye.

It will be noted that the brightness temperatures in Figure 5-5 for a given value of anode current are somewhat higher than in Figure 5-4. One of the contributing factors to this may be that while the data of Figure 5-4 was obtained without any auxiliary heater power, the data obtained for 5-5 was with 22 watts of heater power or about 55% of the amount that is normally supplied to the tube in its microwave oven application. The increase in cathode temperature at 300 milliamperes of current at the higher magnetic field may be caused by gaseous poisoning of the cathode as discussed in Section 5.6.

Figure 5-6 indicates the independence of the cathode temperature from the microwave loading (external Q) of the tube over a range of nearly three to one as determined by the locking range since it was inconvenient to make loaded Q measurements. The most heavily loaded point is the one corresponding to the largest locking range. It corresponds to higher circuit and overall efficiency as indicated by the relative microwave power output.

5.3 Correlation of Operating Temperature with the Richardson-Dushman Equation for Primary Emission

One of the characteristics of a carburized thoriated tungsten cathode is that it has very little secondary emission and can therefore be treated to a first approximation as a primary emitting cathode. Under these conditions the cathode must operate at a temperature sufficiently high to at least supply the anode current in the magnetron. If the anode current is increased then the cathode must operate at a higher temperature to supply the additional current.

Under these circumstances it is of interest to determine how closely the experimentally observed relationship between observed cathode temperature and

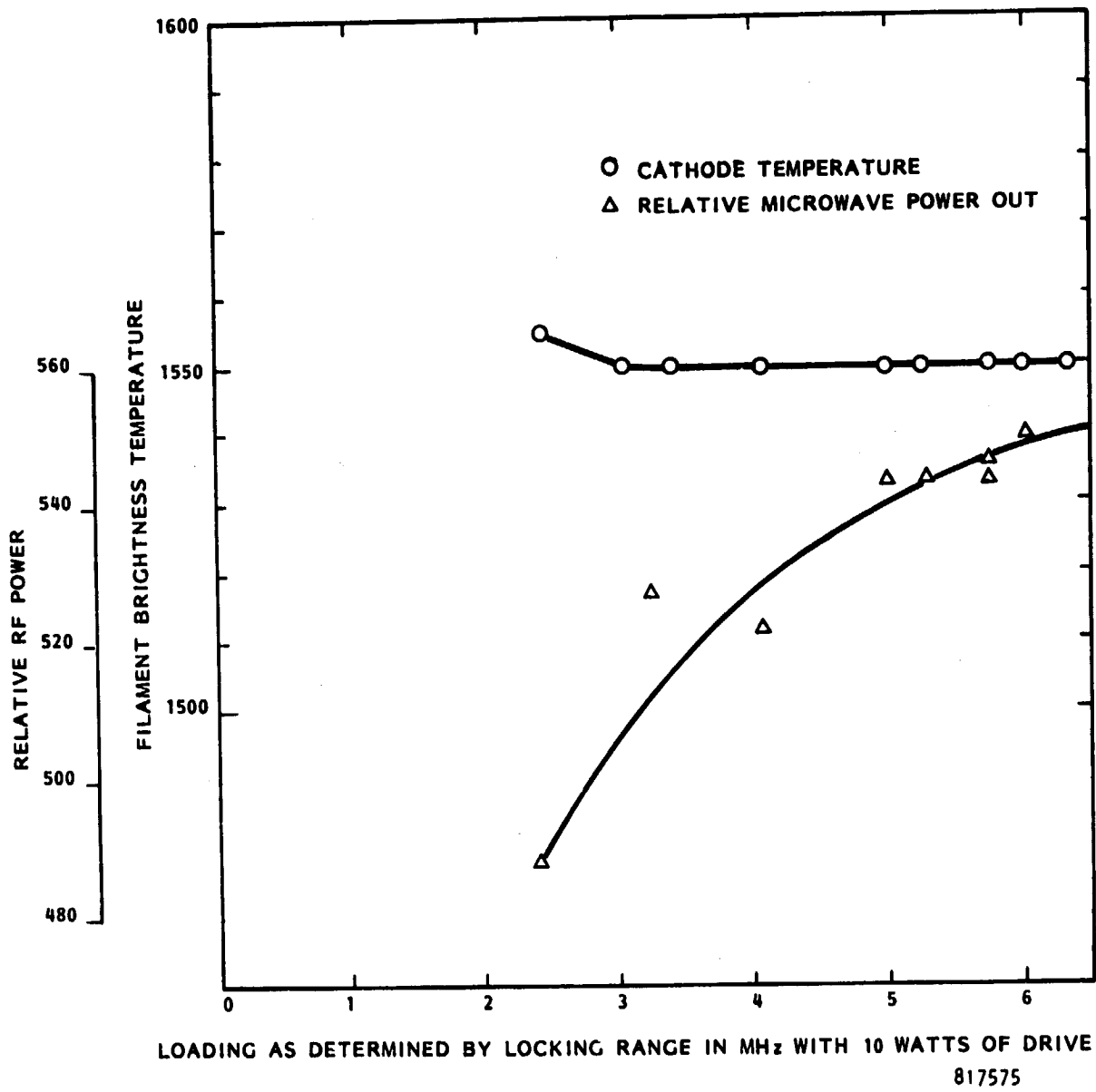


Figure 5-6. Cathode Brightness Temperature and Power Output as Function of Loading.

anode current is predicted by the Richardson-Dushman equation which gives the relationship between saturated thermal emission current and the absolute temperature of the cathode.

$$J_s = A_0 T^2 e^{-\frac{\phi}{kT}}, \text{ where} \quad (5-1)$$

J_s = Saturated thermal emission current density in A/cm²

A_0 = Dushman's constant; the theoretical value is 120.4/cm²deg²

T = Temperature in degrees Kelvin

e = 2.71828

ϕ = True work function in electron volts

k = Boltzmann's constant = 8.6×10^{-5} eV/°K

In the case with which we are concerned, the actual value of A_0 may be considerably different than the theoretical value, and the effective area of the emitting surface of the filament is not accurately known. Because we are primarily interested in comparing the slopes of the experimentally observed anode current versus cathode temperature with the theoretical prediction of the equation, we will rewrite the expression (5-1) as follows:

$$I_1 = KT^2 e^{-\frac{\phi}{kT_1}} \quad (5-2)$$

where I_1 is the measured current at observed temperature T_1 and K is a proportionality constant which we will solve for and assume to be constant subsequent use of (5-2) with other temperatures T . From Figure 5-4 we have the point of data at which I_1 is 0.190 amperes and T_1 is 1.893° Kelvin (after using Figure 5-2 to convert from the observed brightness temperature of 1500° centigrade to 1893° Kelvin). The value of 2.85 that is used for the work function is that generally accepted for the carburized thoriated tungsten cathode. When the 1893° K value of temperature and work function are inserted into equation (5-2) the value of K is computed to be 1.99.

This value was used for determining the emission as a function of brightness temperature from 5-2 and the resulting relationship was plotted in Figure 5-4. It may be seen that there is a close correspondence between slopes of the observed relationship and that predicted by the Richardson-Dushman equation.

Although we are primarily interested in comparing the slopes of the experimental and theoretical relationships it may be of interest to make an estimate of the effective cathode emission area and solve for the A_0 in equation (5-1) to see how well this value agrees with typical values reported in the literature. An effective emission area of 1.0 square centimeters is estimated. With previously used values of emission current of 0.190 amperes and of the temperature of 1893°K, the value of A_0 is $1.99/\text{cm}^2\text{deg}^2$. This value is within the range of commonly observed values for the carburized thoriated tungsten cathode (the theoretical value is never achieved).

Another set of data that may be useful is derived from using the magnetron as a simple cylindrical diode without any magnetic field present. Under these circumstances the current varies as the $3/2$ power of the anode voltage because of space charge limitations until the emission from the cathode becomes temperature limited. This data is shown in Figure 5-7 and indicates that a filament temperature in the range of 1525° is necessary to reach a value of anode current in the range of 200 to 250 milliamperes.

5.4 A Review of the Engineering Background on the Life of the Carburized Thoriated Tungsten Cathode Including Experimental Data

This section reviews some of the extensive engineering background that exists on the carburized thoriated tungsten cathode and experimental data that has been accumulated. The Machlett company was helpful in both selecting key articles in the literature and also in supplying life test information on carburized thoriated tungsten cathodes that have been used in high power negative grid tubes of comparable power rating to that of the proposed magnetron for SPS use.

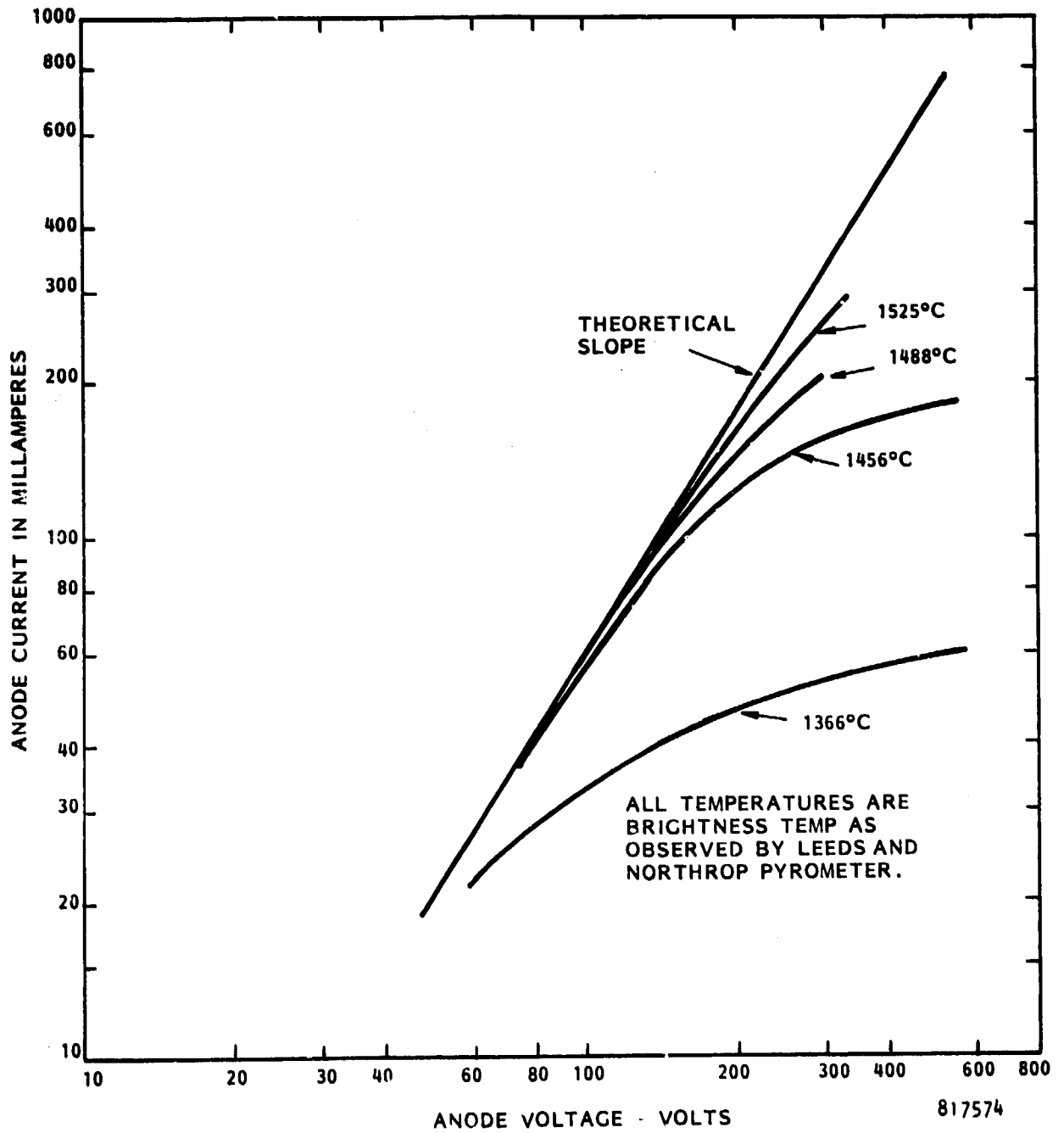


Figure 5-7. Relationship of Diode Current to Anode Voltage as Function of Observed Brightness Temperature.

From this material and the observed behavior of the thoriated tungsten cathode in the microwave oven magnetron a very good case can be made for a carburized thoriated tungsten cathode that will last fifty to 100 years in a magnetron in the SPS application. In addition to the low operating temperature that can be designed into the filament, the SPS application contains an unusually favorable set of other operating conditions for ensuring the long life of a filamentary type cathode: (1) there is no current flow through the filament except for short periods of time during start up operations; (2) the zero-g condition eliminates the sag problem that can occur in terrestrial applications; (3) there should be no mechanical shock; (4) the input power and match to the microwave antenna is always carefully controlled; and (5) the vacuum conditions are either inherently very good or can be made so by appropriate measures.

The technical argument for such long life is based upon data that are given in W.H. Kohl's "Handbook of Materials and Techniques for Vacuum Devices", Reinhold Publishing Corporation, and upon references given there which have been researched. According to experts at Machlett Corporation the Ayer Reference "High-power industrial vacuum tubes having thoriated tungsten filaments" AIEE Trans., 72, Pt. 1, 121-125 (May 1953) is an authoritative reference. As shown in the attached illustration Ayer shows life of up to 75,000 hours at a temperature of 2000° Kelvin, and three times that at a temperature of 1950°, as shown in Figure 5-8.

The predicted life data of 75,000 hours in Figure 5-8 are based upon observed life times in excess of 30,000 hours at 2000 degrees Kelvin, and an extrapolation to 75,000 hours based upon the recognition that it is the decarburization of the cathode which limits life and that the reservoir of carburized material and therefore the life of the cathode is proportional to the thickness of the carburized layer and therefore to the diameter of the wire.

Other data, shown in 5-9 and taken from R. B. Ayer "Use of Thoriated Tungsten Filaments in Transmitting Tubes", Proceedings of I.R.E..

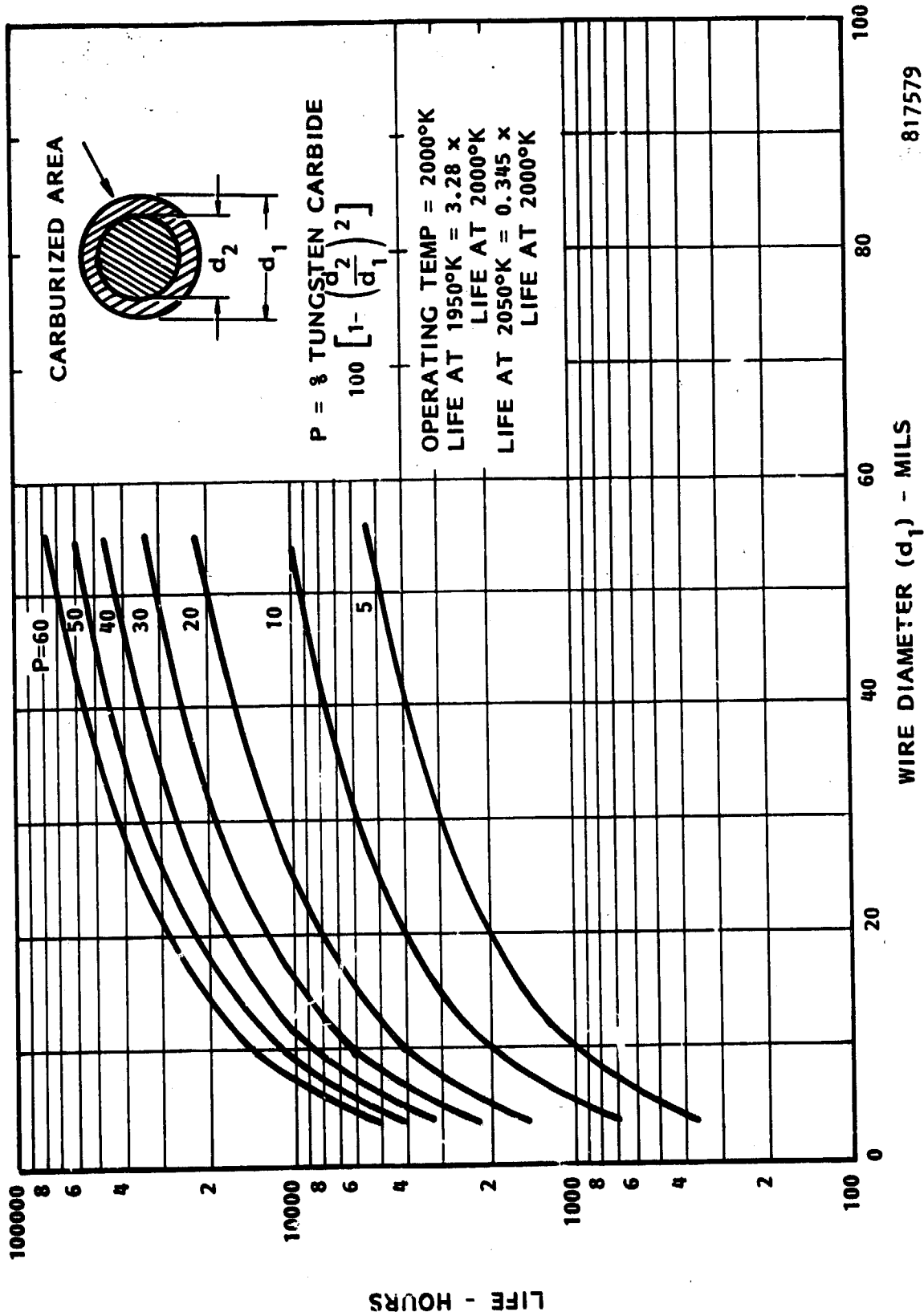


Figure 5-8. Cross section of a carburized thoriated tungsten filament and curve showing life for different thicknesses of carbide shell. After Ayer.

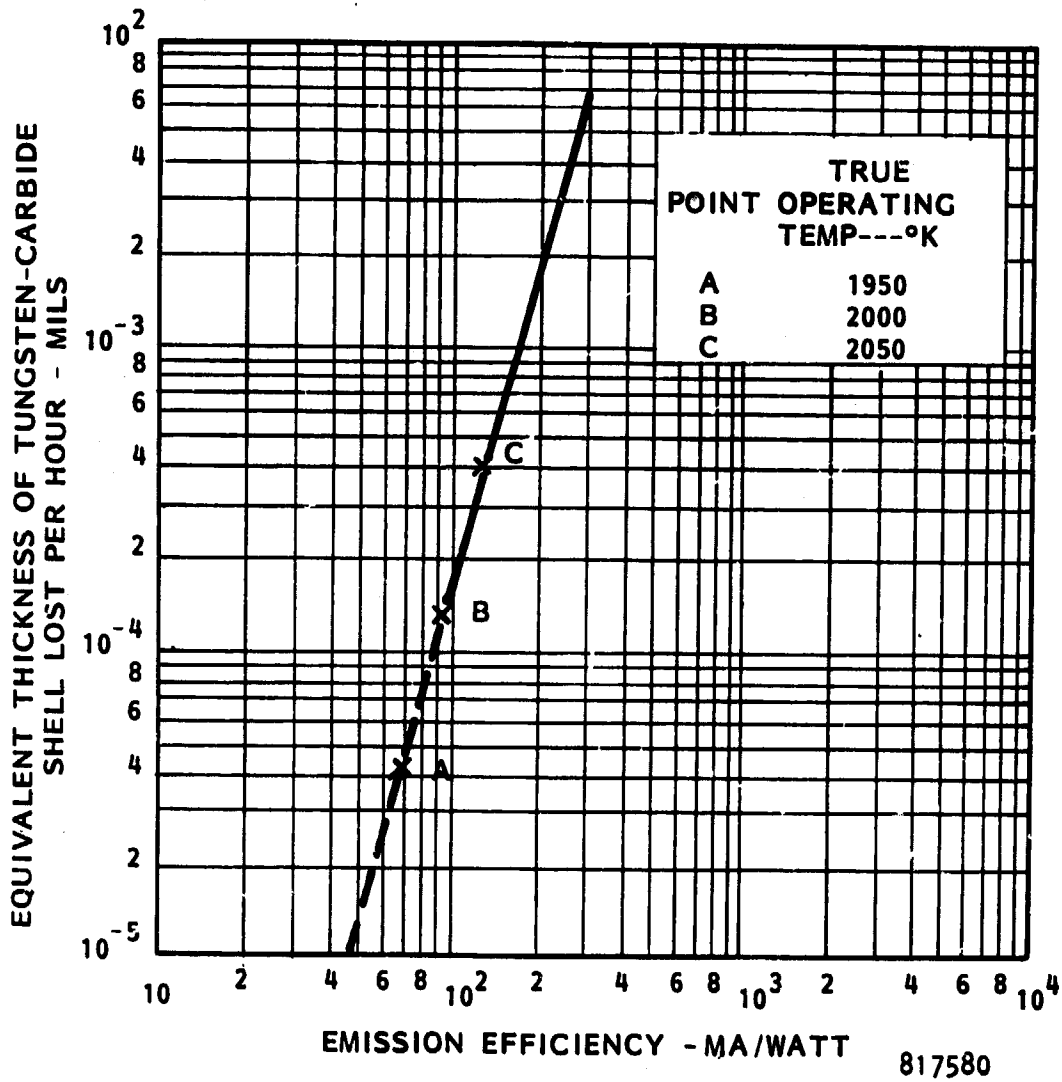


Figure 5-9. Carbide Loss Versus Operating Temperature.

Volume 40, May 1952, Pages 591-94, indicate the reduction in carburized material as a function of temperature. As shown in Figure 5-9 a reduction of 50 Celsius degrees decreases the loss by a factor of 3 and therefore increases the life by a factor of 3. An extrapolation of this data to lower operating temperatures would provide a factor of 27 in increased life if the temperature were reduced to 1850°. If the factor of 27 is used to multiply the 75,000 hour life shown in Figure 5-8, the resulting predicted life is 230 years. The corresponding predicted life for 1900°K and 1950°K, are 77 years, and 26 years, respectively.

How good is the information in Figure 5-8 in predicting the life of carburized thoriated tungsten cathodes? It is surprisingly good, as the experimental data to be presented indicates.

Table 5-1 presents data on 12 high voltage, medium-power ML6421F and ML5541 triodes that show individual lifetimes of up to 86,930 hours or over ten years of continuous running in the WWV CW time signal station of the Bureau of Standards. The twelve tubes had a total running time of 850,000 hours with no failures. In checking with WWV to see if there were additional hours of running time, I was told that the equipment had been retired in 1965 and disposed of so the end-of-life of these tubes was never determined.

However, it is known that the low operating temperatures played an important part in the life of these tubes. The expected lifetimes of these cathodes, which utilized a wire diameter of 0.035" which was 20% carburized, would be 13,000 hours if run at 2000° Kelvin according to Figure 5-7. However, they were run at a reduced temperature of approximately 1900° Kelvin. According to an extrapolation of the Ayer data, the life would thereby be increased by a factor of ten, to 130,000 hours. The running times that were obtained without failure were therefore consistent with that number.

This experimental data can be applied to the life expectation of a filament type cathode that could be designed for a magnetron or amplatron for the SPS application. The filament could be made from 0.050" diameter wire whose cross

TABLE 5-1

Transmitter Frequency	Tube Type	Serial Number	Tube Position	Hours Life As Of 11-1-65	Original Installation Date**
5 Mc	ML-6421F	428425	RFL	71,975	5-7-56
	ML-6421F	426798	RFR	71,975	5-7-56
	ML-6421F	425856	ML	77,284	7-13-55
	ML-6421F	425857	MR	77,284	7-13-55
15 Mc	ML-6421F	428330	RFL	68,025	10-18-56
	ML-6421F	425611	RFR	68,025	10-18-56
	ML-5541	410244	ML	86,930	10-09-53
	ML-5541	410108	MR	86,930	10-09-53
10 Mc	ML-6421F	426800	RFL	70,460	4-05-56
	ML-6421F	428328	RFR	70,460	4-05-56
	ML-6421F	426791	ML	72,100	12-14-55
	ML-6421F	426801	MR	72,100	12-14-55

Legend: RFL -- Radio Frequency, Left ML -- Modulator, Left
RFR -- Radio Frequency, Right MR -- Modulator, Right

General Operating Conditions per Tube

	Filament Volts*	Plate Volts	Plate Amperes
Modulator - 6421	6.0 A.C.	6000 D.C.	0.1
5541	5.3 A.C.	6000 D.C.	0.1
Radio Frequency	6.0 A.C.	6000 D.C.	0.9

Modulators have static current of 0.1 Amps. They are pulsed with a 5 cycle burst of 1000 cycles once per second and voice and telegraphic code announcements for approximately 30 seconds out of each 5 minutes.

* Filaments operate within ± 0.1 volts

** There have been no tube failures in this group of thoriated-tungsten filament tubes. All original thoriated-tungsten tubes are still in operation.

section could be 50% carburized. If this cathode were run at the same temperature of 1900° Kelvin, the life expectancy would be 700,000 hours or over 70 years, if decarburization of the cathode were the failure mechanism, as it usually is in a tube with a good vacuum.

There is no comparable life data on any "CW" magnetrons run on a low-ripple power supply at low cathode temperatures. Because of the lack of such data, we might worry about the potential depletion of the thorium on the surface of the cathode caused by electron bombardment. However, work performed by Danforth* indicates the desorption of thorium on the cathode surface was not affected at all by electron bombardment.

* From Danforth, W.E., "Description of a Thorium Monolayer", *Advances in Electron Tube Technology*, Slater D., ED., Proc. of Fifth National Conference, Sept. 1960, N.Y., pp 143-146, Pergamon Press, New York, 1961.

"We turn now to the subject of desorption by electron bombardment. This matter was previously reported upon in March of 1959 at the M.I.T. Conference on Physical Electrons at which time we had concluded that bombardment of the monolayer by electrons of 350 V energy or less did not remove adsorbed thorium atoms at a rate which we could detect. We calculated at that time if any desorption of this kind existed it was too small to be of any importance in the matter of thorium dispenser cathodes. Since that report we have carried the experiment further, using the tube of Figure 1, and I am now able to speak even more assuringly in this matter of electron desorption of the thorium layer. Using the tube shown, we were able to continue the bombardment for a total of 80 A hr/cm². And it is concluded that such desorption as might exist must have been less than 4×10^{11} electrons removed per bombarding electron. This total bombardment of 80 A hr/cm² is of the order of magnitude of the total bombardment which might be experienced in reasonable life of a CW magnetron. And during this period the number of atoms/cm² removed, if any, was not more than 10^{13} or a very small fraction of one complete monolayer. It may therefore be concluded that removal of electrons by bombardment is of no practical importance even though the cathode concerned be a single and non-replenished layer of thorium atoms. In practical cases the loss of thorium by electron bombardment is probably considerably less than that lost either by thermal evaporation or by the residual ion bombardment from the imperfect vacuum.

It is evident that desorption of thorium by electron bombardment occurs at such a small rate that it need not be considered by the cathode engineer."

5.5 Distribution of Cathode Temperature as a Function of Axial Distance Along the Cathode

It has been observed that at a fixed value of anode current, the resistance of the cathode of the microwave oven magnetron during operation remains nearly unchanged as the power from the external heater supply is raised from zero power to the level at which it is operated in the microwave oven application. The constant resistance implies that the cathode temperature remains the same and that is consistent with the observation that there is an automatic mechanism that supplies the cathode with just enough backbombardment power to heat the cathode hot enough to supply the primary emission. However, it is well known that the use of external heater power makes the tube have a large amount of background noise. It had been assumed earlier that the external heater power resulted in a much higher cathode temperature and that it was the excess number of electrons that were emitted that produced the noise.

Although the cathode resistance measurements are an indirect method of indicating that the cathode temperature as a whole has not changed, direct measurements by the optical pyrometer confirm that there is little difference in cathode temperature between external heater power all the way off and all the way on. It therefore appears that there is a more subtle mechanism having to do with temperature distribution along the cathode that leads to noise when the heater power is turned on.

The purpose of this section is to document observations of distribution of temperature along the cathode with the tube operating normally with the external source of filament power turned off, and with the tube not operating at all but with the external heater power turned on. Unfortunately, no data were taken in the axial distribution of temperature with the external source of filament power on and the tube operating. The data that were taken are shown in Figure 5-10.

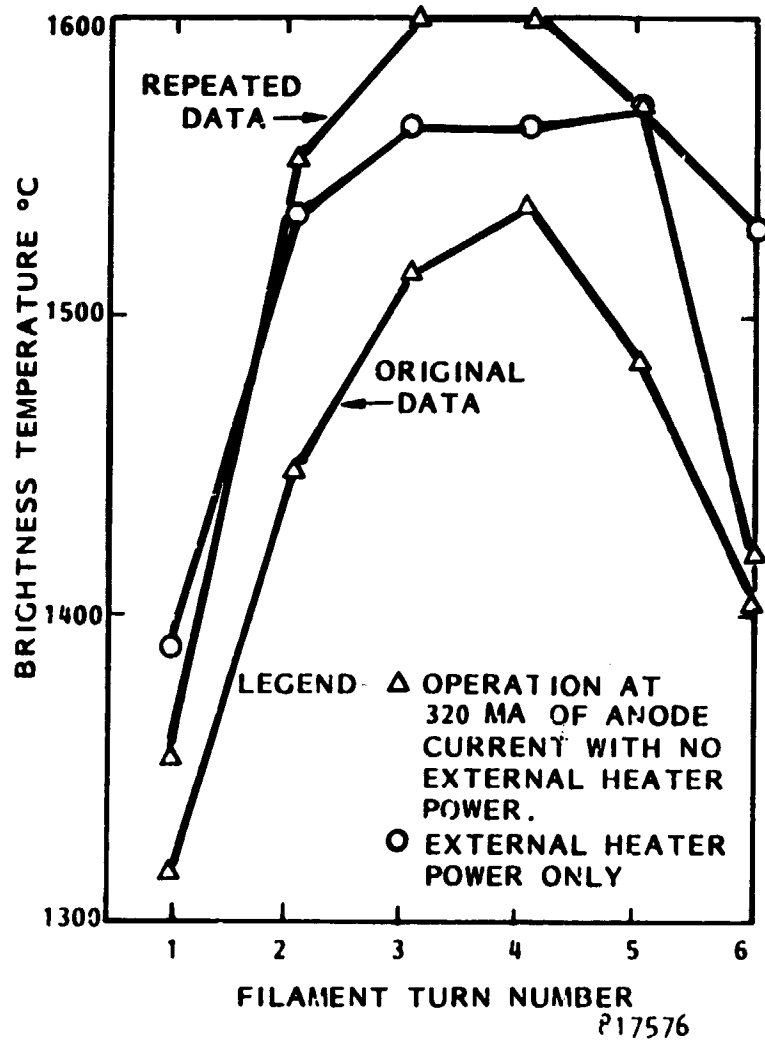


Figure 5-10. Distribution of Temperature Along Filament.

Several things may be noted from the data. The first of these is that there were two sets of data taken for the tube operating and the external source of heater power removed. The two sets of data were taken at two different times, separated by eight days and the higher temperature of the second set may reflect a deterioration or poisoning of the filament, as discussed further in Section 5.6. However, both of these sets of data show a much higher temperature gradient from the center of the filament to the ends than if only external heater power is supplied to the tube.

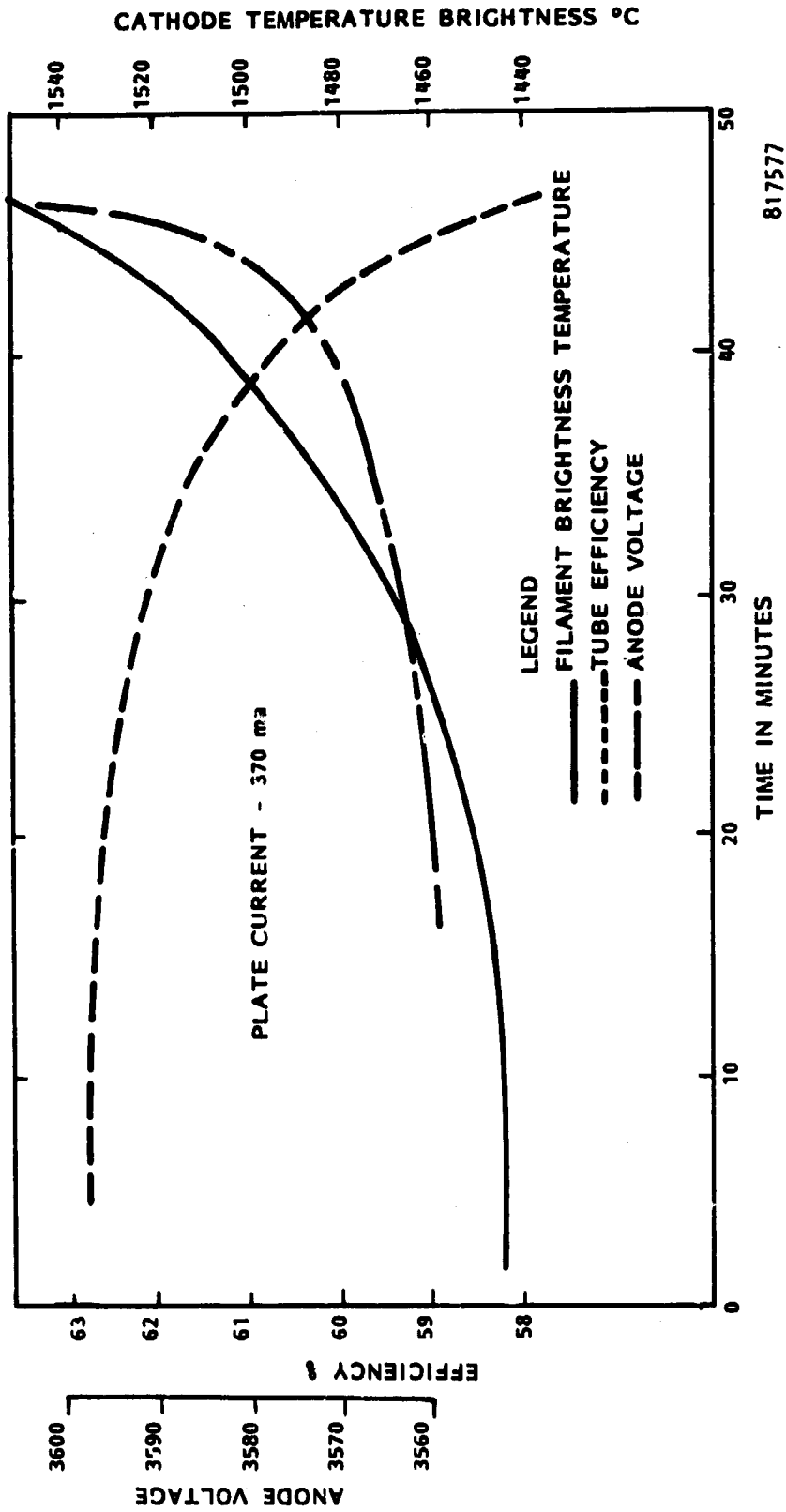
In the case of the tube operating on backbombardment alone, the temperature of the two center turns of the filament is considerably hotter than the adjacent turns, - so much so that with the use of the Richardson-Dushman relationship of Figure 5-4 the emission from the center turns would be double that from the adjacent turns and four to six times that of the next turns. This distribution suggests that most of the magnetron operation occurs near the center of the tube, when backbombardment alone heats the cathode. However, when external heater power is applied, the end turns are relatively hotter, and this has the effect of providing more primary emission from the end turns of the filament.

5.6 Observations of the Impact of Cathode Poisoning upon Cathode Operating Temperature and Tube Efficiency

An unexpected and to some extent an unwelcome experience with the tubes that had windows in them for optical viewing of the filament was that the tubes were "gassy". By that is meant that the tubes had a large amount of residual gas in them. The unwelcome experience was that the gas would poison the cathode so that after a period of operation the tube performance would deteriorate, and the tube would have to go through a "soak" in which the filament is kept hot but no anode current is drawn. During the soak the gas is driven from the cathode and deposited on the anode surface from which it diffuses into the copper for a short distance. When the tube is operated again the anode heats up slightly

and the gas again migrates to the cathode to recycle the poisoning. It was later observed that the tube on which data was taken and which will be reported upon in this section has an unflashed getter. The purpose of the getter when flashed is that it absorbs most of this residual gas.

However, the observation of what happens to the temperature of the cathode, the efficiency, and the anode voltage as a function of time during the operation of the tube is of considerable interest. As shown in Figure 5-11, the tube after a "soak" period operates with a nearly constant filament temperature which is quite low and the efficiency is high. However, as time proceeds portions of the filament are poisoned by the gas so that the remainder of the cathode must supply the emission and it can only do so if the filament is hotter. The automatic mechanism of the tube then causes the backbombardment power to increase to heat the cathode to a higher temperature. The anode voltage then starts to increase and the efficiency decreases, caused in part by the additional backbombardment power that is needed. The deterioration process then increases rapidly and finally a point is reached where the tube can no longer sustain itself with the increased backbombardment power required and the tube ceases to operate.

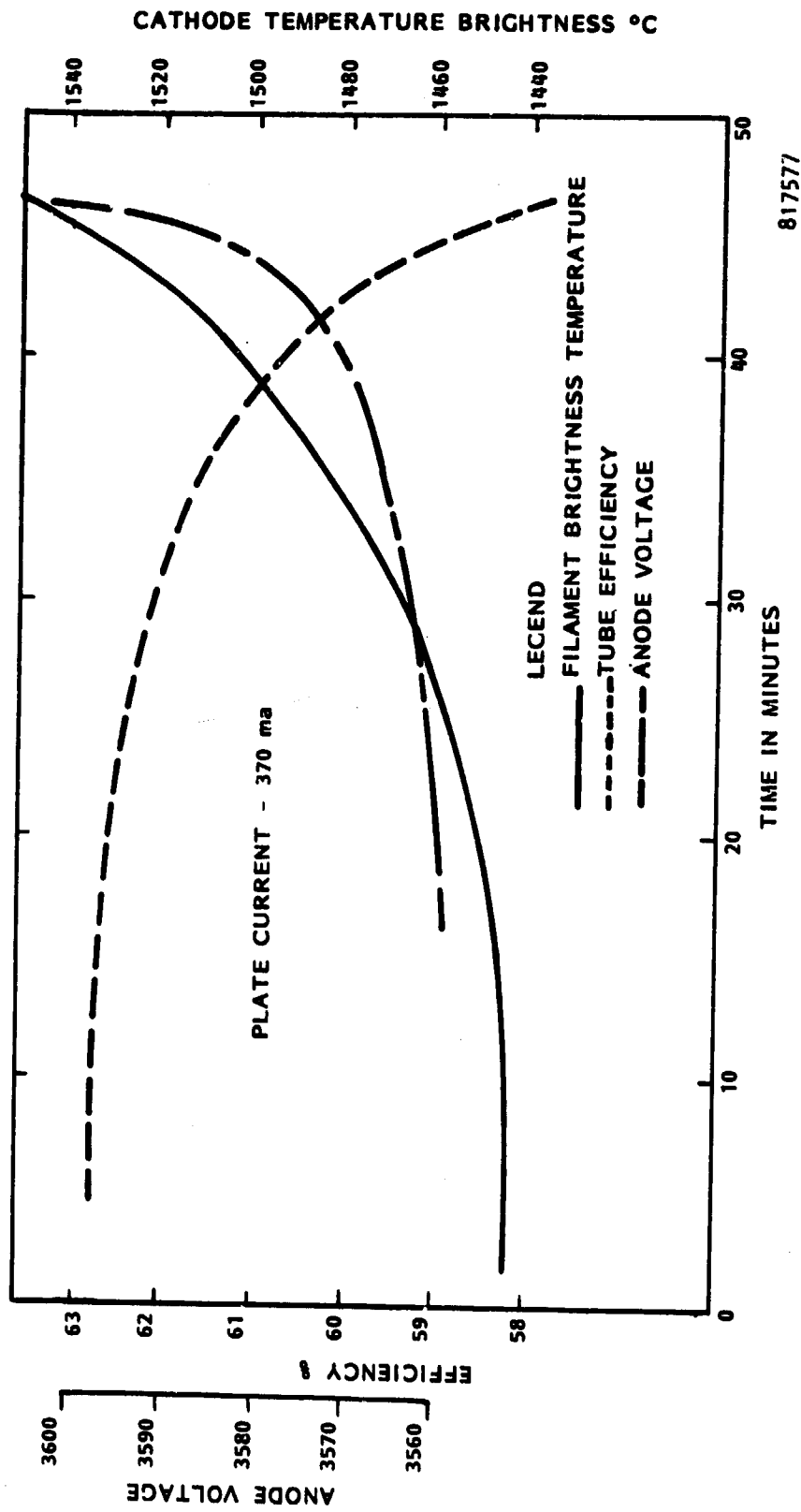


817577

Figure 5-11. Impact of Gas Poisoning on Filament Temperature, Tube Efficiency, and Anode Voltage as Function of Operating Time.

and the gas again migrates to the cathode to recycle the poisoning. It was later observed that the tube on which data was taken and which will be reported upon in this section has an unflashed getter. The purpose of the getter when flashed is that it absorbs most of this residual gas.

However, the observation of what happens to the temperature of the cathode, the efficiency, and the anode voltage as a function of time during the operation of the tube is of considerable interest. As shown in Figure 5-11, the tube after a "soak" period operates with a nearly constant filament temperature which is quite low and the efficiency is high. However, as time proceeds portions of the filament are poisoned by the gas so that the remainder of the cathode must supply the emission and it can only do so if the filament is hotter. The automatic mechanism of the tube then causes the backbombardment power to increase to heat the cathode to a higher temperature. The anode voltage then starts to increase and the efficiency decreases, caused in part by the additional backbombardment power that is needed. The deterioration process then increases rapidly and finally a point is reached where the tube can no longer sustain itself with the increased backbombardment power required and the tube ceases to operate.



817577

Figure 5-11. Impact of Gas Poisoning on Filament Temperature, Tube Efficiency, and Anode Voltage as a Function of Operating Time.

6.0 OPERATION OF THE MICROWAVE OVEN MAGNETRON AT HIGH EFFICIENCY AND POWER LEVEL

6.1 Introduction and Engineering Approach to High Efficiency

This section is devoted to special tests that were run on a microwave oven magnetron in an attempt to maximize the efficiency output of the tube. The maximum overall efficiency that was obtained was 81.7%. The corresponding DC to microwave conversion efficiency was computed to be 87.5% after making allowance for losses caused by circuit inefficiency and backbombardment power for heating the cathode, since no external filament power source was used. Special test arrangements and procedures were used to maximize the confidence in the accuracy of the efficiency measurement.

High efficiency is of great importance in microwave power transmission applications in space where the inefficiency of operation is of primary concern because it represents heat that has to be disposed of by radiation into space, which requires a large expanse and mass of radiating surface.

Although there are many factors which can degrade the efficiency of crossed-field devices and have to be considered, it has been found necessary to operate them at high magnetic fields to maximize the efficiency. This is in accord with theory which indicates that the conversion efficiency of DC power into microwave power, η , should follow the relationship:

$$\eta = \frac{V_h - V_o}{V_n} = \frac{\frac{2B}{B_o} - 2}{\frac{2B}{B_o} - 1} \quad (6-1)$$

where V_h is the operating voltage, B is the applied magnetic field, and V_0 and B_0 are magnetron design parameters. The relationship between the four parameters is:

$$V_h = V_0 (2 B/B_0 - 1) \quad (6-2)$$

In the microwave oven magnetron V_0 is 464 volts and B_0 is 384 gauss. A typical operating value of B is 1760 gauss which results in an operating voltage of 3800 volts. The corresponding theoretical DC to microwave conversion efficiency as given by 6-1 is 88%. To obtain the overall efficiency of the tube, the conversion efficiency must be adjusted for the amount of microwave power that is lost in supplying energy to backheat the cathode and for the circuit losses inside the tube. But obviously the overall efficiency will be higher if the DC to rf conversion efficiency is higher and this can be theoretically achieved by operating at a higher magnetic field. Doubling the magnetic field, for example, would increase the theoretical conversion efficiency from 88% to 94%.

For several practical reasons microwave oven magnetrons are not operated with such high values of magnetic field, but in an application of microwave power transmission, where the highest efficiency is of great importance, operation at these high fields is of great interest. In the SPS application, for example, it is the inefficiency that is of prime interest since this represents heat that must be dissipated by direct radiation into space, as previously mentioned. An 80% efficient tube, for example, will have to dissipate 2.25 times as much power as a 90% efficient tube to radiate the same amount of rf power. Examining the efficiency of the microwave oven magnetron at higher magnetic fields was therefore felt to be of importance in enlarging the data bank of information related to microwave power transmission systems.

6.2 Test Arrangements and Test Results

To carry out this test, a Raytheon magnetron was stripped of its permanent magnets, fitted with a water jacket, and placed into a solenoid magnet so that the magnetic field could be varied. A region of high magnetic field and accompanying high voltage operation was explored with the result that overall efficiencies of as high as 81.7% were achieved. These higher efficiencies were obtained with operating voltages as high as 7500 volts, plate currents as high as 600 milliamperes, and power outputs in excess of three kilowatts. The data in graph form is shown in Figure 6-1. Data is given in tabular form for the highest value of magnetic field employed in Table 6-1.

Special arrangements for measuring output power and dissipated power were made because confidence in efficiency measurements is always a cause for concern in measurements of this type. Confidence in the use of directional couplers and power meters alone is impaired by the accuracy of calibration which for a 50 dB coupler is no better than $\pm 2\%$, and by their frequency sensitivity, particularly to any harmonics. The other approach of measuring the temperature rise of a given volume of water flowing through a thermocouple bridge depends upon an accurate measurement of the water flow, as well as upon the calibration of the thermocouple output in terms of temperature rise. However, the method is insensitive to small amounts of power at other frequencies. Thus, by flowing the water in series through the water load and through a water jacket surrounding the tube, the ratio of useful power output to dissipated power in the tube can be obtained independent of the rate of water flow and independent of errors in the temperature calibrating equipment, if the thermocouple bridges are calibrated with the same equipment. This method is shown schematically in Figure 6-2.

Because this method measures the useful microwave power output as well as the dissipated power, it is possible to add these powers and check their sum against the amount of DC power into the magnetron. This check, of course, depends upon an accurate measurement of water flow and such secondary

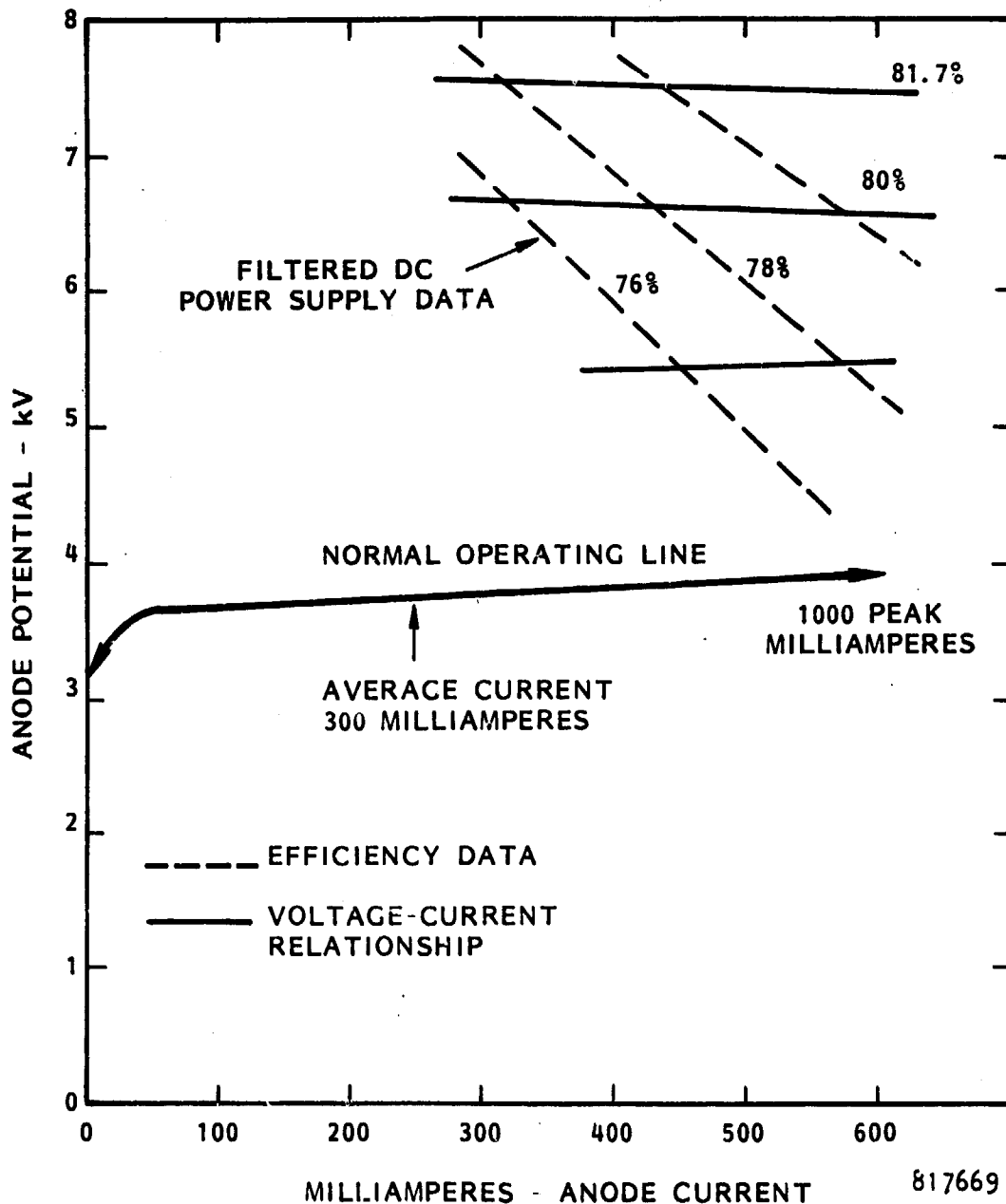
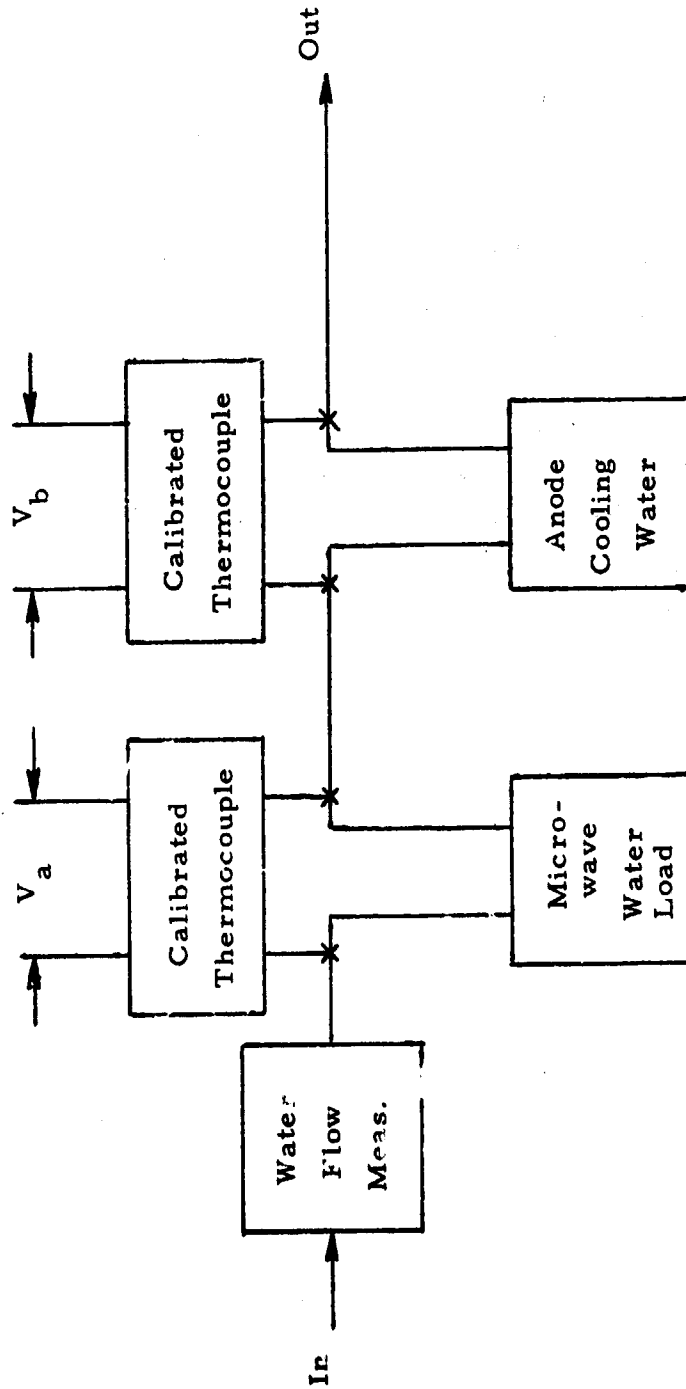


Figure 6-1. Operation of conventional microwave oven magnetron at high magnetic field and voltages on a well-filtered DC power supply. At high voltages and currents, overall efficiency reached 81.7%. Also shown on the chart is the normal operating line for the magnetron which is required in its normal operation to alternate between a peak current of over 900 milliamperes and zero current at a sixty Hz rate.

TABLE 6-1

C S	DC Input			Power Output			Efficiency By Expression (6-1)	Power Balance By Expression (6-2)	
	Anode Current ma	Anode Voltage Volts	DC Power Input Watts	RF Output Watts	Dissipated Power Watts	Total Power Output Watts			Power Output Corrected for Water Temp. Watts
	305	7564	2307	1756	503	2259	2292	77.7	+0.0065
	406	7493	3042	2359	609	2968	3012	79.5	+0.0098
	504	7490	3774	3036	710	3746	3802	81.0	-0.0074
	601	7462	4484	3589	803	4392	4457	81.7	+0.0058
	601	7439	4470	3614	705	4419	4485	81.8	-0.0033

*B/Bo = 7.62



$$\text{Magnetron Efficiency} = \frac{V_a}{V_a + V_b}$$

Figure 6-2. Water flow schematic for eliminating water flow rate and absolute temperature calibration of thermocouples as variables in the measurement of efficiency.

factors as the difference in temperature of the cooling water used in the experiment and that used to calibrate the thermocouples, since the output of the thermocouples is slightly non-linear with respect to temperature. The error caused by the temperature difference in this case was approximately 1.5% in the direction that minimized the power measurement. After a correction of 1.5% was made, the total power output balanced the total power input to within 1%. The DC current and DC voltage were read digitally to better than 0.1% and the voltage and current readings were calibrated by the Standards Department to within 0.2%.

The set of numbers taken from Table 6-1 for a typical high efficiency measurement follows:

- Operating current = 0.601 amperes
- Operating voltage = 7462 volts
- DC power input = 4484 watts
- Power measured in water load - 3589 watts
- Power dissipated in magnetron cooling jacket = 803 watts
- Total measured power output (3589 plus 803) = 4392 watts
- Measured power output corrected for cooling water temperature = $4392 \times 1.015 = 4458$ watts

If the efficiency is computed as

$$\text{then efficiency} = \frac{\text{Power in Water Load}}{\text{Power in Water Load} + \text{Dissipated Power}} = \frac{3589}{3589 + 803} = 81.7\% \quad (6-1)$$

The power balance is defined as

$$\frac{\text{Measured Dc Power Input} - \text{Measured Total Power Output}}{\text{Measured DC Power Input}} \quad (6-2)$$

$$\frac{4484 - 4458}{4484} = 0.0058 = 0.58\%$$

The combined circuit efficiency of the magnetron and the external coupling transition into the water load as seen at the water load flange and as carefully measured by standing wave detector was found to be 94.8%. The corresponding electronic efficiency of the tube would therefore be 81.7/94.8 or 86%.

Electronic efficiency defined in this fashion absorbs the energy required to heat the cathode to the proper emission temperature, since there was no source of external heater power during these measurements. All the power required to heat the cathode comes from microwave energy and must therefore be equated to at least that amount of rf energy. The estimated power to heat the cathode is estimated to be 50 watts, which represents at least 1.5% of the microwave power generated so that the conversion efficiency of DC power into microwave power is at least 87.5%.

This 87.5% efficiency is considerably lower than would be predicted from the relatively high magnetic field that was used. The V_h/V_o ratio was 16.4, which would indicate a theoretical efficiency of 93.8%. While a theoretical number is always open to question, it is a fact that a commercially available magnetron operating at 915 MHz and with about the same V_h/V_o ratio exhibits a DC power to rf power conversion efficiency of 93%.

This "missing" 6% of conversion efficiency in the microwave oven magnetron is not a new discovery; more than this amount of conversion efficiency seems to be missing at the normal operating point of the tube. This is shown

in Figure 6-3, where the theoretical DC to rf conversion efficiency and several experimentally observed points are plotted as a function of the B/B_0 ratio.

Also shown in Figure 6-3 is the 8684 magnetron in which 93% DC to microwave conversion efficiency has been observed. The 8684 magnetron is unusual in that the observed efficiency agrees with the predicted efficiency. In general, as shown in Figure 6-3 the observed efficiency of various crossed-field devices is below the theoretical efficiency. The microwave oven magnetron at its normal operating value of magnetic field is considerably below the theoretical.

It is not the primary function of this contract to examine the causes of inefficiency or to attempt to improve the efficiency by changing the tube design. However, it is known from other sources that the microwave field pattern in the cathode to anode interaction area of the microwave oven tube has a considerable amount of the type of contamination that has been correlated with efficiency degradation in other magnetron types.

7.0 DESIGN, CONSTRUCTION, AND EVALUATION OF A THIN-METAL LOW-COST, LOW-LOSS S-BAND SLOTTED WAVEGUIDE ARRAY.

7.1 Introduction

There is general agreement that the best approach to the transmitting antenna portion of a microwave power transmission system is an active array that is composed of modules whose output phase is orchestrated by means of the retrodirective array principle. Until recently the cost of such an array has been difficult to estimate and this situation had been a deterrent to planning activity associated with applications of microwave power transmission. It is now clear that the microwave power generation portion of the transmitter can use the microwave oven magnetron, whose cost and that of the associated DC power supply can be accurately estimated. However, there had been a very broad range of estimates on the cost of the slotted waveguide antenna modules because it was not known how they would be fabricated. It is believed that problem has now been resolved with the development that will be discussed in this section. Fortunately the method of fabrication indicates that the cost of the slotted waveguide array will be on the low side or even below the previous lowest estimates for the array.

The development that will be discussed in this section may be considered a joint effort of JPL and the Raytheon Co. The electrical design of the slotted waveguide array module is essentially that of JPL. The basic fabrication method is one that Raytheon had previously conceived and which had been pursued to the point of some preliminary forming of the thin sheet metal which is a basic feature of the fabrication.

Tests of the finished product were made by both Raytheon and JPL. Lacking an antenna test range that could be made available for testing the antennas, the Raytheon approach consisted of a special arrangement in which the phase and the amplitude of the output of each slot was measured in the immediate

area of the slot. From this data an estimate of scatter losses of 2.5% could be made based upon the 8.9% value of the mean square phase deviation. The JPL tests consisted of field patterns obtained on their test range. Although the field patterns were quite symmetrical, the predicted gain was considerably less than expected. Judged on the basis of gain alone the efficiency was only 70%.

Several causes for this low efficiency were subsequently considered. One suggested cause was the edge effects of the array so that it could not be treated as a uniformly illuminated area equal to the physical dimensions of the array. Another was that the energy scattered by the array was considerably larger than the Raytheon data would indicate, reflecting doubt as to the validity of the Raytheon testing approach - certainly a possibility. A third was that the I^2R losses in the array as constructed were much higher than anticipated.

This latter suggestion was made at the SPS workshop in Houston and although primarily pointed at losses that might occur in that particular array because of its welded construction, there was the impression left in the minds of some that the 98% slotted waveguide efficiency given in the overall efficiency budget of the SPS microwave power transmission system might be highly suspect. For this reason a special test was run at Raytheon in which the heating losses caused by any skin losses in the antenna were actually measured. That test and the results which indicated that the losses were well less than 2% are included in this section.

7.2 Basic Approach to the Fabrication Method

The proposed method for slotted waveguide array fabrication is shown in Figure 7-1. The design consists basically of a folded top plate whose corrugations contribute the three sides of the waveguide and a bottom into which the radiating slots are punched. The two sections then flow together and are joined to each other either by resistance spot welding or by laser beam welding to form the finished assembly shown in Figure 7-1.

7.0 DESIGN, CONSTRUCTION, AND EVALUATION OF A THIN-METAL LOW-COST, LOW-LOSS S-BAND SLOTTED WAVEGUIDE ARRAY.

7.1 Introduction

There is general agreement that the best approach to the transmitting antenna portion of a microwave power transmission system is an active array that is composed of modules whose output phase is orchestrated by means of the retrodirective array principle. Until recently the cost of such an array has been difficult to estimate and this situation had been a deterrent to planning activity associated with applications of microwave power transmission. It is now clear that the microwave power generation portion of the transmitter can use the microwave oven magnetron, whose cost and that of the associated DC power supply can be accurately estimated. However, there had been a very broad range of estimates on the cost of the slotted waveguide antenna modules because it was not known how they would be fabricated. It is believed that problem has now been resolved with the development that will be discussed in this section. Fortunately the method of fabrication indicates that the cost of the slotted waveguide array will be on the low side or even below the previous lowest estimates for the array.

The development that will be discussed in this section may be considered a joint effort of JPL and the Raytheon Co. The electrical design of the slotted waveguide array module is essentially that of JPL. The basic fabrication method is one that Raytheon had previously conceived and which had been pursued to the point of some preliminary forming of the thin sheet metal which is a basic feature of the fabrication.

Tests of the finished product were made by both Raytheon and JPL. Lacking an antenna test range that could be made available for testing the antennas, the Raytheon approach consisted of a special arrangement in which the phase and the amplitude of the output of each slot was measured in the immediate

area of the slot. From this data an estimate of scatter losses of 2.5% could be made based upon the 8.9% value of the mean square phase deviation. The JPL tests consisted of field patterns obtained on their test range. Although the field patterns were quite symmetrical, the predicted gain was considerably less than expected. Judged on the basis of gain alone the efficiency was only 70%.

Several causes for this low efficiency were subsequently considered. One suggested cause was the edge effects of the array so that it could not be treated as a uniformly illuminated area equal to the physical dimensions of the array. Another was that the energy scattered by the array was considerably larger than the Raytheon data would indicate, reflecting doubt as to the validity of the Raytheon testing approach - certainly a possibility. A third was that the I^2R losses in the array as constructed were much higher than anticipated.

This latter suggestion was made at the SPS workshop in Houston and although primarily pointed at losses that might occur in that particular array because of its welded construction, there was the impression left in the minds of some that the 98% slotted waveguide efficiency given in the overall efficiency budget of the SPS microwave power transmission system might be highly suspect. For this reason a special test was run at Raytheon in which the heating losses caused by any skin losses in the antenna were actually measured. That test and the results which indicated that the losses were well less than 2% are included in this section.

7.2 Basic Approach to the Fabrication Method

The proposed method for slotted waveguide array fabrication is shown in Figure 7-1. The design consists basically of a folded top plate whose corrugations contribute the three sides of the waveguide and a bottom into which the radiating slots are punched. The two sections then flow together and are joined to each other either by resistance spot welding or by laser beam welding to form the finished assembly shown in Figure 7-1.

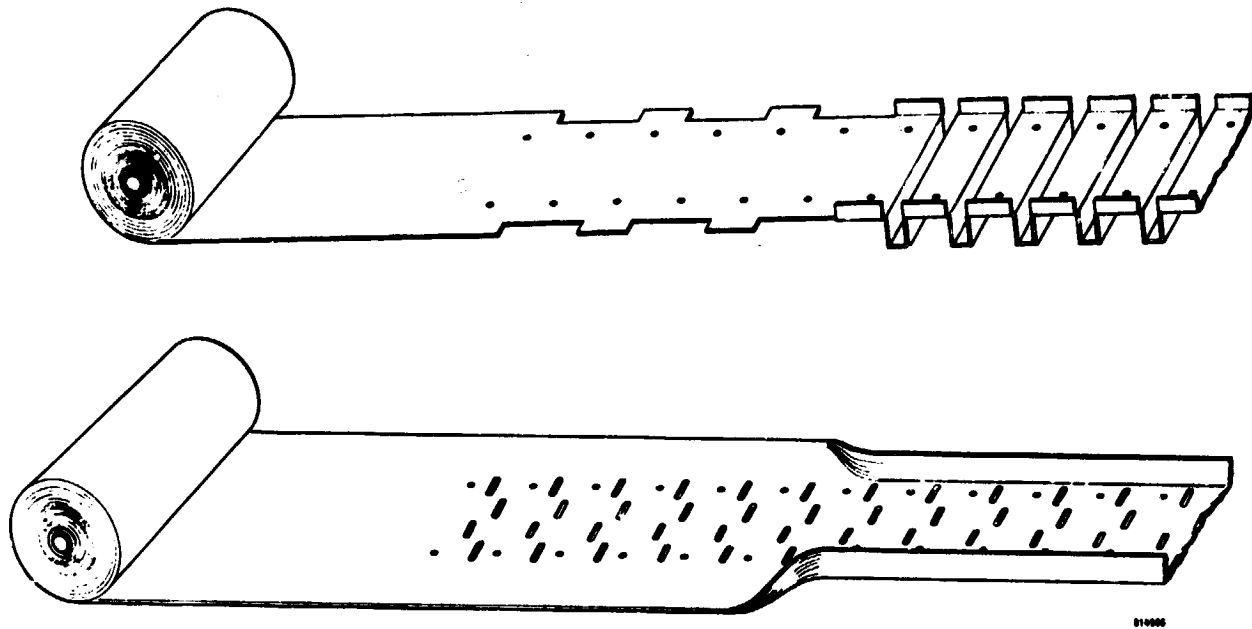


Figure 7-1A.

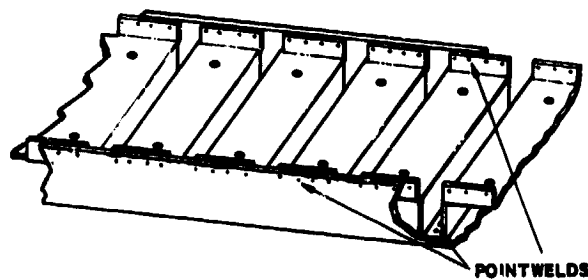


Figure 7-1B.

Figure 7-1. Proposed Method for Precision Forming and Assembly of Low-Cost, Thin-Walled, Slotted Waveguide Arrays for the SPS. Figure 7-1A shows the forming of the top and bottom section. Figure 7-1B shows the assembly of the top and bottom.

The holes which are punched into the material are spaced accurately from each other and serve to accurately locate the material in the bending fixture which is also accurately machined and ground. The holes also serve to jig the top and bottom halves to each other for accurate assembly.

The method as originally proposed by the author utilized a third piece in the assembly that joined the top and bottom at their ends as shown in Figure 7-2. An improvement to simply eliminate the end plate by the upward fold of the end of the top and bottom pieces as shown in Figure 7-1 is the suggestion of R.M. Dickinson.

The variation of the general fabrication procedure that was actually used was that shown in Figure 7-2, because of commitments on tooling and material size that had already been made. But the fabrication method as described in Figure 7-1 appears to be superior in holding close tolerance of construction as well as being lower in cost.

Two 8x8 (8 slots in 8 waveguides) arrays were constructed from 0.020 inch aluminum with the use of temporary tooling of a simple nature. The 1/2 inch separation between waveguides that is necessary in the forming process and which has become attractive as a region in which to mount solid state devices and through which to run cables made it necessary to adjust the dimensional specifications of the JPL design which was designed for a different fabrication method.

The slotted face plate, folded waveguide section, and the end channels were assembled to each other by spot welding. The individual slotted waveguides in the array are fed from a feed waveguide. Transfer of energy is made through diagonal slots between the feed waveguide and radiating waveguides. The feed waveguide is attached to the array by means of pop rivets.

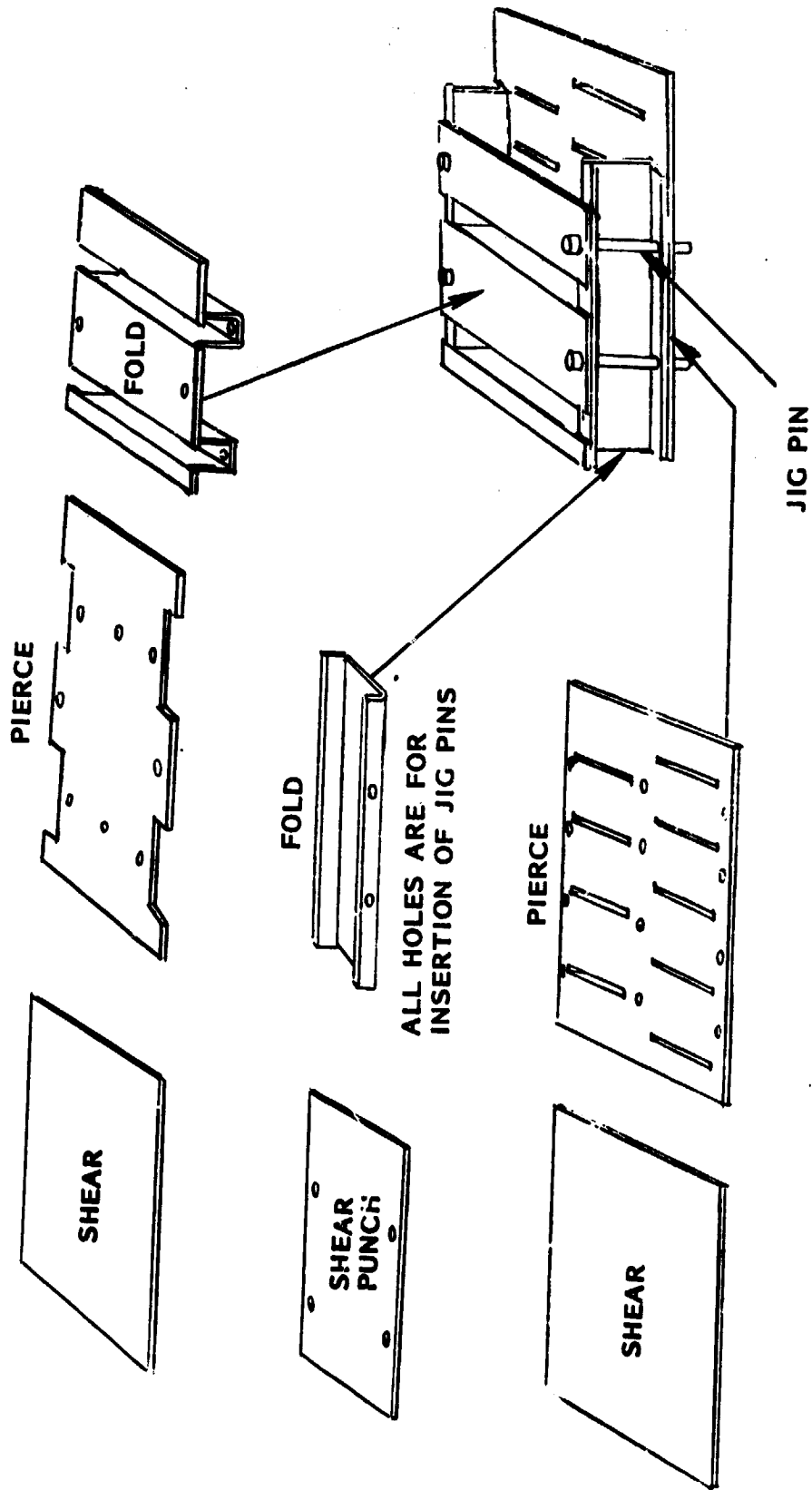


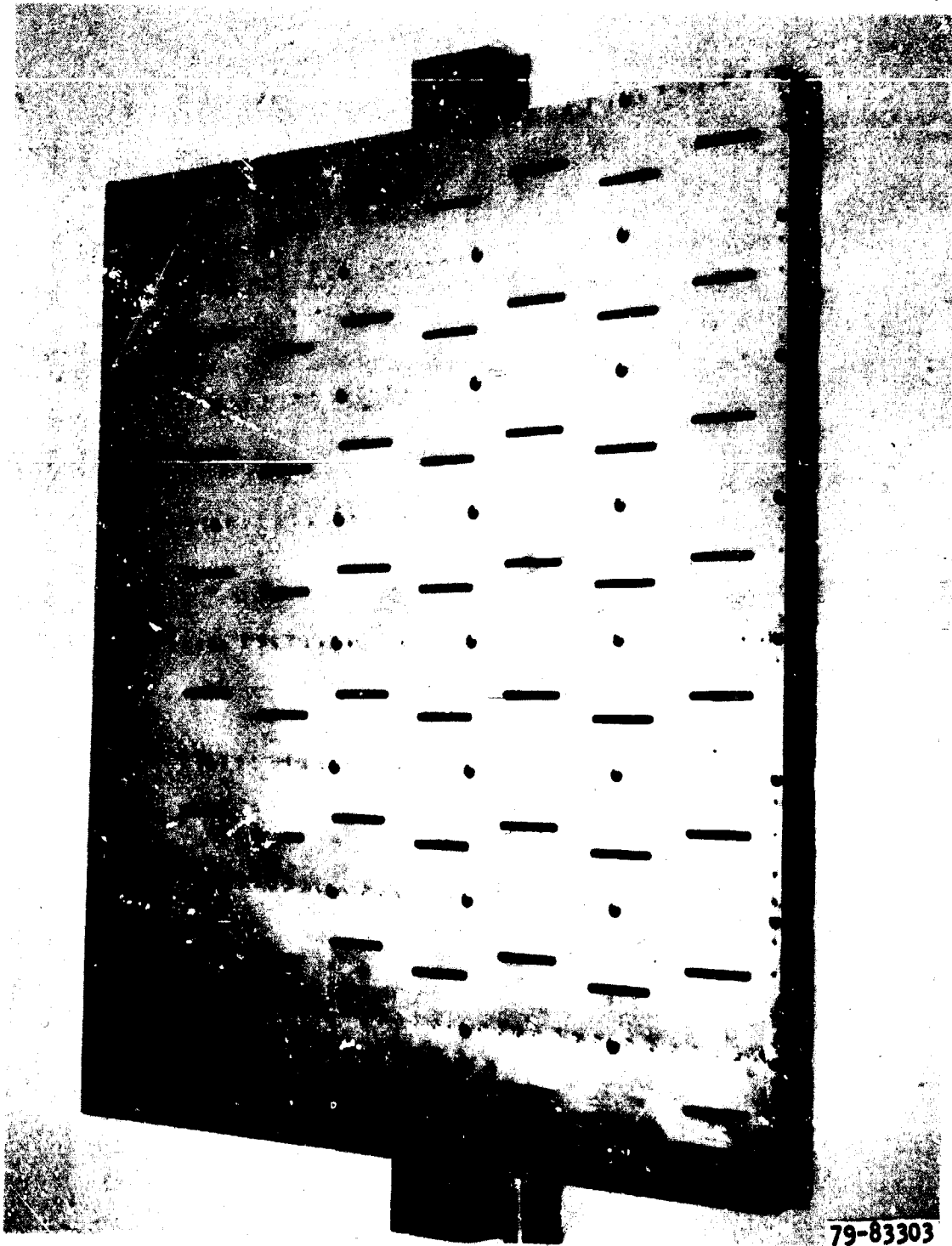
Figure 7-2.

Front and back view of the finished assembly are shown in Figures 7-3 and 7-4, respectively. The arrays are approximately 0.75 x 0.75 meters in size. The finished weight was 3.2 kilograms (7 lbs) or about 5.7 kilograms per square meter.

The resulting product was structurally very stiff and strong even though it was fabricated from 0.020" thick aluminum material which would be considered thin by most standards. A force-deflection curve was performed on an assembly that was two waveguide sections wide. The waveguide "beam" was supported at both ends with the supports 29" apart. The structure was then point loaded at the center with the resulting force deflection curve shown in Figure 7-5. A maximum deflection of 0.136 cm was obtained with the center point loading of 34.5 kilograms. This same deflection would also occur with a total distributed loading of 55.2 kilograms or 368 KG/m^2 (56 lb/ft^2). The maximum deformation would correspond to only 4.1 degrees of phase shift in the radiated power, and it is difficult to imagine a distributed loading equal to 56 lbs per square foot on a flat surface parallel to the earth's surface (the orientation for use in a microwave powered atmospheric platform or for powering a spacecraft from a location near the earth's equator).

7.3 The Electrical Design and Its Development

The electrical design of the slotted waveguide array is based upon the JPL design as shown in Figure 7-6. This design in turn had been scaled (with some changes) from a JPL X-band design that had been built and tested. At the time the 2.45 GHz design was sent to Raytheon, JPL had not yet constructed a model. The design shown in Figure 7-6 would have been used directly for the unit fabricated at Raytheon except that the method of fabrication required a one-half inch separation between the waveguide sticks to permit bonding the top slotted plate to the folded waveguide section. This difference in fabrication techniques made it necessary to change the width of the feed waveguide section. The significant dimensions of the two designs are shown in Table 7-1. The dimensions that are different in the Raytheon design are underlined.



79-83303

Figure 7-3. Front View of the 8x8 Slotted Waveguide Array as Constructed from 0.020 Inch Aluminum Sheet Throughout and Assembled by Means of Spot Welding.

ORIGINAL PAGE IS
OF POOR QUALITY

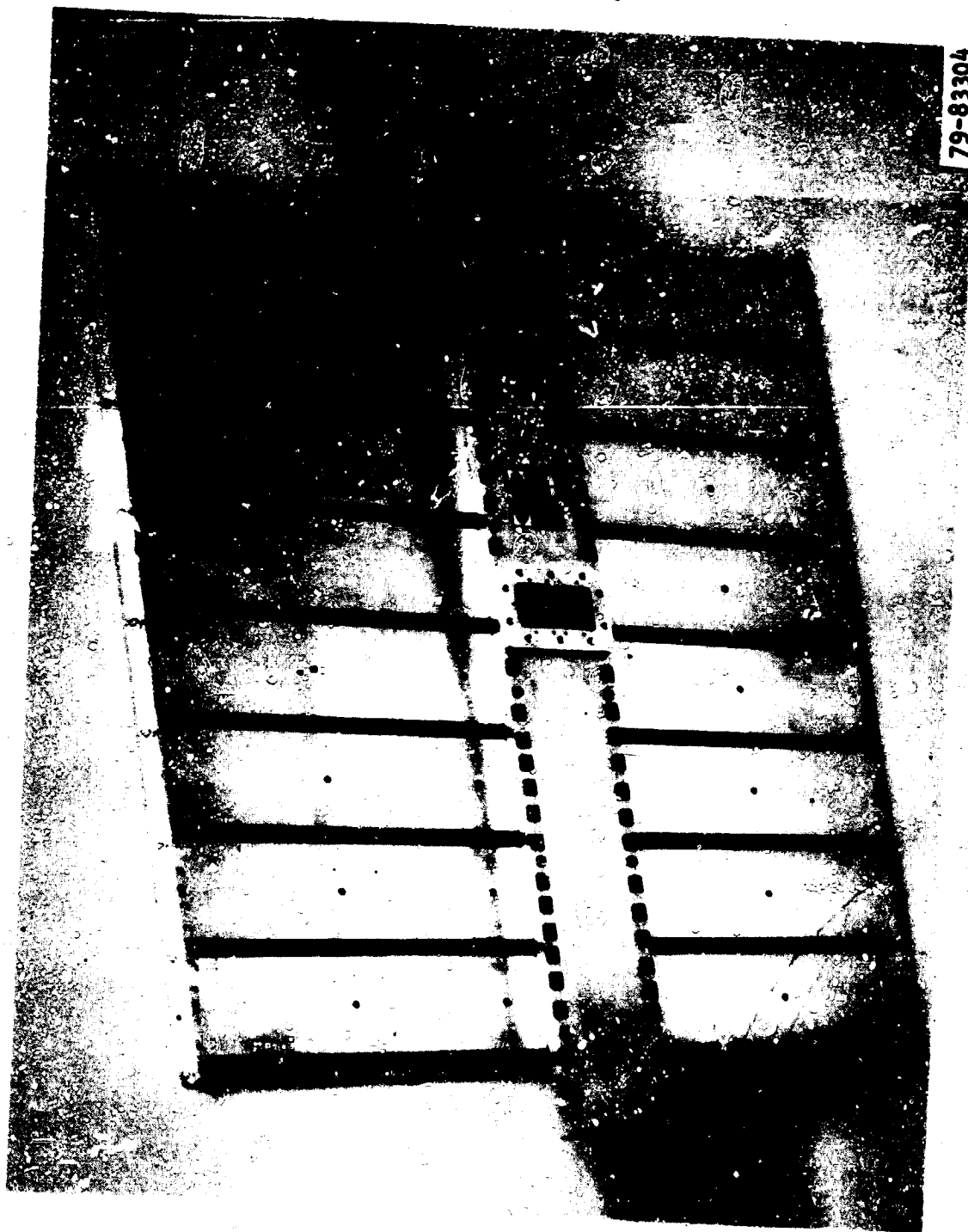


Figure 7-4. Back view of the 8x8 slotted waveguide array as constructed from 0.020" aluminum sheet throughout and assembled by means of spot welding.

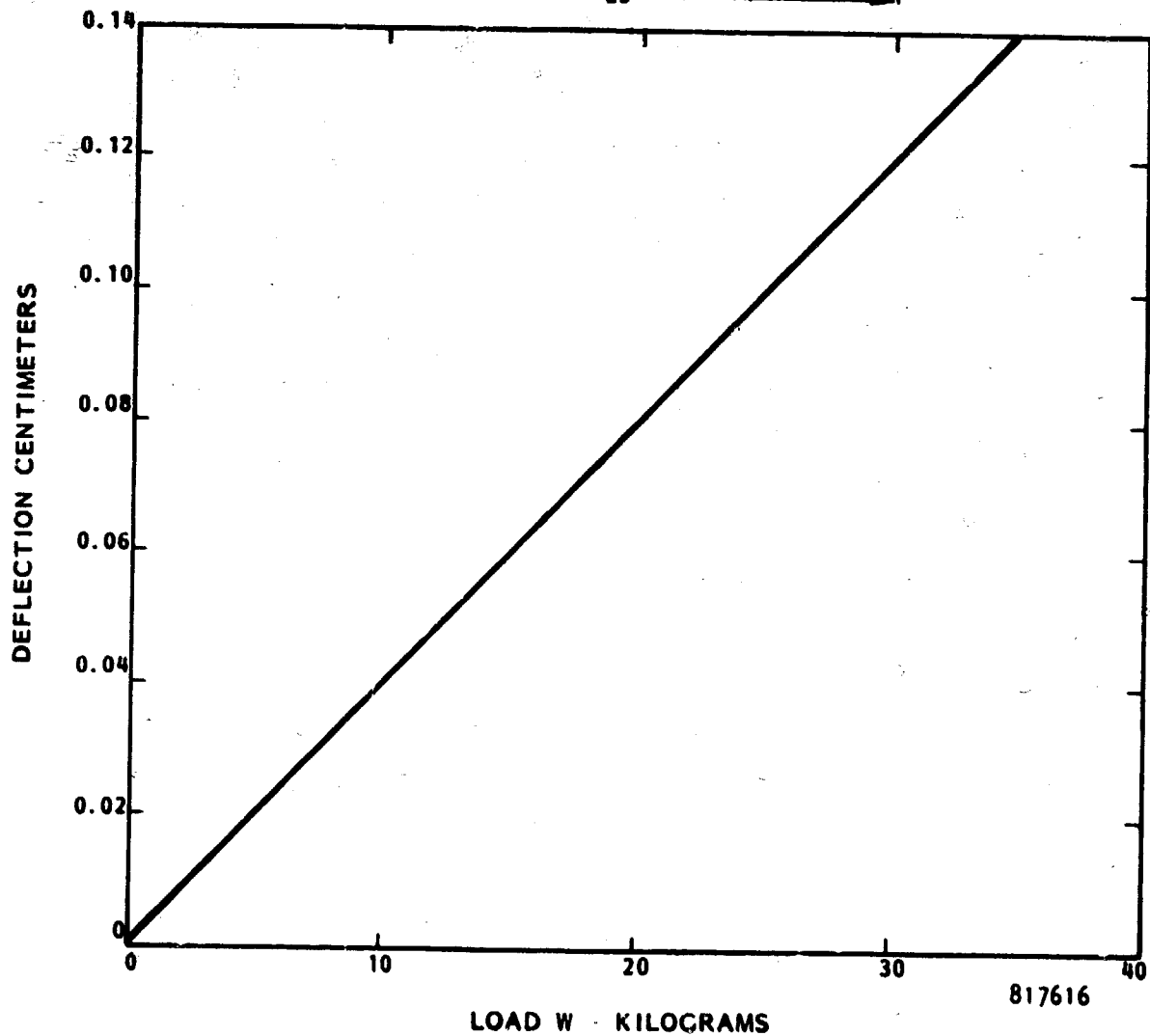
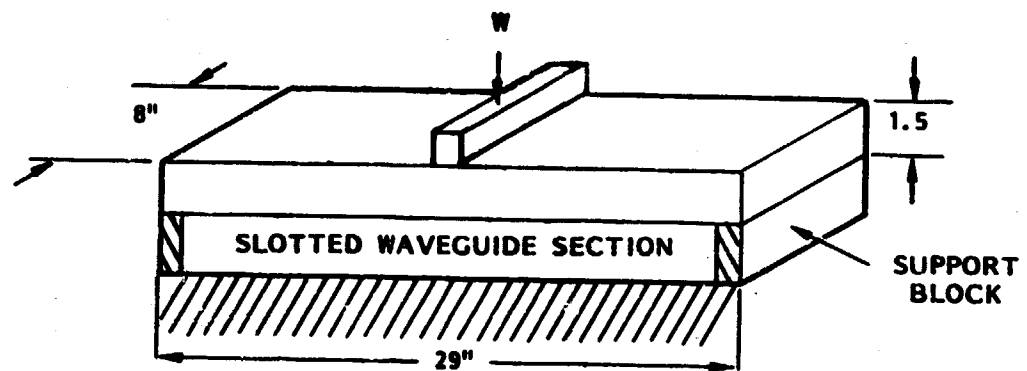
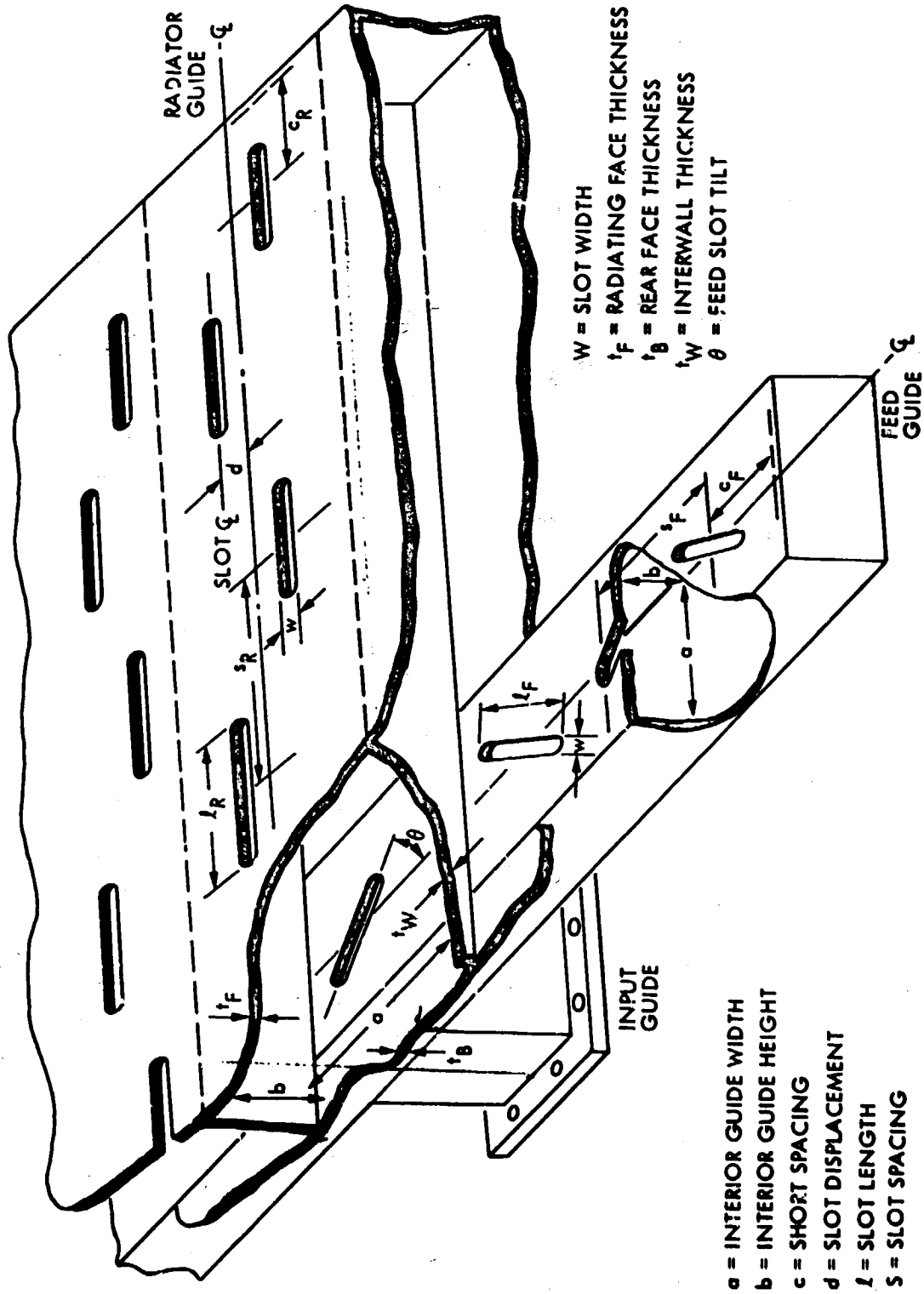


Figure 7-5. Load deflection curve for section of slotted waveguide array made from 0.020" material and spot welded together.



BEAMED RF POWER TECHNOLOGY S-BAND SLOTTED WAVEGUIDE SUBARRAY

PT-5613



- a = INTERIOR GUIDE WIDTH
- b = INTERIOR GUIDE HEIGHT
- c = SHORT SPACING
- d = SLOT DISPLACEMENT
- l = SLOT LENGTH
- s = SLOT SPACING

- w = SLOT WIDTH
- t_f = RADIATING FACE THICKNESS
- t_b = REAR FACE THICKNESS
- t_w = INTERVAL THICKNESS
- θ = FEED SLOT TILT

Figure 7-6.

TABLE 7-1

<u>Item</u>	<u>Description</u>	<u>Original JPL Design</u>	<u>Raytheon Design</u>
a	Interior Radiating Guide Width	3.240"	3.240"
	Interior Feed Waveguide Width	3.240"	<u>3.127"</u>
b	Interior Guide Height	1.440"	1.440"
c_r	Short Spacing	1.800"	1.800"
d	Slot Displacement	0.331"	0.331"
l_R	Slot Length in Radiating Guide	2.274"	2.274"
l_F	Slot Length in Feed Waveguide	2.342"	<u>2.396"</u>
s_r	Slot Spacing	3.600"	3.600"
W	Slot Width	0.1875"	0.1875"
t_f	Radiating Face Thickness	0.1875"	<u>0.020"</u>
t_B	Rear Face Thickness	0.1875"	<u>0.020"</u>
t_W	Internal Wall Thickness	0.360"	<u>0.540"</u> *
O	Feed Slot Tilt	26°	<u>18°</u>

* Includes the spacing of 0.500" between waveguide sections and two wall thicknesses of 0.020" each.

Aside from the change in the width of the feed waveguide, the difference in the thickness of the stock in which the radiating slots were cut was probably the most significant dimensional change from an electrical point of view. The slot length was not changed but subsequent measurements indicated that the slot was not resonant but had a substantial reactive component. One measurement was derived from physically terminating a waveguide standing wave detector with a plate with the radiating slot cut into it. These measurements indicated that the resonant frequency of the slot was 2650 and not 2450, and that therefore the slot should be 0.180" longer. It indicated that the reactive component was equal to the resistive component. Another measurement was made of the impedance of the outboard slot (furthest away from the feed waveguide) of the radiating waveguide by probing the standing wave pattern through a series of probe holes drilled in the waveguide, and noting both phase and amplitude information to make a polar coordinate plot from which the minimum and the standing wave ratio could be accurately ascertained. This measurement gave a ratio of reactive to resistive component of approximately one half. The measurements do not agree and both are subject to measurement error, but both indicate that the slot should be longer.

The resulting reactive load of the waveguide radiating stick presented at the coupling slot between the feed waveguide and the radiating waveguide may have impacted the JPL design values of the angle of the coupling slot and its length. Because it had been anticipated that there could be a change in the angle and length of the coupling slot, the first engineering model of the array was equipped with slotted plates that could be rotated between the feed waveguide and the radiating waveguides as shown in Figure 7-7. A substantial effort was made to find the combination of slot length and rotational angle to establish the desired slot resistance of $0.25 Z_0$ and to minimize the reactive component. The result of this study is shown in Figure 7-8. This data was reviewed and a decision made to set the slot rotation at 18° and to make the slot 2.396" long.



79-82836

Figure 7-7. Engineering model of slotted waveguide array showing provision for rotation of coupling slots and their removal for making change in slot length.

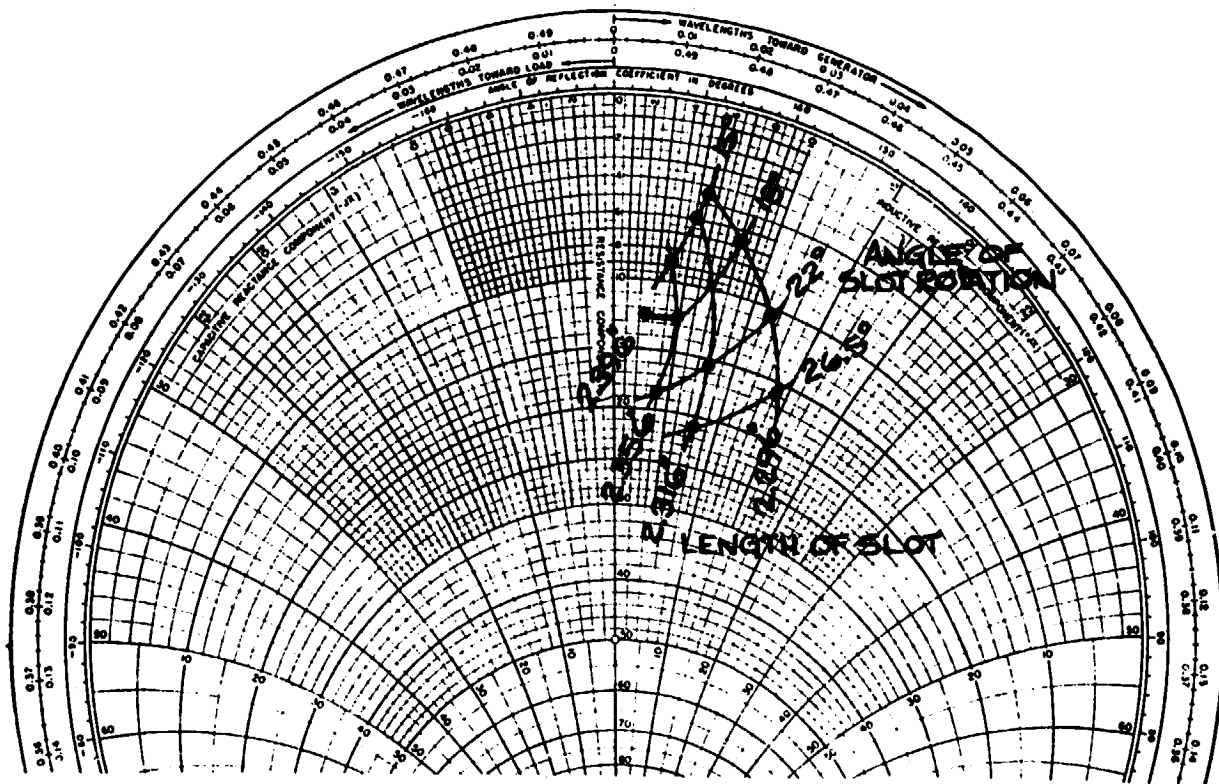


Figure 7-8. Impedance as seen at the center line of coupling slot looking into radiating waveguide as a function of coupling slot rotation and length of coupling slot. Feed waveguide was used as standing wave detector. All coupling slots in feed waveguide were sealed off to set shorting plunger at end of feed waveguide to produce a minimum at center of outboard coupling slot. The shorting tape was then removed from the outboard coupling slot and the measurements made as shown above. Holes in the feed waveguide cover plate that were used to obtain standing wave information are shown in Figure 7-7. Phase information as well as amplitude information was taken when the probe was inserted into the holes to obtain accurate minimum data from plotting phase and amplitude information on polar coordinate paper. Impedance values above have been normalized to the 50 ohm Smith chart paper. Actual values, of course, are related to the characteristic impedance of the feed waveguide.

Although the testing of the 8x8 array had begun with exciting it from one end as shown in Figure 7-7, the arrangement was soon changed to excite the array at the middle which had been the eventual goal. Although some dissymmetry of excitation of the two waveguide radiators in the immediate vicinity of the waveguide T junction was expected, the dissymmetry, if there, is relatively minor.

7.4 Testing Methods and Test Results for the Finished Arrays

As indicated in the Introduction (7.1) tests of the finished product were made by both Raytheon and JPL. The Raytheon testing method and results will be discussed in considerable detail. The JPL tests were made on their antenna range and are included for comparison purposes and documentation.

The Raytheon method that was used for testing the completed arrays originated in response to a need to evaluate the phase and amplitude of the power coming out of each radiating slot in the face of the antenna during the early development phase of the project. The measurement technique is discussed in conjunction with Figure 7-9. The method consists basically of the use of a dipole probe that is visually centered on the slot at a fixed physical distance from it. Readings from the probe are insensitive to any reasonable departure (say a three millimeter deviation) from a visual centering and separation distance, although critical, is kept constant in the sequence of slot measurements by means of a piece of styrofoam placed under the supporting coaxial feedline. Readings can be repeated to within a probable error of one degree in phase and 2% in amplitude.

The validity of the technique was studied to some degree. There is apparently no gross impact of an error signal that might be introduced by an rf signal picked up from other slots and feeding up to the dipole through the supporting line. This conclusion was reached after placing aluminum tape over all of the slots immediately adjacent to the one being measured but leaving several slots open immediately below the support rod for the probe as shown in Figure 7-10. Measurements of the probe pickup were taken with the arrange-

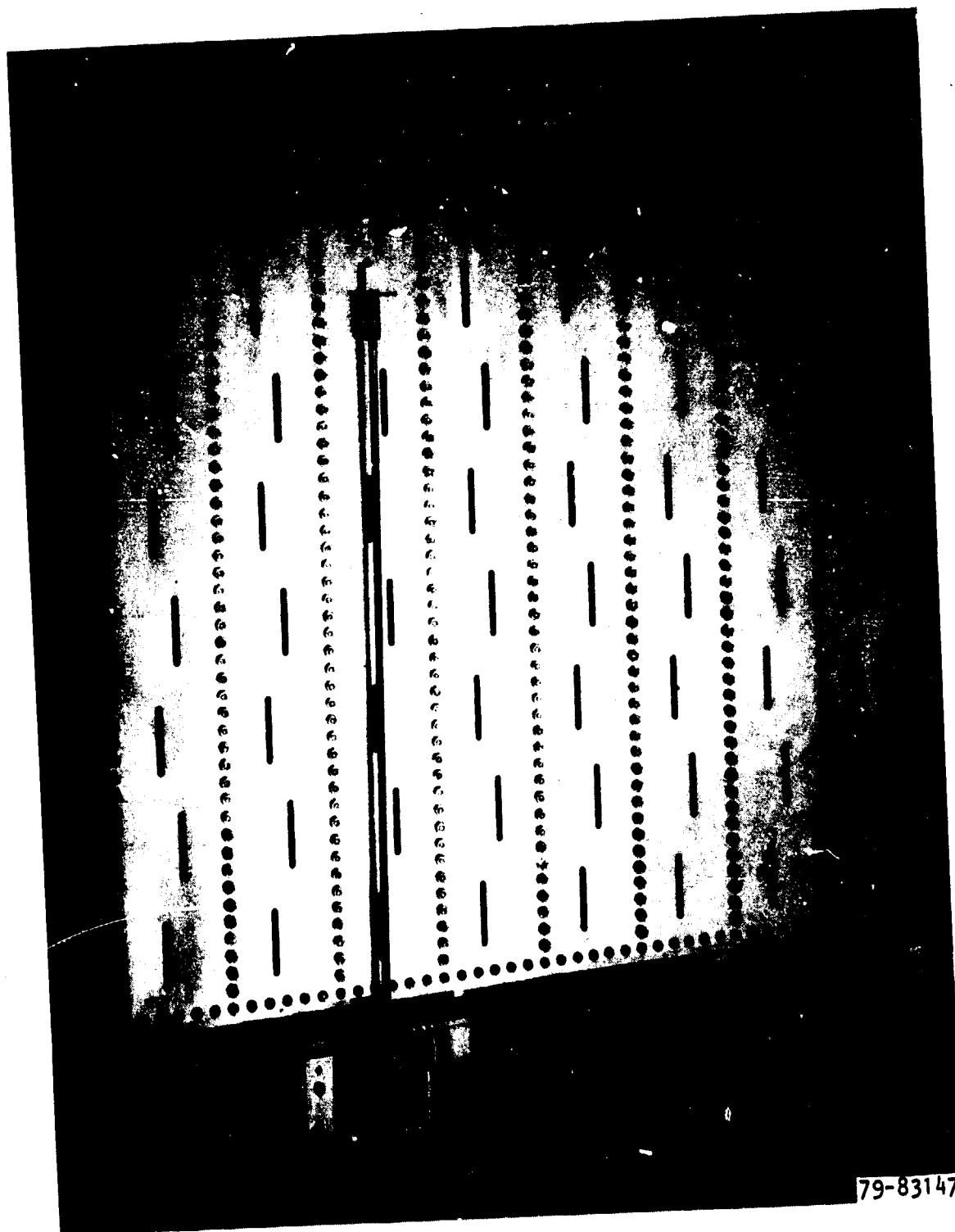


Figure 7-9. Probe arrangement for measuring phase and amplitude of microwave power radiated at individual slots. The phase and amplitude sensed by the probe were compared by means of a Hewlett-Packard network analyzer with the amplitude and phase of the power input to the single waveguide feed to the slotted waveguide array.

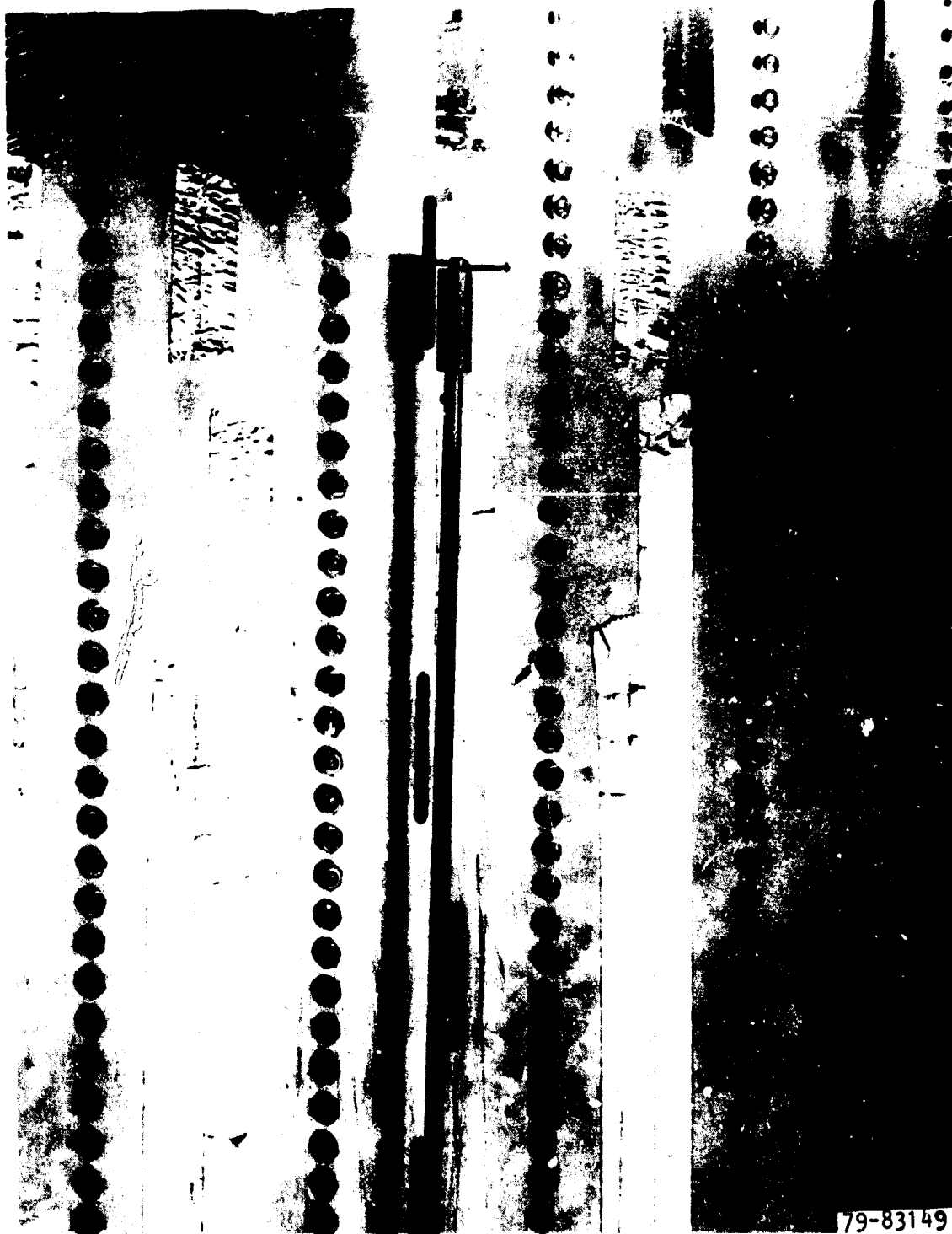


Figure 7-10. Arrangement for checking for any error in phase and amplitude slot measurements introduced by rf pickup of the support rod for probe. Data indicated no significant error was introduced.

ment shown in Figure 7-10, and then the single slot underneath the probe was covered over. The residual pickup of the probe was found to be more than 30 dB below that received with the slot open. This experiment tends to eliminate pickup of microwaves by the support as a source of error in the measurements.

The large size of the dipole undoubtedly disturbs the measurement being made but it should treat all slots the same. Using a shorter probe was prevented because the output of a network analyzer was used to excite the array directly and the probe pickup was therefore relatively weak. The full pickup was needed to provide a reasonably small spot size on the polar plot provided by the network analyzer.

It was logical to use this same equipment for testing the final arrays. The matrix array of amplitude and phase information on the first welded model that was shipped to JPL, designated Array #1, is shown in Figure 7-11.

Assuming the validity of these data, several interesting uses of them can be made. The first of these is that the rms phase deviation of the internal array is 6.22 degrees while the rms phase deviation of the overall array is 8.89 degrees. If the phase deviation is statistically random the inefficiency of the internal array caused by scattering is 1.2% while that of the overall array is 2.4%. The rms of the amplitude variation of the internal array is 0.0628 from a mean value of 0.627. However, it can be shown that the amplitude variation is far from random and that indeed much of it is associated with systematic errors in the placement of the radiating slots (originating from errors in milling the slots in the front plate) from the center of the waveguide.

It is important to understand that the amplitude variation is related to voltage and not to power. The amplitude variation has to be squared in order to compare variations in the power radiating from the slots. The amplitude was read from the radial position of the spot on the oscilloscope of the polar coordinate presentation on the Hewlett Packard network analyzer.

Col \ Row		1	2	3	4	5	6	7	8
1	Phase Amp	105 .53	100 .57	109 .67	110 .70	103 .64	96 .61	93 .62	105 .62
2	Phase Amp	104 .61	84 .51	80 .59	82 .67	91 .71	94 .72	79 .59	90 .40
3	Phase Amp	94 .45	80 .58	88 .63	89 .71	85 .64	85 .58	94 .56	106 .56
4	Phase Amp	105 .61	79 .56	80 .60	73 .73	80 .73	89 .69	72 .65	94 .40
5	Phase Amp	120 .50	81 .60	86 .59	76 .72	70 .68	85 .52	84 .58	120 .50
6	Phase Amp	96 .60	80 .53	74 .57	83 .68	92 .72	90 .69	79 .60	91 .39
7	Phase Amp	89 .49	73 .60	83 .67	82 .69	80 .61	86 .60	91 .54	104 .55
8	Phase Amp	100 .59	86 .60	90 .53	93 .63		96 .70	88 .57	160 .45

Overall array is an 8x8 matrix

"Internal" array is a 6x6 matrix

Coupling slots between feed waveguide and radiating waveguides are 2.396 inches long and are rotated to an angle of 18° from the feed waveguide longitudinal axis.

Test data obtained by dipole probe placed on front of each radiating slot.

RMS of phase deviation of internal array is 6.22°.

RMS of phase deviation of overall array is 8.89°.

RMS of amplitude variation of internal array is 0.0628 from a mean value of 0.627.

Figure 7-11. Matrix Array of Amplitude and Phase Information on Thin Metal Slotted Array #1.

It is interesting to observe that the variation in measurements of amplitude from one slot to the next along the two outside waveguides is definitely correlated with the distance of the slots from the outside edge of the array. The data show that the outside slots radiate less power than the inside slots. The average measured amplitude of the 8 outside slots is 0.45 while for the inside slots it is 0.58, or a ratio of amplitude of 1.26 and a ratio in power of 1.66. However, it should be recognized that the dipole that is making the measurement is also closer to the edge in one set of measurements than it is in the other, so the validity of the measurement could be involved. If the reader wishes to refer to a photograph to see what is meant by "inside" and "outside" slot, he should refer to Figure 7-3 rather than Figure 7-9. The probe measuring technique is illustrated with the engineering model whose inside and outside slots are transposed from those of Array #1 (Figure 7-3) on which the matrix measurements in Figure 7-11 were made.

Another observation of importance is that the amplitude of the slots in waveguide #5 (column #5) is definitely greater than for the other guides. Here the average value of the amplitude is 0.67 versus the average value of 0.627. This may be caused by the lack of symmetry in the physical region of the T junction at the center of the array. In fact, intuition would indicate that the coupling would be less symmetrical than the measurements indicate.

It was not possible to find a correlation between the phase variation within the internal matrix and any other parameter, such as variation in slot length or position of the slot from the waveguide centerline. Although there were some errors in slot length on the top and bottom row, the slot lengths were very uniform within the internal matrix, and no correlation could be established. There did not appear to be any correlation between phase and errors in position of the slot from the center line.

Figures 7-12 and 7-13 are of the antenna patterns in the E and H planes that were recorded at JPI. The measured gain was 25.42 dB as compared with a theoretical gain of 26.9 dB for uniform illumination of the 29.6"x30.7" maximum dimensions of the array. The effective aperture area, however, may be considerably smaller than this. The 25.42 dB gain would be associated with a uniformly illuminated aperture 25.4" on a side. It is of interest to note that the distance between the centers of the end slots in each waveguide is 25.2" and the distance between the outside slots in waveguide #1 and waveguide #8 is 27.5". It was also noted that the outside slots in waveguides #1 and #8 radiate appreciably less power than do other slots, so that the array has a small amount of illumination taper on it.

At examination, the position of the first nulls on the graphs, although difficult to read accurately, appears to be between ten and eleven degrees. The theoretical nulls for the 29.6 and 30.7" maximum dimensions of the array are 9.33 degrees and 8.99 degrees respectively, while for the 25.4" dimension that would match the observed gain the null occurs at 10.87 degrees.

Nevertheless, there was understandable concern that the lower gain figure could be caused by dissipative losses within the slotted array waveguide itself. This item will be discussed in the next section.

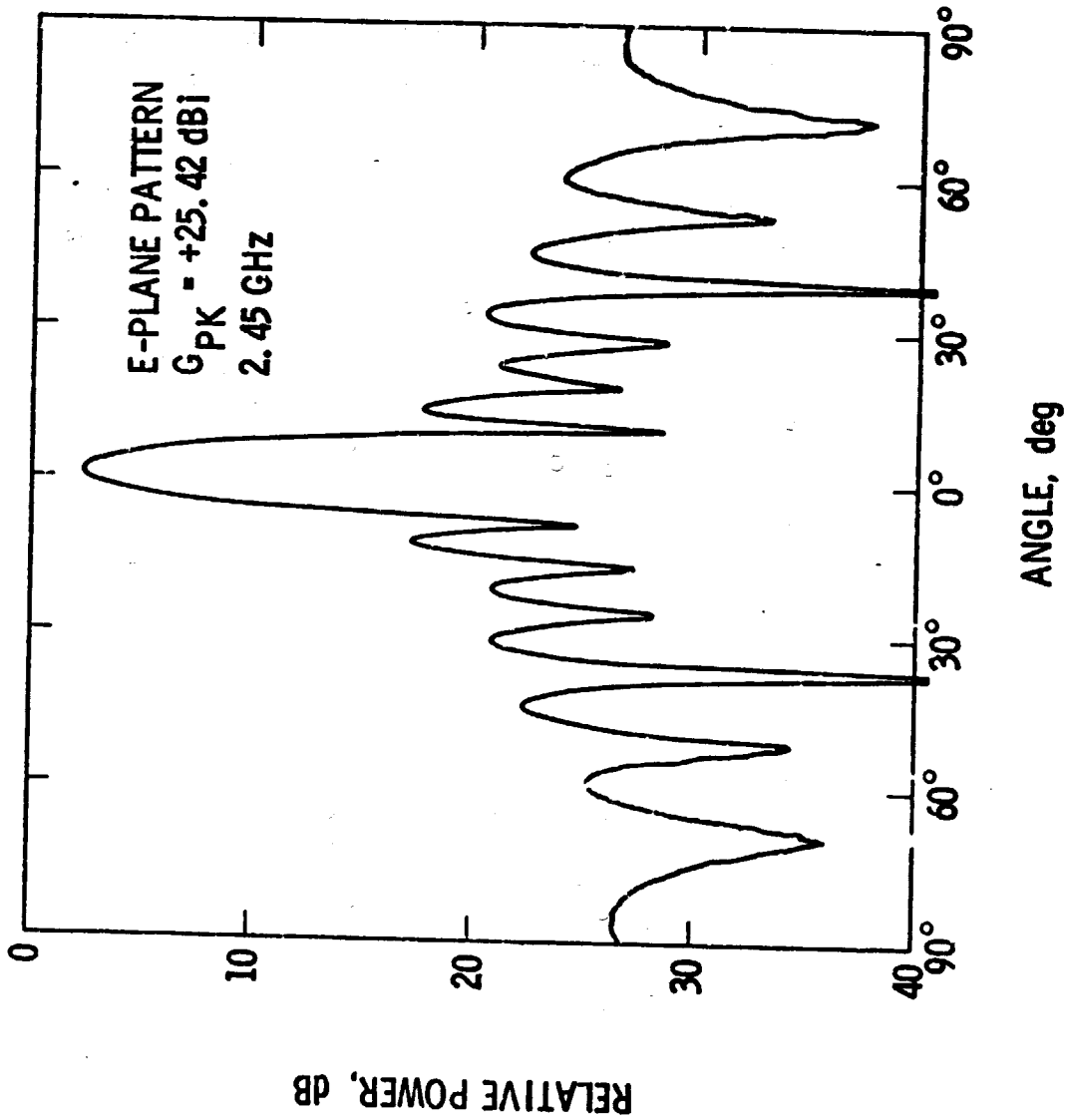
7.5 Measurement of the Dissipative Loss in the Slotted Waveguide Array

It would be difficult to imagine serious losses in the walls of a slotted waveguide structure of the area under consideration unless there were losses at the junction of the slotted face plate to the folded waveguide section. This was an early concern and one of the first items addressed in the development of the fabrication of approach described in Section 7.1. The matter became of concern again in an effort to account for a possible disagreement between the experimentally measured gain of the antenna and the theoretical gain for the



BEAMED RF POWER TECHNOLOGY

8-SLOT x 8-STICK SLOTTED WAVEGUIDE ANTENNA



PT-5613

Figure 7-12.



BEAMED RF POWER TECHNOLOGY

8-SLOT x 8-STICK SLOTTED WAVEGUIDE ANTENNA

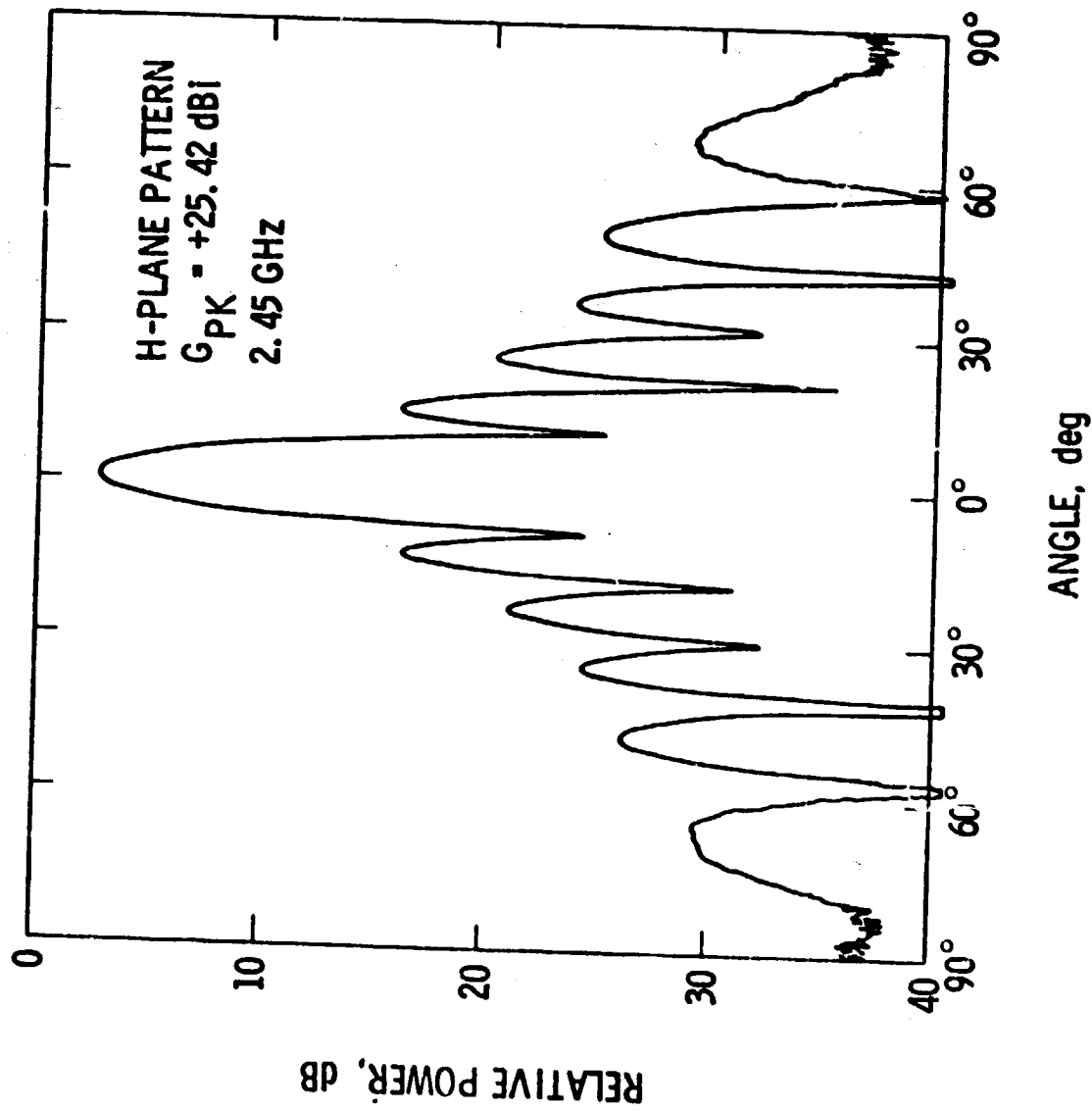


Figure 7-13.

maximum dimensions of the array. The early concern prompted the use of cold test measurements to investigate dissipative losses, while the later concern motivated the measurement of antenna internal losses by measuring the temperature rise in a known rate of water flow that was used to cool a section of the slotted waveguide antenna.

The initial measurement activity on losses within the array were made on an assembly consisting of two waveguide sticks that were assembled together by means of machine screws and nuts. A welded but similar assembly is shown in Figure 7-15. Measurements on the degree of coupling between the two guides as a function of the spacing between the machine screws which served to bond the slotted face plate to the folded waveguide sections were made.

The first set of measurements made on coupling between the waveguides was made under conditions where both were treated as resonant cavities. To obtain any measurable coupling, it was necessary to have both cavities at the same resonant frequency, and to have a reasonably good match at the input under these conditions. The waveguide resonances were so close together that it was possible to shift the resonance of one to coincide with that of the other by a small distortion of the sides of the waveguide. Under these measurement conditions, the feedthrough power was down 27 dB for a 3.0 centimeter spacing of the bolts on the mutual boundary, and 35 dB for a 1.5 centimeter spacing of the bolts.

A significant finding in this aspect of the testing was that because of the high cavity Q's that were found to be present (approximately 10,000) there could have been little radiation from the sides of the waveguides which were left unbonded at the shorted ends of the waveguides. Leaving this point unbonded greatly simplifies the construction procedures and is considered to be one of the desirable features of the basic fabrication approach described in Section 7.2.

The second set of measurements made on coupling between the waveguides was under more normal operating conditions in which radiating slots were present in the waveguide receiving the input power. The input matching arrangement was revised to provide low reflection of input power under these new conditions. The slots in the second waveguide were covered over with aluminum tape to prevent mutual coupling to the first guide. The output coupling in the second waveguide was a duplicate of that used on the input waveguide. Under this new set of conditions, the feedthrough power was down 49 dB with the use of bolts every 3.0 cm in the mutual boundary and down 60 dB with the bolts positioned every 1.5 cm.

Finally, the metal tape was removed from the slots of the second waveguide and the mutual coupling between the two guides determined. This was determined to be -19.8 dB.

The data that were taken on the feedthrough of power from one waveguide to the other are tabulated in Table 7-2. The quality of the input match may be ascertained from the reflected power measurement. The resonant frequency of the waveguide, 2443 MHz, is close to the design point of 2450 MHz.

From these measurements it may be seen that the coupling between waveguide sections through the mutual boundary may be kept low if the points of contact in the mutual boundary are in the range of 1.5 to 3.0 cm. The coupling is about 40 dB less than that of the mutual coupling of the waveguides through the slots in their faces. Finally it is noted from the high Q's that were obtained that the method of forming the waveguides by bolting a flat top to a folded section introduced negligible losses.

The second set of measurements having to do with dissipative losses in the slotted waveguide were motivated by questions raised concerning the efficiency of arrays made by this technique at the SPS microwave workshop held

TABLE 7-2

Test	Conditions	Separation Between Bolts on Common Waveguide Wall	Incident Power at Waveguide #1 Terminal		Reflected Power at Waveguide #1 Terminal		Transmitted Power at Waveguide #2 Terminal		Ratio of Transmitted Power to Incident Power dB	Frequency MHz
			Microwatts		Microwatts		Microwatts			
#1	Both waveguides operated as resonant cavities having same resonant frequency.	3.0 cm	1,250,000	1,500	1,500	2,500			-27	2444
#2	Same as #1 except for separation of bolts.	1.5 cm	1,650,000	2,000	2,000	8			-53.1	2443
#3	Waveguide #1 radiating through slots. Slots in #2 waveguide covered over.	3.0 cm	500,000	40,000	40,000	6			-49.2	2444
#4	Same as #3 except for separation of bolts.	1.5 cm	1,050,000	27,000	27,000	0.9			-60.7	2442
#5	Slots in both waveguides left open for mutual coupling.	1.5 cm	1,050,000	24,000	24,000	11,000			-19.8	2441

at the Johnson Space Center on January 15 to 18, 1980. Measurements of antenna gain made by JPL on the array sent to them by Raytheon in the spring of 1979 were less than anticipated and could be explained only by edge effects greater than anticipated or by internal losses in the array itself. Measurements of variations of phase and amplitude among the slots made at Raytheon, if assumed to be valid, were not sufficient to explain the loss of gain.

The ensuing discussion took two directions to explain the loss. One was that the waveguide array was internally lossy because of the spot welds that were used to join the slotted face to the back of the array. The other was that all slotted waveguide arrays are inherently lossy, and that the 98% radiation efficiency figure utilized in the estimate of the overall efficiency of the SPS microwave power transmission might be much too high. This latter consideration elevated the importance of resolving the issue.

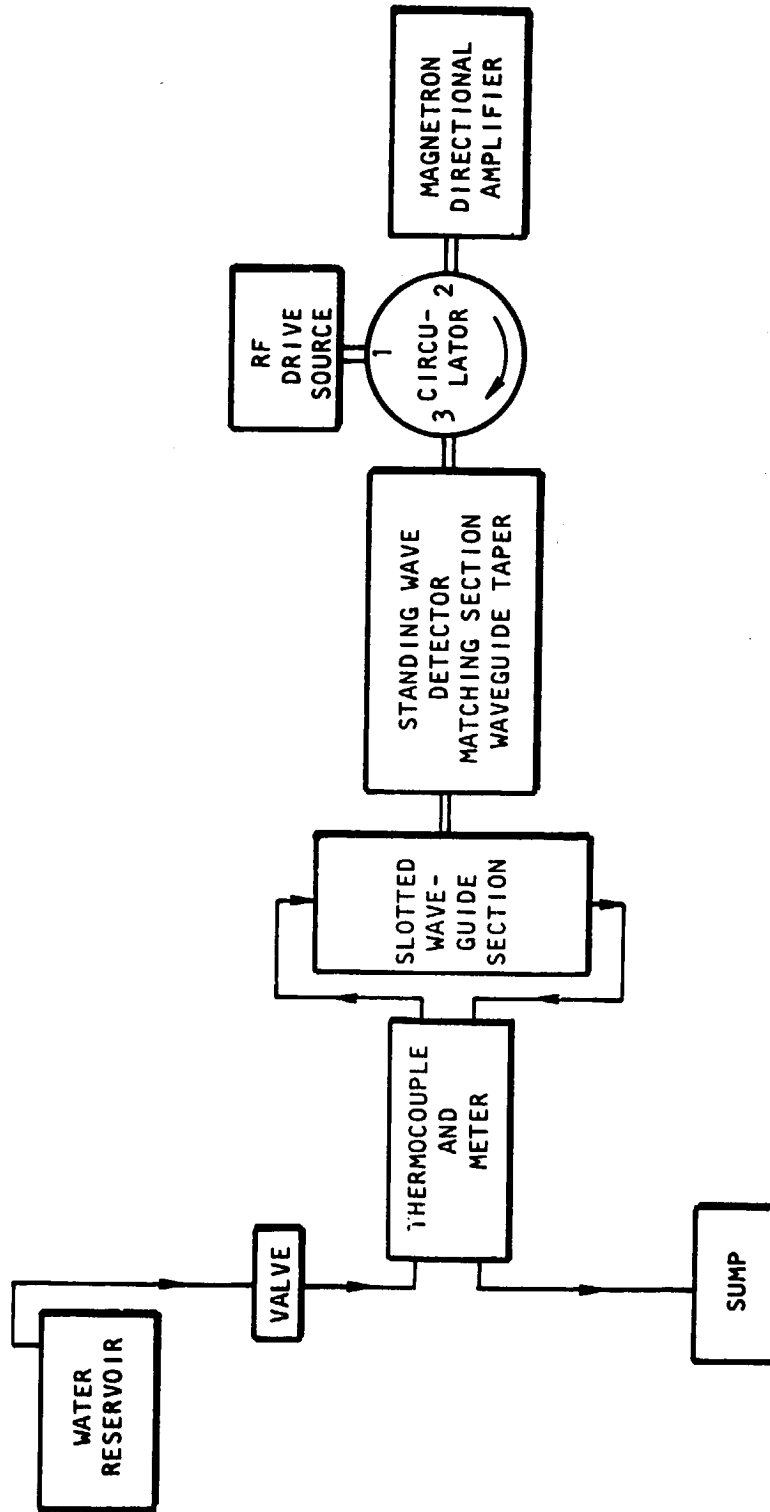
It was recognized that the 1/2 inch wide channel that separates the waveguides in the array could be used as a channel for the flow of water. The rise in temperature in this flow of water could then be used as a means of measuring the losses that were incurred in the waveguide radiator when normally high power levels of operation were employed. Unfortunately, the large eight by eight waveguide array was in use and could not be used for this purpose. However, a two by eight (two waveguides with eight slots each) made with identically the same spot welded construction and with the same spacing of the welds was available. The measurement does not lose any of its validity if a single waveguide radiator is used providing some allowance is made for losses in the feed waveguide.

Using a radiated power level of 480 watts, the loss measurements that were made with refined measurement methods indicated that the internal losses of this radiator assembly were $1.0 \pm 0.1\%$ of the radiated power. These losses include feed waveguide losses as well as losses in the slotted waveguide section. It is therefore concluded that the poor efficiency of 70 to 80% inferred from antenna gain measurements must be caused by some other factor.

While these measurements should reaffirm faith in the use of a 98% efficiency for the slotted waveguide array, they should not be generalized for all arrays and all constructions. For example, the welds may indeed be a source of loss and a continuous weld could appreciably decrease the losses. Also, the array is small in size (30 inches x 30 inches). A much larger array would have significantly larger internal losses because the power has to flow further before it is radiated along the waveguide. Even this small array has a waveguide length long enough to account for a 0.3% loss.

The experiment also provided the opportunity to operate the array at near the power densities expected from it in actual operation for either space or ground arrays. For the intended SPS application each magnetron would supply sixteen radiating slots with a total microwave power of three to five kilowatts. Thus, the eight slot array which we were testing should be operated at 1500 watts or more of power to duplicate the space application. The array was operated with a microwave power level of 1450 watts which was approaching the upper limit of the magnetron directional amplifier. Operation of both the array and the magnetron directional amplifier were normal in all respects. No internal loss measurements were made at this power level because of the glass foam load into which it radiated and from which there would have been radiation heating of the slotted waveguide array caused by the elevated temperature of the load.

The general test arrangement for the experiment is shown in Figure 7-14. The detailed arrangements for exciting the slotted waveguide radiator and attaching it to the rest of the system are shown in Figure 7-15. Figure 7-15(a) shows the overall assembly from the feed waveguide side with the water cooled access cover in position. The water cooling feature was not used in the data that will be discussed in this report. Figure 7-15(b) shows the assembly with the access cover removed. The standard 18° excitation slot that was machined into the feed waveguide is shown. The feed waveguide is attached with sheet metal screws to the slotted waveguide radiator. Figure 7-15(c) shows the slotted wave-



TEST SET-UP

816328

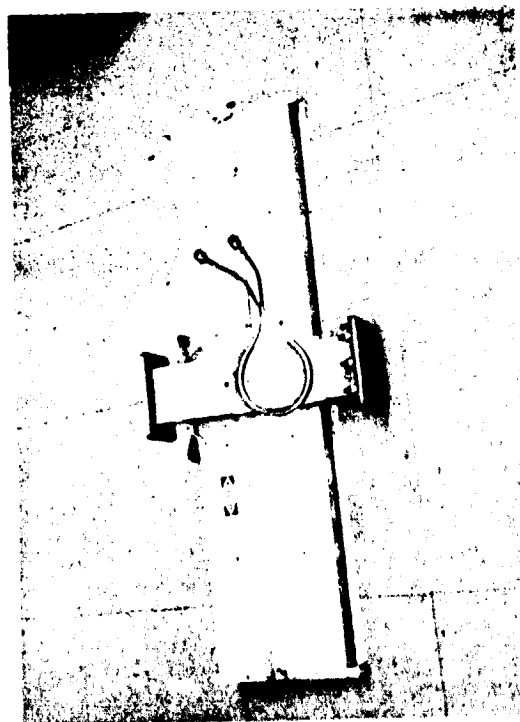
Figure 7-14. Test Arrangement for Measuring Internal Losses of Microwave Slotted Waveguide Radiator.



(b)



(d)



(a)



(c)

Figure 7-15. Arrangements for Checking Slotted Waveguide for Internal Dissipation Losses

guide radiator in position for test with the slots in the adjacent waveguide covered over to eliminate the possibility of mutual coupling. Figure 7-15(d) shows the input matching arrangement for matching the slotted waveguide radiator to the magnetron directional amplifier. The glass-foam load shown in the picture was used only for checking the radiator at power levels in excess of one kilowatt. The load was not used when loss measurements were made because of radiation of heat from the glass-foam load to the slotted waveguide radiator.

The slotted waveguide used in the tests was a two waveguide section assembled with forming and welding techniques identical to the eight-waveguide section delivered to JPL and reported upon in progress report No. 9. It consisted of a slotted section of 0.020 inch thick aluminum flat stock that was resistance welded at approximately 3/4 inch intervals to the formed 0.020 inch thick aluminum waveguide portion. The two 29 inch lengths are separated by a 1/2 inch wide by 1 1/2 inch deep channel. This channel was used as a water cooling channel. A water fitting was adapted to each end of the channel area. The open side of the channel was sealed with a cover and RTV material was used to seal all possible leak areas.

A brass 1 1/2 inch x 3 inch waveguide section with a properly positioned machined slot was mated to the one waveguide section that was used for loss measurements. One end of the feed waveguide was terminated with a short $\lambda/2$ from the center of the slotted waveguide. A thin sheet of insulating material was inserted between the brass waveguide and the unused section of the aluminum slotted waveguide to minimize unwanted heat transfer. Contact and fastening between the brass waveguide and the slotted waveguide to be tested was made with short self tapping screws. Pop rivets were used in the eight waveguide section delivered to JPL. Further rigidity was ensured by strapping the two waveguide assemblies together. No changes in rf losses could be detected during low level microwave testing in which the radiating slots were covered over with tape and sensitive standing wave ratio measurements made while exerting torque on the junction between the slotted waveguide and the feed waveguide.

Formed copper tubing for water cooling was brazed to the copper cover plate located directly opposite the slot feed in the brass waveguide. This cooling feature was a precautionary measure introduced to minimize heat transfer to the aluminum waveguide from abnormally high I^2R losses in the feed waveguide caused by the high standing wave ratio occasioned by the relatively poor match of the feed waveguide to a single waveguide radiator as contrasted to the good match into four waveguide radiators under normal circumstances. Although it did reduce such transfer losses, the reduction was not large and in the final tests this auxiliary cooling feature was not used.

To reduce the flow of heat from the I^2R losses generated in the waveguide attached to the magnetron, non-metallic screws and gaskets were used to join this section to the feed waveguide flange. However, after a long time delay, heat flow across this flange did appear in the measurements. In any future tests this flow of heat would be prevented by cooling the waveguide attached to the magnetron with water just before it entered the sump (Figure 7-14).

Extreme care was used to reduce the impact of the ambient environment upon the measurements. Of particular importance was the need to have the temperature of the slotted waveguide radiator very close to ambient temperature during the measurements to minimize radiative transfer losses. To help bring this about water for the thermal measurements was stored in an open elevated reservoir and was allowed to thermally stabilize to room ambient temperature. The temperature rise in the water and therefore the slotted waveguide radiator was 0.1 degree during the measurements. The increased radiative power transfer from a surface equal to that of the slotted waveguide under test and with an emissivity and absorptance of 0.5 would be only 0.16 watt.

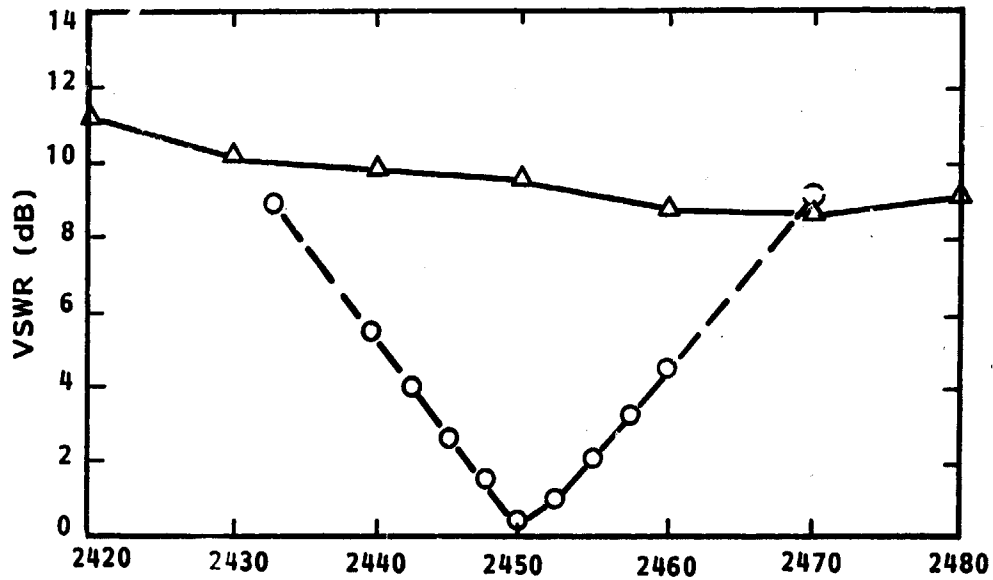
For additional assurance of the validity of the test procedure a well insulated cylinder with an immersion heater in it was inserted into the line in place of the slotted waveguide section. The immersion heater was then adjusted

for a small known amount of power - typically 5 watts. Corresponding power readings were then made using the temperature rise in the thermocouple meter and the measured water flow. The system operation is best illustrated by the transient response of the system to two successive applications and removal of power to the immersion heater, as shown in Figure 7-16.

The data in Figure 7-16 indicates both the degree of sensitivity and repeatability with which the measurement system is capable. The fine structure of the curves is impacted by errors in reading the meter and possibly by the "stickiness" of the meter needle itself. The data also shows an ambient drift of the meter reading when no dissipation is being introduced into the system. It is clear, however, that the sensitivity is well within the 0.2 to 0.3 watt region, and that there is good agreement between the measured power into the dissipation system and the power that is measured by thermal means. The "thermal means" is identified with the carefully calibrated millivolt meter and thermocouple to measure temperature rise in the water, and a carefully measured rate of flow.

The VSWR looking directly into the feed waveguide is shown as a function of frequency in Figure 7-17. A VSWR of 9.5 dB corresponds to a reflection of 25% of the power. The reflection was eliminated by a matching section consisting of a section of waveguide with post tuners. The VSWR as a function of frequency after the impedance matching is also shown in Figure 7-17.

A Raytheon Microwave Oven Magnetron was run as a directional amplifier to supply the microwave power. It was driven with 10 watts of rf feed power at 2450 MHz. The tube was operated in the "locked" condition at 4040 volts with 200 mA of current producing 480 watts of power at the input to the slotted waveguide section. Filament power was maintained at approximately 30 watts during the test runs. The regulated DC Power Supply was operated in the Current Mode during the power runs.



816329

Figure 7-17. VSWR Looking into Feed Waveguide to Slotted Waveguide Before and After Impedance Matching.

It is to be noted that the operation of the magnetron as a directional amplifier was not in the least disturbed by operating into the slotted waveguide array. This was expected because the waveguide load is a relative broadband load. In addition any reactive coupling to the magnetron is eliminated by the ferrite circulator.

The thermal measurements of dissipated power indicated that 4.8 watts of power were dissipated by the combination of a single slotted waveguide radiator and the feed waveguide attached to it. The microwave power fed into the microwave radiator was 495 watts of which 3% was reflected as determined by VSWR measurements during the actual test run. The nature of the test data is shown in Figure 7-18 as a sequence of two applications and removals of a step function of microwave power of 480 watts.

An analysis of the expected heat flow from the slotted waveguide itself and the attached feed waveguide indicates that heat flow from both sources should be detected within the first few minutes and reach a steady state value well within ten minutes. The flow of heat from the aluminum waveguide should take the form of two surges of heat flow separated in time. This is because most of the skin losses are generated along the sides of the waveguide and to a much smaller degree in the top and bottom. There will be almost no time delay in the flow of heat from the side wall adjacent to the cooling channel. However, the heat that is generated in the opposite side wall from the cooling channel will have to flow along the top and bottom surfaces first and will be delayed. In particular the slots in the waveguide top will delay the heat flow through that surface. The data of Figure 7-18 indicates these two surges of heat as A & B separated in time about equal to the time for the heat to flow across the top and bottom. There is also time delay in the data caused by the fill time for the volume of water between the input and exit thermocouple of about 30 seconds. The third observed step in the transient response is the heat flow that is transmitted to the waveguide from the input feed waveguide. This flow is denoted as C in Figure 7-18. About

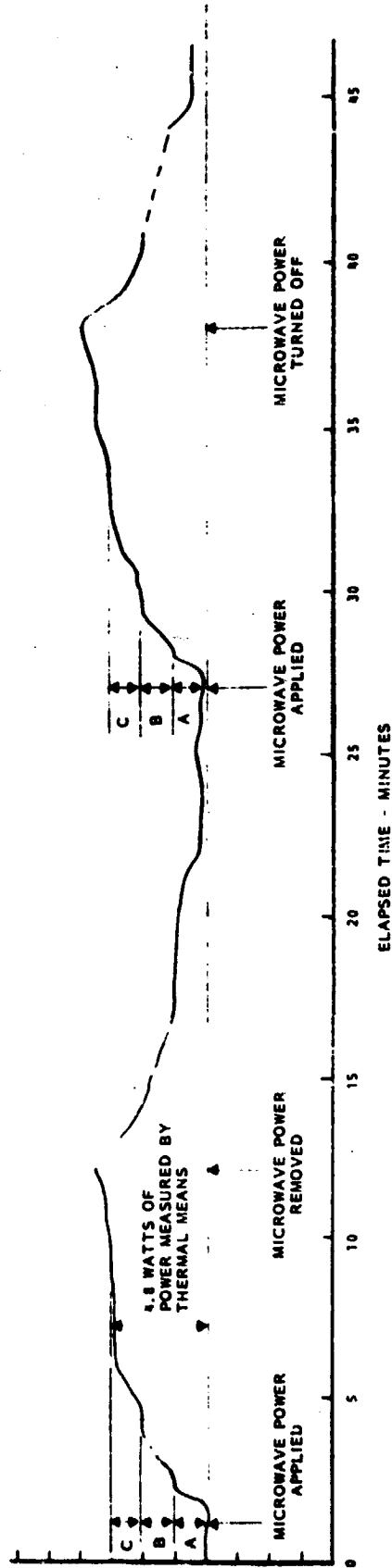


Figure 7-18. Dissipated Power in Slotted Waveguide Section Measured by Thermal Means. Microwave Power of 480 Watts Enters the Slotted Waveguide and All But 4.8 Watts is Radiated Through the Slots. Microwave Power is Applied as a Step Function for Approximately Ten Minutes and Then Turned Off.

PT-5613

nine minutes after the application of a step function of microwave power, a fourth flow of heat input is detected. This comes about, it is believed, as a flow of heat from the waveguide system which feeds the flanged input of the feed waveguide and which is only partially thermally isolated from it by a Kapton gasket 0.015 inch thick. Calculations indicate that if the gasket had perfect thermal contact to the two flanges, 0.25 watts could be conducted for each degree centigrade differential between the flanges. The flow of heat across the flange increases with time as the waveguide on the magnetron side of the flange heats up with continued operation. In any future rerun of this test this delayed source of heat could be eliminated by simply water cooling the waveguide flange on the magnetron side of the coupling by the waterflow after it had exited the second thermocouple.

One additional perspective on the tests is the time required for the waveguide system to store the energy represented by an average increase in the water temperature of 0.05 centigrade degrees. The mass of the entire two section aluminum waveguide is 581 grams. The additional heat stored is 120 calories or 501 watt seconds for each centigrade degree rise in temperature. Since the rise in temperature is 0.05 degrees, 25 watt seconds of energy are stored. On the other hand, the feed waveguide and flange weighed 2400 grams and represented a storage of approximately 40 additional watt seconds of energy for the 0.05° centigrade increase in average temperature.

It is believed that the foregoing analysis of the test results in combination with the use of the immersion heater as a check upon the carefully made thermal measurements has established the validity of the test results. The probable error is in the range of 5 to 10% of the power measurement or 0.25 to 0.5 watt or about 0.1% of the microwave power level radiated.

It is also interesting to consider what the attenuation losses would be in the aluminum waveguide itself. The attenuation is about 0.01 dB per foot. The length of waveguide of either side of the feed waveguide is 15 inches or

1.25 feet. The predicted waveguide loss in this length of guide would be 0.28%. The situation in the slotted waveguide radiator is much more complicated, however. The standing wave ratio would increase the loss but much of the power is radiated before the region of high standing wave ratio is reached which is at the ends of the slotted waveguide. It is also possible that the slotted waveguide losses would be considerably lower if the welds were closer together, or ideally, a continuous weld.

During the tests in which the microwave power was radiated directly into space, precautions were taken to ensure that personnel making the test were not exposed to an excessive amount of microwave radiation. No other people were in the vicinity. A Narda Microfilm Electromagnetic Monitor, Model 8110, was used during the radiating periods to check the immediate area for personnel safety. Most exposure levels did not exceed 1 milliwatt/cm². In no instances were personnel exposed to more than 10 milliwatts/cm².

8.0 CONCLUSION AND SUMMARY OF RESULTS

The study consisted of (1) an evaluation of several characteristics of the magnetron directional amplifier that are critical to its application to an active phased array in microwave power transmission and (2) the evaluation of a novel method of making slotted waveguide arrays from thin sheet metal by fabrication and testing of a 64-slot array. The results of the magnetron amplifier evaluation program are summarized in the material immediately following. The conventional microwave oven magnetron was the specific tube used for the investigation.

8.1 Phase Shift and Power Output as a Function of Anode Current, Anode Voltage, and Drive Level

Several sets of data involving the phase shift across the magnetron directional amplifier and its power output were taken with the anode current, voltage, and rf drive level as input variables. The operating range in current was found to vary as the one-half power of the rf drive level, as expected. The phase shift data appeared to be without discontinuities.

Data was also taken on the frequency range of locked operation as a function of drive and current level.

It was determined that the current range over which the magnetron directional amplifier was operative was limited for the most part by the frequency-shift-with-current characteristic of the free-running magnetron.

The data was taken without any external heater power being applied to the tube. All characteristics appeared to be acceptable.

8.2 Evaluation of Noise Properties

Measurements of broadband noise removed in frequency from the main signal, close-in noise, and harmonic generation were made.

Broadband background noise is characterized by continuous spectra whose amplitudes fall rapidly at frequencies removed from near the carrier. A noise spectral density that was at least 155 dB below the carrier was obtained in the normal operating range of voltage at frequencies removed from the carrier frequency by more than 10 MHz. Background noise increased with operating voltage.

The level of the background noise was determined to be independent of the level of rf drive and of the frequency of the rf drive over the range of locked frequency operation.

Measurement of noise close to the carrier was also made with special equipment. The spectral density of the noise was 145 dB below the carrier at a frequency removed from the carrier by 50 kHz.

Both the background noise removed from the carrier as well as the close-in noise represent excellent performance. The major factor in obtaining such low noise is removing any external source of heater power after the tube has been started.

Harmonic noise measurements were also made with a special test arrangement that attached a small diameter coaxial line directly to the output probe of the tube to eliminate higher modes of propagation that would normally confuse the measurements. The average harmonic levels on two tubes were -70, -86, -89 and -63 below the carrier for 2nd, 3rd, 4th, and 5th harmonics respectively.

8.3 Investigation of Long Cathode Life Potential

Measurements of cathode temperature as a function of anode current, anode voltage, magnetic field, and coupling to the external load were made with the use of special tubes with windows in them so that an optical pyrometer could be

used to measure these temperatures. It was found that the cathode temperature was uniquely dependent upon the value of anode current. The increase in temperature with an increase in anode current corresponded closely to such an increase in temperature predicted by the Richardson - Dushman equation for temperature limited emission. The implication is that the magnetron has an internal feedback mechanism that adjusts the backbombardment power from the electrons that return to the filament to just the amount needed to heat the cathode to a temperature to provide the primary emission required by the increase in anode current.

The cathode temperatures observed at an operating current of 200 milliamperes (the normal value is 300 milliamperes) was so low that a life of 5 to 10 years could be predicted on the basis of well-established engineering data on carburized thoriated tungsten cathodes. It follows that a tube could be designed for the SPS application that could provide fifty or more years of life because of the low emission current density and associated low filament temperature that could be designed into the tube.

8.4 Investigation of High Efficiency in the Microwave Oven Magnetron

An overall efficiency of 81.7% defined as the ratio of microwave power output to DC power output was obtained by operating the tube at higher voltage and current levels. This corresponds to a DC to rf conversion efficiency of 86 - 87% after taking into consideration the loss of microwave power in circuit losses and in backbombardment power to heat the cathode.

Special care was taken to assure the accuracy of the efficiency measurement by using a special test arrangement. A balance of DC input power against the sum of measured microwave output and anode dissipation was also made to provide additional confidence in the accuracy of the efficiency measurement. A probable error of $\pm 1\%$ of the 81.7% efficiency measurement resulted.

As anticipated, the high efficiency measurements were about 6% less than theoretically predicted and were consistent with reduced efficiencies obtained at lower values of the applied magnetic field. The microwave oven magnetron has a degraded efficiency not only from that predicted from theory but also from that exhibited by a commercially available magnetron at 915 MHz.

8.5 Investigation of a Novel Method for Fabricating Slotted Waveguide Arrays from Thin Sheet Metal

Although slotted waveguide arrays are an established antenna technology, there has been little effort to develop a low-cost high-speed method of fabricating them. There has been a critical need for such a method because of its influence on the cost of microwave power transmission which has been a sensitive element in its acceptance.

A novel method for fabrication was investigated by adapting it to a JPL electrical design for a 64 slot array and fabricating the design with the use of temporary tooling. To reduce the cost of material as well as to ease the fabrication process, 0.020" thick aluminum sheet was used. The resulting product was adequately strong and rigid.

The resulting array was tested for radiation patterns both at Raytheon and JPL. Although more evaluation needs to be made, the measurements indicated that it compared favorably with arrays made from specially drawn waveguides which were assembled into an array.

A special effort was made to measure the skin losses in the array. These skin losses manifest themselves in the form of heat which was measured with a special test setup. Such losses were well below 2% of the microwave input power. A further benefit of the test was successful operation at a power density level approaching that required from the SPS transmitting antenna.

9.0 RECOMMENDATIONS

The following recommendations are made for further improvement of Microwave Beamed Power Technology:

- The capability to follow a reference phase and a reference amplitude needs to be added to the magnetron directional amplifier in order to qualify it for use in a phased array transmitting antenna.
- The capability of the magnetron directional amplifier to operate stably into a slotted waveguide array antenna section needs to be demonstrated, preferably with a simultaneous demonstration of a capability to track a phase and amplitude reference.
- Although significant carrier to noise ratios have been demonstrated, the residual noise level of the instrumentation now limits the sensitivity of these measurements. It would be desirable to increase the sensitivity of these noise measurements.
- The various kinds of noise and their sources need to be better identified and their control better understood.
- The sources of inefficiency in the magnetron need to be better identified and their control understood.
- An approach to a low-cost slotted waveguide array has been investigated and its advantages have been demonstrated. The construction and use of a sizeable number of these in some form of phased array is the next logical step to be taken. It would be logical to combine the low-cost slotted waveguide array with the low-cost magnetron directional amplifier with a phase and amplitude tracking capability.

10.0 NEW TECHNOLOGY

No reportable items of new technology have been identified. The nature of the study was investigative rather than innovative. Although the 64-slot slotted waveguide array was made with a novel fabrication approach, the approach had been previously conceived and described and the key fabrication step reduced to practice by experiment.